Ioannis Poulopoulos

Modelling and Simulation of Carbonated Water Injection

Master's thesis in Exchange Student

Supervisor: Even Solbraa

July 2020

Master's thesis

NTNU
Norwegian University of Science and Technology
Faculty of Engineering
Department of Energy and Process Engineering

NTNU
Kunnskap for en bedre verden

Acknowledgements

This master thesis is a result of many hours of work and I would not have been able to complete it without the help and the guidance of several individuals. Therefore, I would like to express my special thanks of gratitude to my supervisor Epaminondas Voutsas and my co-supervisor Georgia Pappa at NTUA. Moreover, I would like to thank my supervisor at NTNU Even Solbraa as well as my co-supervisor Efstathios Skouras-Iliopoulos for their advice and support. Last but not least, I would like to thank all the people that kept encouraging me during this project.

Abstract

Carbonated Water Injection (CWI) is considered as one of the most sustainable solutions in response to CO_2 emissions in oil and gas processes. It has the potential to store CO_2 in geological formations, while recovering oil, reducing this way the carbon footprint. This advantage is a key asset of CWI, comparing to other enhanced oil recovery methods (EOR). In this technique, recovering oil is achieved through the dissolution of CO_2, which transfers to the oil phase improving the oil mobility and causing oil swelling, both enhancing the sweep efficiency.

In this work, two models are presented for the prediction of CO_2 solubility in water and NaCl brines. A third model is, also, presented for the prediction of CO_2 solubility, taking into consideration the presence of O_2 and N_2, in water and NaCl brines. The first model is the model of Duan and Sun, which is based on the theoretical basis that at equilibrium the chemical potential of CO_2 in the liquid phase is equal with the chemical potential of CO_2 in the vapor phase. The second model is the equilibrium model, which is based on the theoretical basis that in equilibrium the fugacities of CO_2 and water in the vapor phase are equal to the fugacities of CO_2 and water in the liquid phase. The third model is the model of Li, which is based on the Henry constant, that is valid only when the system is at equilibrium state and interrelates the gas fugacity coefficient of a component with its activity.

The advantage of Duan and Sun's model is that they developed a non-iterative method to calculate the fugacity coefficient of CO_2 in the vapor phase, whereas in the equilibrium model an equation of state is used in order to calculate the fugacity coefficients of CO_2 and water in the vapor phase. The advantage of the equilibrium model is that it predicts better the CO_2 solubility in higher salinities, higher than 4 molality. The advantage of Li's model is that, despite the not so accurate prediction of CO_2 solubility in the CO_2-water-salts system, it includes the effect of impurities, such as O_2 and N_2, on the CO_2 solubility in the CO_2-O_2-N_2-water-salts system.

The effect of pressure, temperature, salinity and impurities' content on the solubility of CO_2 is studied. It is observed that the solubility increases with pressure, decreases with salinity and impurities' content. The influence of the temperature is more complex. Its effect varies according to the values of the aforementioned factors. In general, in temperatures below 100^o C the solubility decreases, whereas over 100^{o}C it increases with it.

The process simulation for the production of carbonated water is developed in Unisim. Owing to the fact that the already existing thermodynamic models don't describe well the equilibrium of the CO_2-O_2-N_2-water-salts system, the model of Li et al. is implemented via CAPE-OPEN. This model, though, is not able to calculate the thermodynamic properties of the fluid. Subsequently, a comparison is made between the existing complete thermodynamic models, so as to decide which one simulates in a better way the behavior of Li's model and is going to be used for the calculation of the rest of the properties.

The process simulation is studied based on a case study provided by Equinor. More specifically, it is referring to an offshore process, that produces carbonated water, by mixing a water and a carbon dioxide stream, in the pressure of 180 bar. Since, the CWI is not a mature process, the modelling/simulation studies are not extensive. In this master thesis, a multistage compression of the CO_2 stream and the pumping of water in the same pressure, before their mixing, is proposed.

Two cases are studied in order to reach this pressure. The first one is by immediately pumping the water and compressing the carbon dioxide in the pressure of 180 bar. The second one is by pumping the water and compressing the carbon dioxide in an intermediate pressure and then pumping the carbonated water in the pressure of 180 bar. The scheme of the intermediate pressure is conceived since it is noticed that the given amount of CO_2 can be dissolved in the given amount of water at a pressure lower that this of 180 bar. The criterion, on which the selection is based, is the comparison of the cooling, compression and water pumping duties.

The simulation's results indicate that the water pumping duties have similar values. Thus, the compression and the cooling duties are of greater importance. The results indicate that in terms of required compressed and cooling duties, the intermediate pressure case is more profitable.

A sensitivity analysis is conducted in order to examine the effect of some of the most important operational parameters of the CWI on the aforementioned duties. Therefore, the effect of the type of compression (single vs multi-stage), the thermodynamic approach to equilibrium, the pressure drops of each heat exchanger and the mixer and the pressure ratio is studied.

The compression requirements are lower when the pressure ratio of the compression stages is the same and the multistage compression is chosen. The required pressure for the complete dissolution of the given amount of CO_2 decreases with the thermodynamic approach to equilibrium and increases with the pressure drops of each heat exchanger and the mixer. The higher the compression pressure, the higher the cooling and the compression duties.

As a result, it is concluded that the most profitable way, in terms of required duties, of producing the carbonated water is by pumping the water and compressing the carbon dioxide stream in an intermediate pressure and then pumping the mixture in the desired pressure.

KEY WORDS: Carbonated Water Injection, Carbon dioxide, Thermodynamic Modelling of carbon dioxide-water-brine system

Contents

List of Tables

List of Figures

Nomenclature

Latin Letters

Symbol	Description	Unit
b	covolume parameter of t-mPR	L/mol
k	binary interaction parameter	-
m	parameter in α parameter of t-mPR	-
P	pressure	bar,Pa
R	gas constant	L*bar/mol/K
T	temperature	K,°C,F
V	molar volume	L/mol
x	molar fraction for the liquid phase	mol/mol
y	molar fraction for the vapor phase	mol/mol
f	fugacity	bar
m	molarity	mol/kg solvent
Par	parameter in λ,ζ,μ/RT	-
c_1-c_{11}	parameters in Par	-
c_1-c_{15}	parameters in ϕ	-
K	equilibrium constant	bar,Pa
A_0-A_5	parameters in K	-
Q	born function	-
B	parameter in ε^o	-
C	parameter in ε^o	-
S	salinity	mol NaCl/kg solvent
t	translation factor correcting the volume in t-mPR	L/mol
a_1-a_7	parameters in K	-
a_1-a_5	parameters in $\bar{V}$	-
U_1-U_9	parameters in ε^o	-
a	parameter in α	-
α_c	parameter in α	bar*L^2/mol^2
m	parameter in a	-
t_o	parameter in t	L/mol
Z	compressibility factor	-
H	henry constant	bar
H^*	henry constant asterisk	bar
ΔP	pressure drop	bar
f/2	friction factor	-
Re	Reynolds number	-
v	superficial velocity	m/s
L	mixer length	m
D	inner pipe diameter	m
$\dot{Q}$	volumetric flow rate	m^3/s
PR	pressure ratio	-
SG	specific gravity	-
$\dot{m}$	mass flow rate	kg/s
Q	duty	kW
Cp	specific heat capacity	kJ/kg/°C
ΔT	temperature difference	K

Greek Letters

Symbol	Description	Unit

α	attractive parameter of t-mPR	bar*L^2/mol^2
ϕ	fugacity coefficient	-
μ	chemical potential	L*bar/mol
γ	activity coefficient	-
λ	interaction parameter	-
ζ	interaction parameter	-
ω	acentric factor	-
ω	parameter in $\bar{V}$	-
ε^o	dielectric constant	-
β	parameter in t	-
A	parameter in Z	-
B	parameter in Z	-
ρ	density of the fluid	kg/m^3
μ	absolute viscosity	kg/m/s

Abbreviations

Symbol	Description
CO_2	carbon dioxide
H_2O	water
O_2	oxygen
N_2	nitrogen
NaCl	sodium chloride
t-mPR	translated-modified Peng-Robinson
EoS	equations of state
WAG	water alternating gas
CWI	carbonated water injection
KCl	potassium chloride
$CaCl_2$	calcium chloride
NeqSim	Non-Equilibrium Simulator
PR	Peng-Robinson
SRK	Soave-Redlich-Kwong
HP	High Pressure
IP	Intermediate Pressure

Subscripts

Symbol	Description
i	component
ij	cross parameter
c	cation,critical,cold
a	anion
ref	reference state
r	reduced
m	mixture
h	hot
in	inlet
out	outlet

Superscripts

Symbol	Description

l	liquid
v	vapor
(0)	standard state
-	average
sat	saturated
^	mixture
∞	infinite dilution
+	cation
-	anion

1 Introduction

As the global energy demand continues to increase and many of the existing oil fields are in the tail end production, the need has risen for development of improved oil recovery methods. At the same time, as the global concentration of CO_2 in the atmosphere has been rising, carbon geo-sequestration has been considered as one of the most important technologies to reduce the carbon footprint. In order to overcome these two phenomena, methods such as CO_2, after water injection, water alternating gas (WAG), simultaneous water alternating gas and carbonated water injection (CWI) have been developed.

From the aforementioned techniques, carbonated water injection presents some very important advantages over the others. During CWI, CO_2 stays dissolved both in the oil and the water phases, as a result it leads to a better sweep efficiency in comparison with CO_2 injection. In addition, CWI needs less amount of CO_2 than the CO_2 injection. This is a very critical factor for offshore processes where the supply of CO_2 is limited. Moreover, at the end of the CWI process a significant amount of CO_2 has been stored in the reservoir as it is dissolved in the remaining oil and water. Whereas, in the CO_2 injection, the CO_2 sequestration could be failed because of gas leakage due to the fact that CO_2 is free and mobile. Premature gas breakthrough caused by gas overriding puts some additional risk to the process. WAG injection, as mentioned above is another viable method that can be used. The main disadvantage is that water shielding could have a negative effect in the oil recovery efficiency. Efficiency decreases if diffusion process is not completely accomplished. The water between the oil and gas phases can be an obstacle to gas diffusion.

The availability of a model that accurately predicts the solubility of CO_2 in saline aqueous solutions for a wide range of pressures, temperatures and salinities is very important for the simulation and CWI process development. In this work two approaches for the prediction of CO_2 solubility in water and NaCl brines are presented. The first one is the model proposed by Duan and Sun 2003 and the second one is a model based on the methodology followed by Pappa. A third approach is also studied, that consists of the model proposed by Li et al. 2018. This model predicts the solubility of CO_2 in water and NaCl brines, while impurities as oxygen and nitrogen are present.

Since there is not a widely known process simulation for the production of carbonated water, its development is studied. In this thesis, the multistage compression of the carbon dioxide and then its mixing with the water injection stream is suggested. The pressure is considered the most critical design variable and it is calculated so that the carbon dioxide is dissolved in the water injection stream. The compression, cooling and water pumping duties are estimated. The effect of the type of the compression, the thermodynamic approach to equilibrium, the pressure drops of each heat exchanger and the mixer and the diverse pressure ratios in the compression stages on the dissolution pressure and the aforementioned duties is studied.

In the beginning of this master thesis (Chapter 2), the existing thermodynamic models for the systems: CO_2-NaCl brines (or pure water) and CO_2-N_2-O_2-NaCl brines (or pure water) are presented. Moreover, the effect of pressure, temperature, salinity and impurities' content on the CO_2 solubility is studied. In Chapter 3, the solubility data of CO_2 in these systems are reviewed and the behavior of the model of Li et al. 2018 in the aforementioned systems is studied. Next, in Chapter 4, the thermodynamic model, for the prediction of CO_2 solubility in

water-NaCl brines, that is developed in this work, is introduced. The implementation of Li et al's 2018 model in Unisim via CAPE-OPEN is shown in Chapter 5. In Chapter 6, the theoretical development of the carbonated water injection process is presented. Chapter 7 represents the Case Study provided by Equinor and its process flow diagram in Unisim. The simulation results of this Case Study are presented in Chapter 8. In Chapter 9, the sensitivity analysis studying the effect of the different factors on the dissolution pressure is presented. The discussion of the results and the conclusions are presented in Chapters 10 and 11 respectively.

2 Thermodynamic Models

The solubility of CO_2 in water is described by the equilibrium between the vapor and the liquid phase. This equilibrium is usually expressed by the equality of fugacities of CO_2 and water in the vapor and liquid phase:

$$f_i^l = f_i^v$$

$$x_i \varphi_i^l P = y_i \varphi_i^v P$$

where f_i^l and f_i^v are the fugacities of the component i in the water-rich and the CO_2-rich phase respectively, φ_i^l and φ_i^v are the fugacity coefficients of the component i in the water-rich and the CO_2-rich phase respectively, x_i and y_i are the mole fractions of component i in the water-rich and the CO_2-rich phase respectively and P is the pressure.

In systems without strong interactions the calculation of the fugacity coefficient can be achieved through a cubic equation of state. This calculation can also be done in the case of slightly polar molecules, like CO_2, by using the binary interaction parameter k_{ij} in the calculation of the attraction term α_{ij} (Tassios, 2001, p.358). In the systems studied in this thesis, CO_2-water, CO_2-brine and CO_2-N_2-O_2-brine, the standard equations of state cannot be used. The main reasons for that is that they can neither describe the hydrogen bonding that characterizes the equilibrium nor the effect of polar molecules, like the inorganic salts (NaCl) that are present.

After reviewing the literature, the main modifications in a standard cubic equation of state that are proposed, are the following: a) introduction of a new expression for the dependence of the attraction parameter a from the temperature and b) different values of binary interaction parameters for the aqueous and non-aqueous phase (Søreide and Whitson, 1992; Firoozabadi et al., 1988; Peng and Robinson, 1980). Some other more advanced thermodynamic models have also been used (Pappa et al., 2009; Ji et al., 2005).

Another common strategy that is used for the description of the aforementioned systems is a activity coefficient-fugacity methodology (Li and Nghiem, 1986; Enick and Klara, 1990; Diamond and Akinfiev, 2003; Spycher and Pruess, 2003; Nighswander and Kalogerakis, 1986; Duan and Sun, 2003; Duan et al., 2006; Sørensen et al., 2002). Their main advantages are that they are simpler methods and they require less computational time.

As a result, in this work, the model of Duan and Sun (2003) is presented and studied. The effect of impurities like N_2 and O_2 in the CO_2 solubility is described by the model of Li et al. (2018).

2.1 The model of Duan and Sun

Duan and Sun (2003) presented a thermodynamic model for the calculation of CO_2 solubility in pure water and NaCl brines for a temperature range 273-533 K, a pressure range 0-2000 bar and an ionic strength range 0-4.3 m. Their work is based on the study made by Duan et al. (1992). The theoretical basis of their model is that at equilibrium the chemical potential of CO_2 in the liquid phase is equal with the chemical potential of CO_2 in the vapor phase. The equation obtained is the following:

$$\ln \frac{y_{CO_2} P}{m_{CO_2}} = \frac{\mu_{CO_2}^{l(0)}(T,P) - \mu_{CO_2}^{v(0)}(T)}{RT} - \ln \varphi_{CO_2}(T,P,y) + \ln \gamma_{CO_2}(T,P,m)$$

where $\mu_{CO_2}^{l(0)}$ is the chemical potential in hypothetically ideal solution of unit molality, $\mu_{CO_2}^{v(0)}$ is the hypothetically ideal gas chemical potential when the pressure is equal to 1 bar, φ_{CO_2} is the fugacity coefficient of CO_2 in the vapor phase and γ_{CO_2} is the activity of CO_2 in the liquid phase.

The mole fraction of CO_2 in the vapor phase, due to the lack of experimental measurements, assuming that water vapor pressure of the mixtures is the same as pure water saturation pressure, is calculated from the following equation:

$$y_{CO_2} = \frac{\left(P - P_{H_2O}\right)}{P}$$

where P_{H_2O} is the pure water pressure.

The fugacity coefficient of CO_2 in the vapor phase is calculated from the equation of state for pure CO_2, as it is observed that it differs very little from that in the CO_2-H_2O mixture, proposed by Duan et al. (1992).

The activity of CO_2 in the liquid phase is calculated from a virial expansion of excess Gibbs energy proposed by Pitzer (1973) and described by the following equation:

$$\ln \gamma_{CO_2} = \sum_c 2\lambda_{CO_2-c}\, m_c + \sum_a 2\lambda_{CO_2-a}\, m_a + \sum_c \sum_a \zeta_{CO_2-\alpha-c}\, m_c m_\alpha$$

where λ is a second-order interaction parameter, ζ is a third-order interaction parameter, c means cations and a means anions.

In the parameterization, $\mu_{CO_2}^{v(0)}(T)$ is set to zero and following Pitzer et al. (1984) the parameters λ,ζ and $\frac{\mu_{CO_2}^{l(0)}(T,P)}{RT}$, are described by the following equation:

$$\text{Par(T,P)}=c_1 + c_2 T + \frac{c_3}{T} + c_4 T^2 + \frac{c_5}{(630-T)} + c_6 P + c_7 P \ln T + \frac{c_8 P}{T} + \frac{c_9 P}{(630-T)} + \frac{c_{10} P^2}{(630-T)^2} + c_{11} T \ln P$$

Duan et al. (2006) presented an improved model over the aforementioned for a temperature range 273-533 K, a pressure range 0-2000 bar and an ionic strength range 0-4.5 m. They ameliorated their previous model by developing a non-iterative method for the calculation of the fugacity coefficient of CO_2 in the vapor phase, instead of using the equation of state as mentioned above, and by also improving their accuracy below 288 K, through fitting of new solubility data.

The non-iterative equation that is proposed in order to calculate the fugacity coefficient as a function of temperature and pressure is the following:

$$\varphi_{CO_2} = c_1 + \left[c_2 + c_3 T + \frac{c_4}{T} + \frac{c_5}{(T-150)}\right] P + \left[c_6 + c_7 T + \frac{c_8}{T}\right] P^2 +$$

$$\left[c_9 + c_{10} T + \frac{c_{11}}{T}\right] lnP + \frac{[c_{12} + c_{13} T]}{P} + \frac{c_{14}}{T} + c_{15} T^2$$

The parameters $c_1, c_2, \ldots, c_{14}, c_{15}$ were fitted to the fugacity, that is calculated by the equation of state, proposed by Duan et al. (1992). The T-P range has been divided into six sections and there is a set of parameters for each one of them.

2.2 The model of Li

Li et al. (2018) presented a thermodynamic model that is based on a fugacity-activity method. The gas fugacity coefficients are calculated using a cubic model and the activity coefficients are calculated using the Pitzer theory. The equation obtained, that describes the model, is the following:

$$m_i = \frac{P * y_i * \varphi_i}{\gamma_i * K_H(T, P_{ref}) * \exp\left(\frac{\overline{V_{m,i}}(P - P_{ref})}{RT}\right)}$$

where P is the pressure, y_i is the mole fraction in the vapor phase, ϕ_i is the fugacity coefficient in the vapor phase, γ_i is the activity coefficient of component i, $K_H(T,P_{ref})$ is the equilibrium constant at reference state, usually set as 1 atm, $\overline{V_{m,i}}$ is the average partial molar volume and $\frac{\overline{V_{m,i}}(P-P_{ref})}{RT}$ is the poynting factor.

The fugacity coefficients are calculated based on the Peng-Robinson equation of state as described above.

The equilibrium constant for the component i is expressed by the following equation:

$$K_i = K_H(T, P_{ref}) * \exp\left(\frac{\overline{V_{m,i}}(P - P_{ref})}{RT}\right)$$

For H_2O, the following equation is used:

$$K_{H_2O} = (a_1 + a_2T + a_3T^2 + a_4T^3 + a_5T^4)\exp\left(\frac{(P-1)(a_6+a_7T)}{RT}\right).$$

For CO_2, O_2 and N_2, the following equation is used:

$$\log\left(K_H(T, P_{ref})\right) = A_0 + A_1 + \frac{A_2}{T} + A_3 * \log(T) + \frac{A_4}{T^2} + A_5T^2.$$

The average partial molar volume is expressed by the following equation:

$$\overline{V_{m,i}} = 41.84(0.1a_{1,i} + \frac{100a_{2,i}}{2600+P} + \frac{a_{3,i}}{T-288} + \frac{10^4a_{4,i}}{(2600+P)(T-288)} - \omega_i * QBrn).$$

The Born function as presented by Helgeson et al. (1981) is the following:

$$Q = \frac{1}{\varepsilon^o}\left(\frac{\partial ln\varepsilon^o}{\partial P}\right)_T$$

where ε^o denotes the dielectric constant of the solvent-water. The dielectric constant (ε^o=EPS) of water as a function of pressure at constant temperature is described by the following equation suggested by Bradley and Pitzer (1979):

$$EPS = EPS_{1000} + C * \ln\left(\frac{B + P}{B + 1000}\right)$$

where P is the pressure, EPS is the dielectric constant and EPS_{1000} was chosen arbitrarily as a reference value (EPS at 1000 bar). EPS_{1000}, B and C are temperature dependent parameters described by the following equations:

$$EPS_{1000} = U_1 \exp(U_2T + U_3T^2)$$

$$B = U_4 + \frac{U_5}{U_6 + T}$$

$$C = U_7 + \frac{U_8}{T} + U_9 T$$

The activity of component i in the liquid phase is calculated from a virial expansion of excess Gibbs energy proposed by Pitzer (1973) and described by the following equation:

$$\ln \gamma_i = \sum_c 2\lambda_{\mathrm{i}-c}\, m_c + \sum_a 2\lambda_{\mathrm{i}-a}\, m_a + \sum_c \sum_a \zeta_{\mathrm{i}-a-c}\, m_c m_a$$

where λ is a second-order interaction parameter, ζ is a third-order interaction parameter, c means cations and a means anions.

The main factors that affect the dissolution of CO_2 in the water-brine stream are the pressure, the temperature, the salinity and the impurities' content. These factors are studied through the model of Li et al. (2018).

2.2.1 CO_2 solubility as a function of pressure

With increasing pressure, at constant temperature, salinity and impurities' content, the solubility of CO_2 in solution increases. The solubility is more affected by pressure at lower ones. As a result, the pressure effect diminishes with increasing pressure (Hangx, 2005; Esene et al., 2019).

The conditions that are studied, are presented in the following table:

Table 2.1 Conditions studied for the pressure's effect

Temperature (K)	P (bar)	Salinity (mol/kg solvent)
293.15-303.15	1-200	0-1

In the following diagram (see also Appendix A), the relation between the carbon dioxide solubility and the pressure is presented for standard conditions of temperature, salinity and impurities' content.

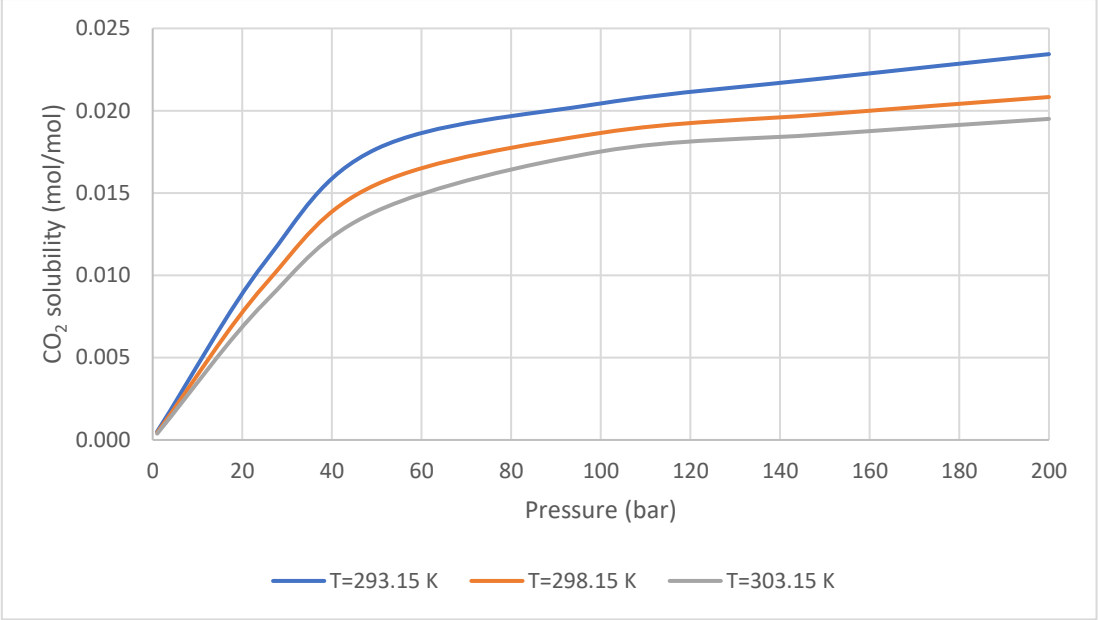

Figure 2.1 CO_2 solubility using Li et al.'s (2018) model for the different temperatures (S=1 mol/kg solvent) as a function of pressure

2.2.2 CO_2 solubility as a function of temperature

The effect of the temperature varies according to the pressure and salinity. In general, with increasing temperature, at temperatures below 100 °C and at constant pressure, salinity and impurities' content, the solubility of CO_2 in solution decreases. Regarding the pressure, the solubility could either decrease or increase over this temperature (Hangx, 2005; Esene et al., 2019).

The conditions that are studied, are presented in the following table:

Table 2.2 Conditions studied for the temperature's effect

Temperature (K)	P (bar)	Salinity (mol/kg solvent)
273.15-473.15	1-300	0-1

In the following diagrams (see also Appendix A), the relation between the carbon dioxide solubility and the temperature is presented for standard conditions of pressure, salinity and impurities' content.

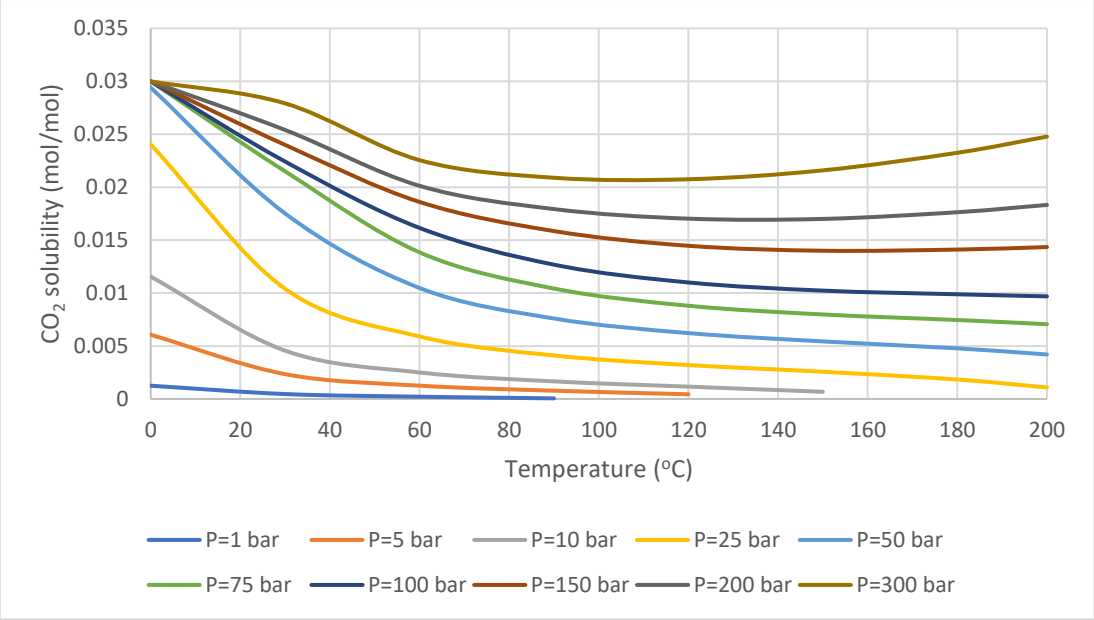

Figure 2.2 CO_2 solubility using Li et al.'s (2018) model for the different pressures (S=0 mol/kg solvent) as a function of temperature

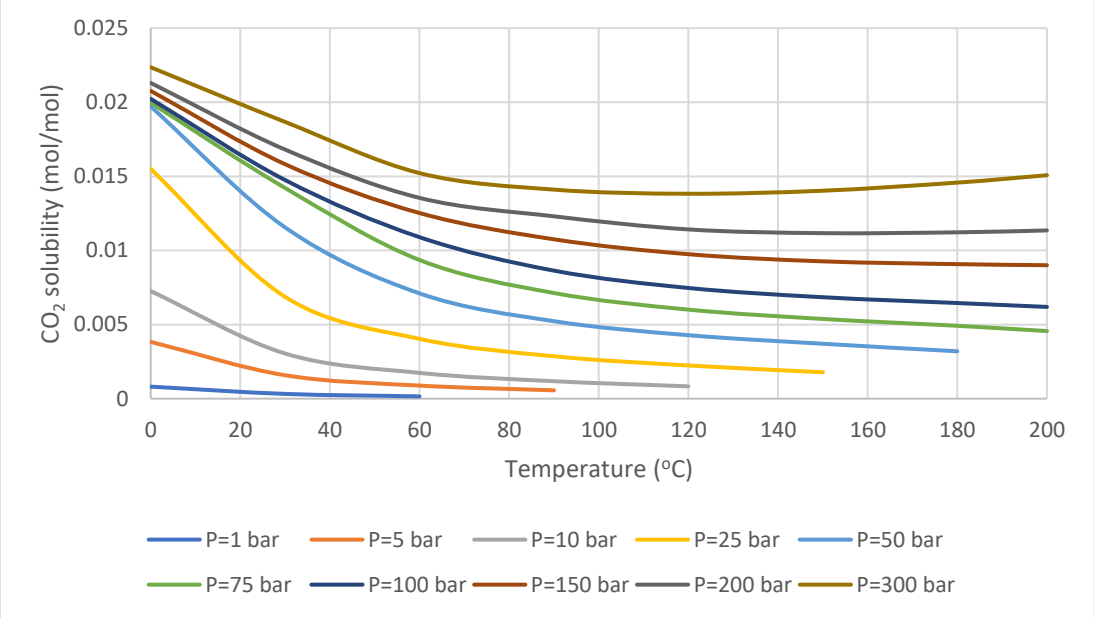

Figure 2.3 CO_2 solubility using Li et al.'s (2018) model for the different pressures (S=1 mol/kg solvent) as a function of temperature

2.2.3 CO_2 solubility as a function of salinity

Salinity is one of the most significant factors that affects the solubility of carbon dioxide in aqueous phases. Sodium chloride and other salts enhance the structuring of aqueous phases and thus the cohesive energy in water due to their strong interactions with water dipoles. As the salt content increases, the partition equilibrium of neutral organic solutes is shifted toward nonaqueous phases (salting-out effect). In a brine formation, except sodium chloride (NaCl), potassium chloride (KCl) and calcium chloride ($CaCl_2$) may be dissolved. Pure sodium chloride is the worst case regarding the lowering of the carbon dioxide's solubility. The hydration action of K^+ is smaller than that of Na^+ and there are more free H_2O molecules interacting with the CO_2 molecules in aqueous KCl solution. The reason for this is that the size

of K^+ is larger than that of Na^+. Furthermore, the molecular weight of NaCl is smaller than that of KCl, therefore there are less ions in the KCl solution. Comparing NaCl and $CaCl_2$, Ca^{2+} has two positive charges, that make the salting-out effect greater. However, the size of Ca^{2+} is close to that of Na^+. Moreover, the molecular weight of $CaCl_2$ is about twice as large as that of NaCl, which means lower salting-out effect. These lead to the conclusion that, the salting-out effect of NaCl is greater than this of KCl and similar to that of $CaCl_2$. This means that mixtures of different salts will be less challenging than pure NaCl, considering that the g/litre concentration is the same (Liu et al., 2011; Boström and Ninham, 2004; Ervik, Westman, Hammer, Skaugen and Lilliestrale, 2012). As a result, all the salts are considered to be NaCl.

The conditions that are studied, are presented in the following table:

Table 2.3 Conditions studied for the salinity's effect

Temperature (K)	P (bar)	Salinity (mol/kg solvent)
293.15-303.15	1-200	0-4

In the following diagram (see also Appendix A), the relation between the carbon dioxide solubility and the salinity is presented for standard conditions of pressure, temperature and impurities' content.

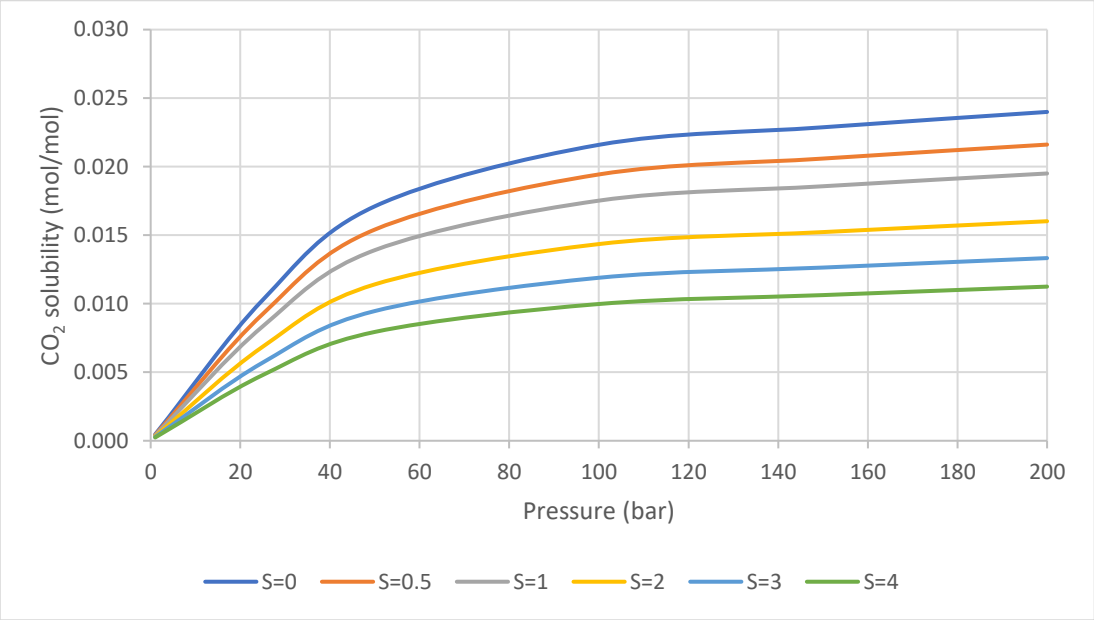

Figure 2.4 CO_2 solubility using Li et al.'s (2018) model for the different salinities (T=303.15 K) as a function of pressure

From these diagrams, it is shown that as the salinity increases and considering that the other conditions remain constant the solubility of carbon dioxide decreases.

2.2.4 CO_2 solubility as a function of impurities' content

Nitrogen and oxygen are considered non-condensable gases which leads to the increase of vapor-liquid saturation pressures and the decrease of the critical temperature, regarding their lower critical ones. As a result, their solubilities are negligible at low pressures. Therefore, when they are mixed with carbon dioxide, they cause a decrease in its solubility in water. Another reason for this, is the decrease in the partial pressure of carbon dioxide due to their presence, since they have lower solubilities in water than it. Thus, the higher the impurities

content in a nitrogen-oxygen-carbon dioxide mixture, the lower is the carbon dioxide partial pressure (Wang, Ryan, Anthony and Wigston, 2011; Nguyen and Ali, 1998).

The effect of oxygen is studied considering the following streams that enter a flash separator. The cases of 100, 500, 1000, 5000 and 10000 ppm are studied.

The conditions that are studied, are presented in the following table:

Table 2.4 Conditions studied for the O_2 content's effect

Temperature (K)	P (bar)	Salinity (mol/kg solvent)
293.15-303.15	1-200	0-1

In the following diagrams, the relation between the carbon dioxide solubility and the O_2's content is presented for standard conditions of pressure, temperature and salinity.

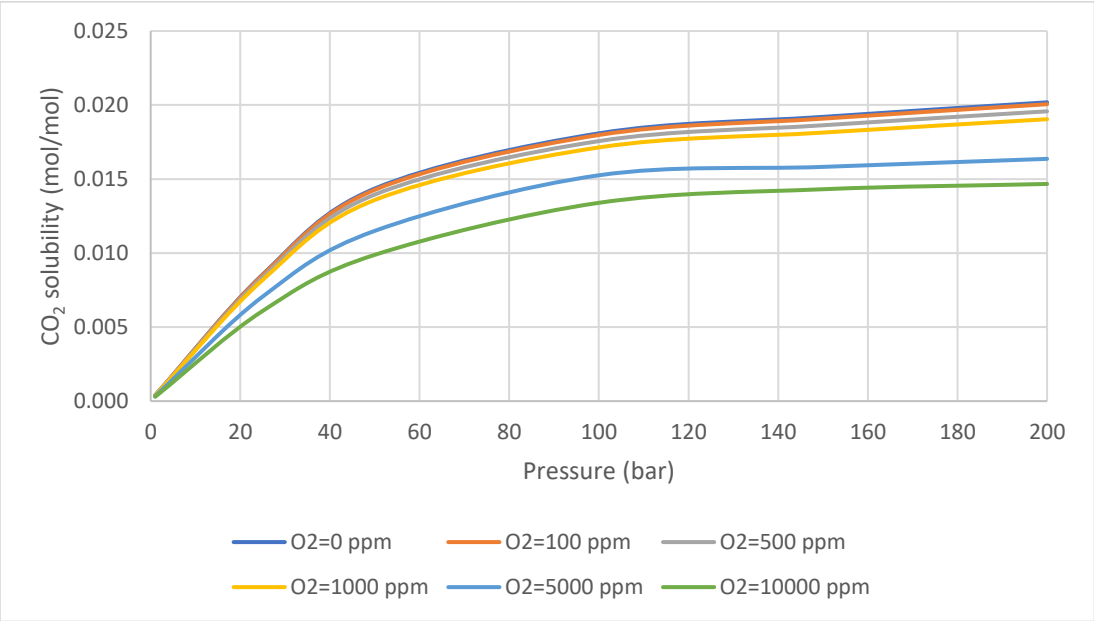

Figure 2.5 CO_2 solubility using Li et al.'s (2018) model for the different O_2's contents (T=303.15 K and S=1 mol/ kg solvent) as a function of pressure

From these diagrams, it is validated that as the oxygen's content increases and considering that the other conditions remain constant the solubility of carbon dioxide decreases.

The effect of nitrogen is studied considering the following streams that enter a flash separator. The cases of 500, 1000, 5000, 10000 and 50000 ppm are studied.

The conditions that are studied, are presented in the following table:

Table 2.5 Conditions studied for the N_2 content's effect

Temperature (K)	P (bar)	Salinity (mol/kg solvent)
293.15-303.15	1-200	0-1

In the following diagrams, the relation between the carbon dioxide solubility and the N_2's content is presented for standard conditions of pressure, temperature and salinity.

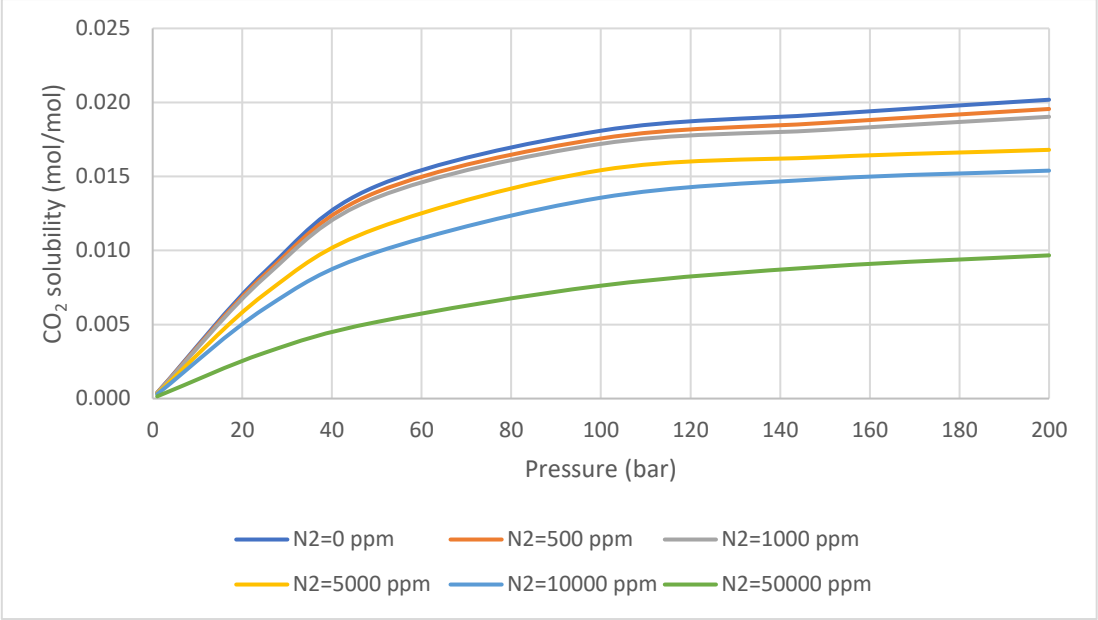

Figure 2.6 CO_2 solubility using Li et al.'s (2018) model for the different N_2's contents (T=303.15 K and S=1 mol/kg solvent) as a function of pressure

From these diagrams, it is validated that as the nitrogen's content increases and considering that the other conditions remain constant the solubility of carbon dioxide decreases. From Figure 2.5 and Figure 2.6, it is observed that for the same concentration, the effect of N_2 is like that of O_2. In higher concentrations the effect of O_2 is a little bit greater.

The effect of the simultaneous presence of oxygen and nitrogen is studied considering the following streams that enter a flash separator.

The conditions that are studied, are presented in the following table:

Table 2.6 Conditions studied for the impurities content's effect

Temperature (K)	P (bar)	Salinity (mol/kg solvent)
293.15-303.15	1-200	0-1

In the following diagrams, the relation between the carbon dioxide solubility and the impurities' content is presented for standard conditions of pressure, temperature and salinity.

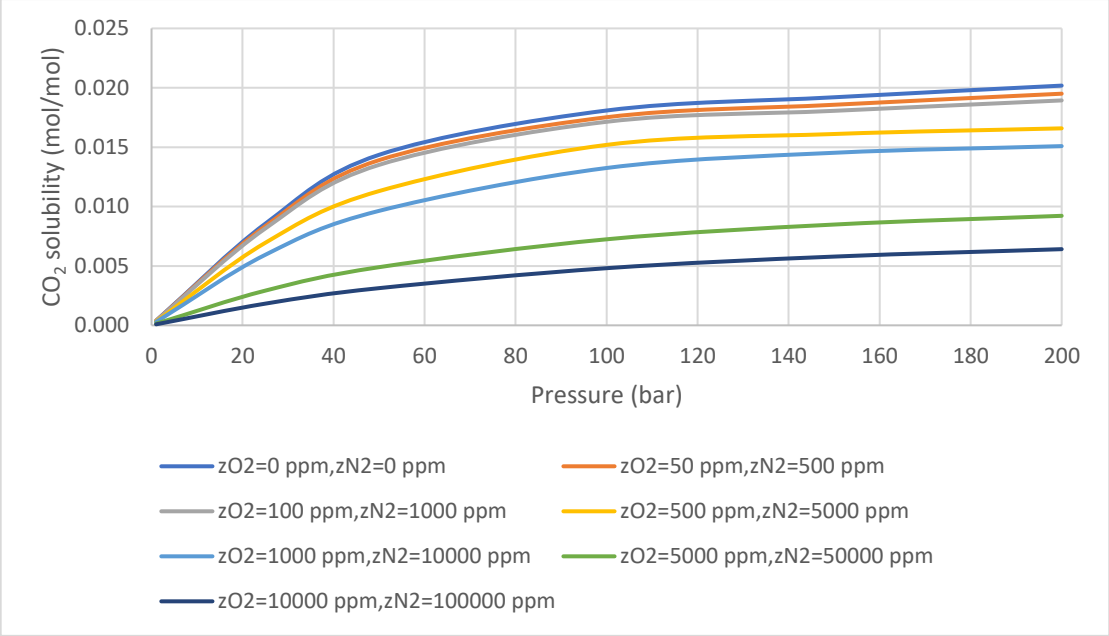

Figure 2.7 CO_2 solubility using Li et al.'s (2018) model for the different impurities' content (T=303.15 K and S=1 mol/kg solvent) as a function of pressure

From these diagrams, it is validated that as the oxygen and nitrogen's contents increase and considering that the other conditions remain constant the solubility of carbon dioxide decreases.

3 CO_2 solubility data and model comparisons

3.1 Solubility Data

The review of solubility data of CO_2 is carried out. In the following table the studies of CO_2 solubility in pure water and in aqueous NaCl solutions, that are studied in this work, are presented. The covered ranges of temperature, pressure and salinity are also presented.

Table 3.1 CO_2 solubility data

Generated data	**Temperature (K)**	**Pressure (bar)**	**Salinity (m)**
Duan and Sun (2003)	273.15-483.15	1-1000	0-4
Experimental data	**Temperature (K)**	**Pressure (bar)**	**Salinity (m)**
Takenouchi and Kennedy (1965)	423.15	100-1000	4.2779
Rumpf et al. (1994)	313.254-433.065	6.02-92.01	5.999
Yan et al. (2011)	323.2-413.2	50-400	5
Bando et al. (2003)	303.15-333.15	100-200	0.1711-0.5292
King et al. (1992)	288.15-298.15	60.8-243.2	0
Wiebe and Gaddy (1940)	285.15-313.15	25.3313-506.625	0

The work of Duan and Sun (2003) is the most extensive study of CO_2 solubilities in pure water and in brines. The data sets of Takenouchi and Kennedy (1965); Rumpf et al. (1994); and Yan et al. (2011) cover the higher ionic strengths, while those of King et al. (1992); and Wiebe and Gaddy (1940) are some of the most comprehensive at low temperatures. The data set of Bando et al. (2003) is one of the most trustworthy close to the sea water's salinity and that of the application that is going to be studied.

For the study of the behavior of the model of Li et al. (2018), the data sets of O_2 and N_2 solubilities that are used, are presented in the following table. The covered ranges of temperature, pressure and salinity are also presented.

Table 3.2 O_2 and N_2 solubility data

Generated data	**Temperature (K)**	**Pressure (bar)**	**Salinity (m)**
Geng and Duan (2010)	273-603	1-1000	0
	273-513	1-400	1-4
Mao and Duan (2006)	273.15-573.15	1-600	0
	273.15-473.15	1-600	2-6
Experimental data	**Temperature (K)**	**Pressure (bar)**	**Salinity (m)**
Liu et al. (2012)	308.15-318.15	80-160	0
	308.15	80	0.9

The generated data of Geng and Duan (2010); and Mao and Duan (2006) are considered to be the most thorough for the solubilities of O_2 and N_2 respectively. In the work of Liu et al. (2012) the solubility of a N_2+CO_2 mixture in water at different pressures, temperatures and salinities is determined.

3.2 Results and discussion

The main disadvantage of the models of Duan (Duan and Sun, 2003; and Duan et al., 2006) is that they are only able to calculate the CO_2 solubility in the liquid phase of the CO_2-water-NaCl system. They are not able to calculate the fugacities of CO_2 in the liquid phase and these of water-NaCl brine in both phases (vapor-liquid). This is a very important fact, since they are needed for the process simulations, when implementing a model through CAPE-OPEN. This leads to the creation of a new model, the equilibrium model (see Chapter 4), which is able to predict the fugacities of both components (CO_2 and H_2O), in both the liquid and the vapor phase.

The behavior of the model of Li et al. (2018) is studied in the conditions of the carbonated water injection. The temperature range is 293.15-303.15K, the pressure range is 1-200 bar and the salinity range is 0-1 mol/kg solvent. The errors in each component's solubility for each experimental or generated point are presented. The model was compared both to binary and ternary systems.

The main advantage of Li et al.'s (2018) model is that it includes the effect of O_2 and N_2 on the CO_2 solubility. It is also able to predict in a very good way the solubilities of O_2 and N_2 in both binary and ternary systems, as it can be observed from the following figures and tables (see also Appendix B). On the other hand, as it is also noticed its main disadvantage is that it underestimates the solubility of CO_2.

Table 3.3 Errors % in O_2 solubility in binary system: Model of Li et al. (2018)

O_2 solubility (mol/kg solvent)					
Salinity (mol/kg solvent)	T(K)	P(bar)	Model of Li et al. (2018)	Geng and Duan (2010)	% error
1	303	10	0.01949	0.02072	5.92
		50	0.03784	0.04035	6.20
		100	0.07151	0.07572	5.55
		200	0.12967	0.13358	2.93
Average (%) error					**5.03**

Table 3.4 Errors % in N_2 solubility in binary system: Model of Li et al. (2018)

N_2 solubility (mol/kg solvent)					
Salinity (mol/kg solvent)	T(K)	P(bar)	Model of Li et al. (2018)	Mao and Duan (2006)	% error
0	303.15	50	0.02879	0.02787	3.27
		100	0.05393	0.05173	4.25
		150	0.07628	0.07239	5.38
		200	0.09650	0.09056	6.55
Average (%) error					**4.86**

Table 3.5 Errors % in CO_2 solubility in binary system: Model of Li et al. (2018)

CO_2 solubility (mol/kg solvent)					
Salinity (mol/kg solvent)	T(K)	P(bar)	Model of Li et al. (2018)	Duan and Sun (2003)	% error
1	303.15	10	0.21010	0.22940	8.41

		50	0.79400	0.87290	9.04
		100	0.99783	1.09580	8.94
		200	1.11697	1.19900	6.84
Average (%) error					**8.31**

Table 3.6 Errors % in CO_2 solubility in ternary system: Model of Li et al. (2018)

CO_2 solubility (mol/mol) in the ternary system (CO_2-N_2-H_2O)					
Salinity (mol/kg solvent)	T(K)	P(bar)	Model of Li et al. (2018)	Liu et al. (2012)	%error
0	308.15	80	0.01777	0.01980	10.27
			0.01708	0.01910	10.57
			0.01592	0.01740	8.49
			0.01323	0.01500	11.79
			0.01012	0.01100	8.00
Average (%) error					**9.82**

Table 3.7 Errors % in N_2 solubility in ternary system: Model of Li et al. (2018)

N_2 solubility (mol/mol) in the ternary system (CO_2-N_2-H_2O)					
Salinity (mol/kg solvent)	T(K)	P(bar)	Model of Li et al. (2018)	Liu et al. (2012)	% error
0	308.15	80	0.00012	0.00012	0.63
			0.00015	0.00014	9.68
			0.00020	0.00022	8.82
			0.00031	0.00032	2.37
			0.00043	0.00043	0.39
Average (%) error					**4.38**

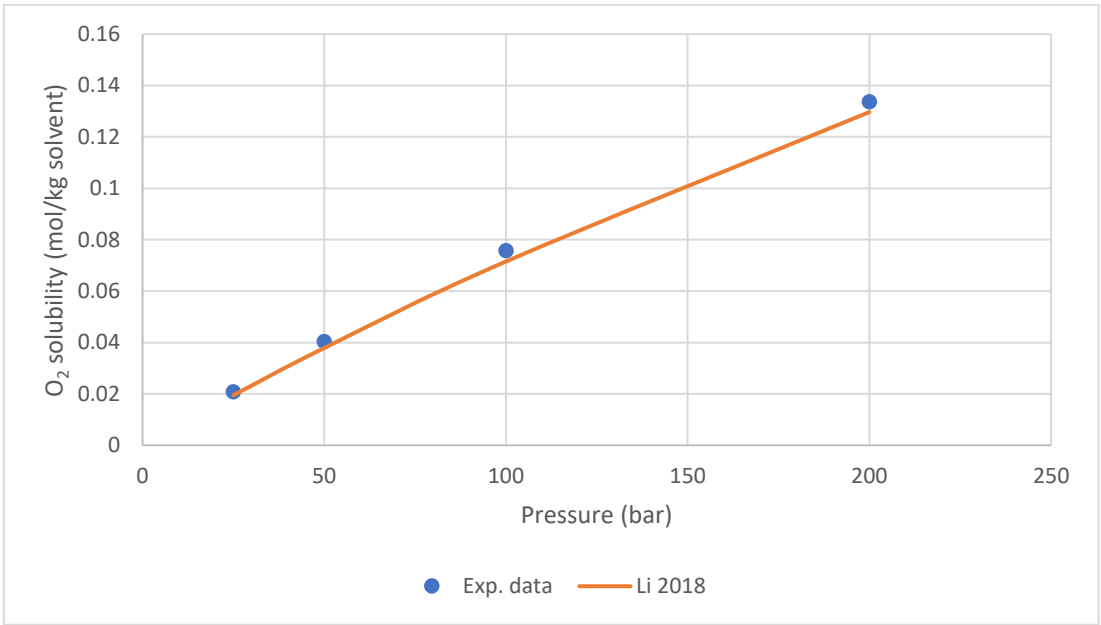

Figure 3.1 Comparison of Li et al. (2018) model's predictions with the generated data of Geng and Duan (2010) (T=303 K, S=1 molality) as a function of pressure

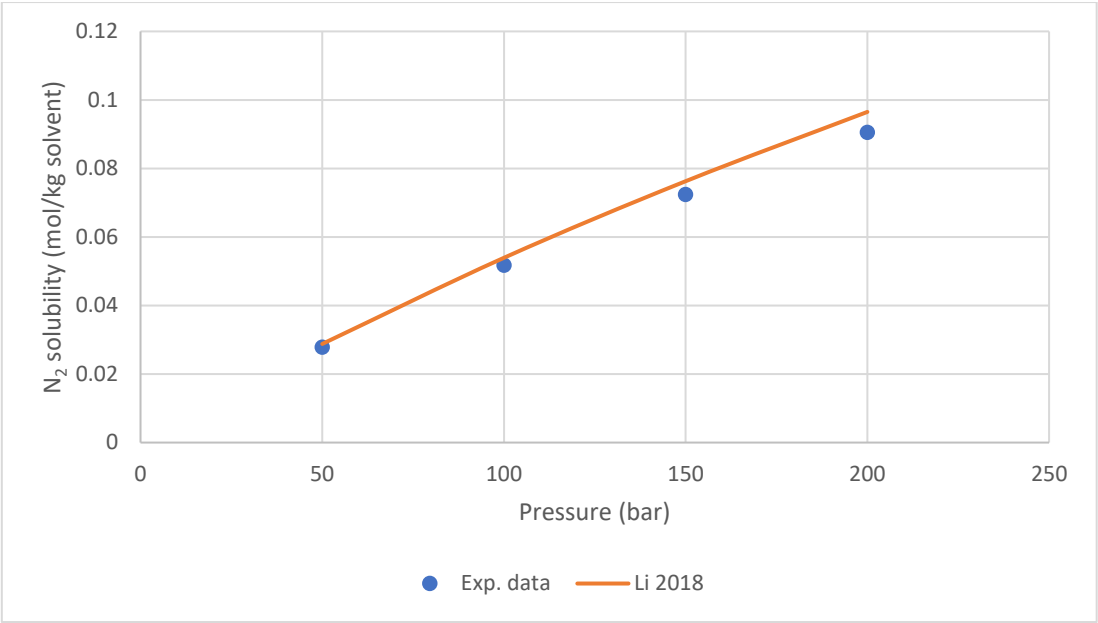

Figure 3.2 Comparison of Li et al. (2018) model's predictions with the generated data of Mao and Duan (2006) (T=303.15 K, S=0 molality) as a function of pressure

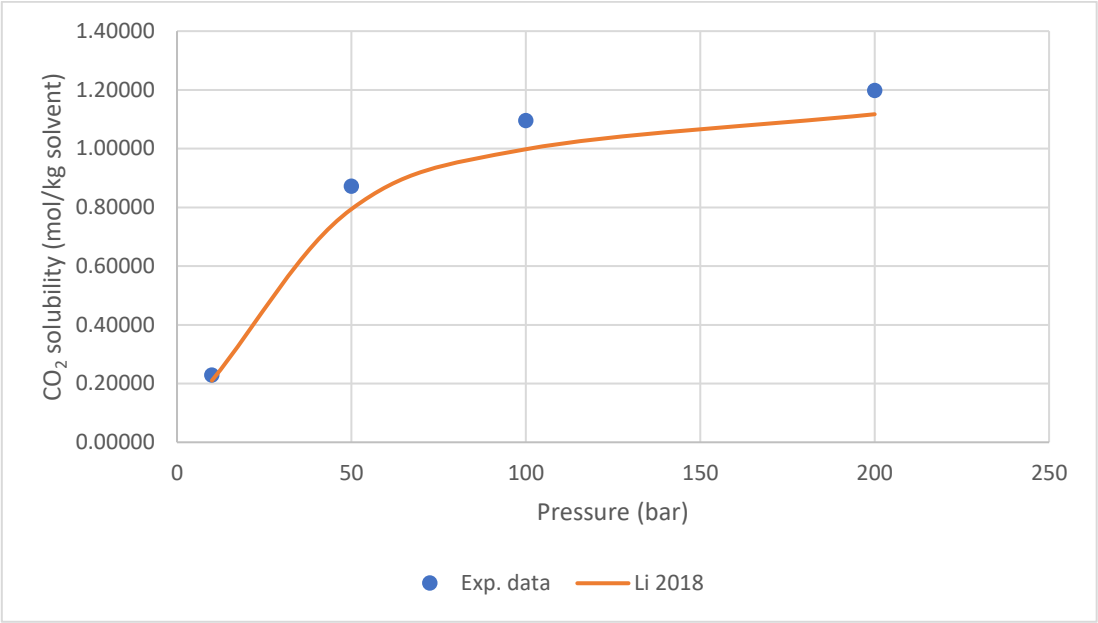

Figure 3.3 Comparison of Li et al. (2018) model's predictions with the generated data of Duan and Sun (2003) (T=303.15 K, S=1 molality) as a function of pressure

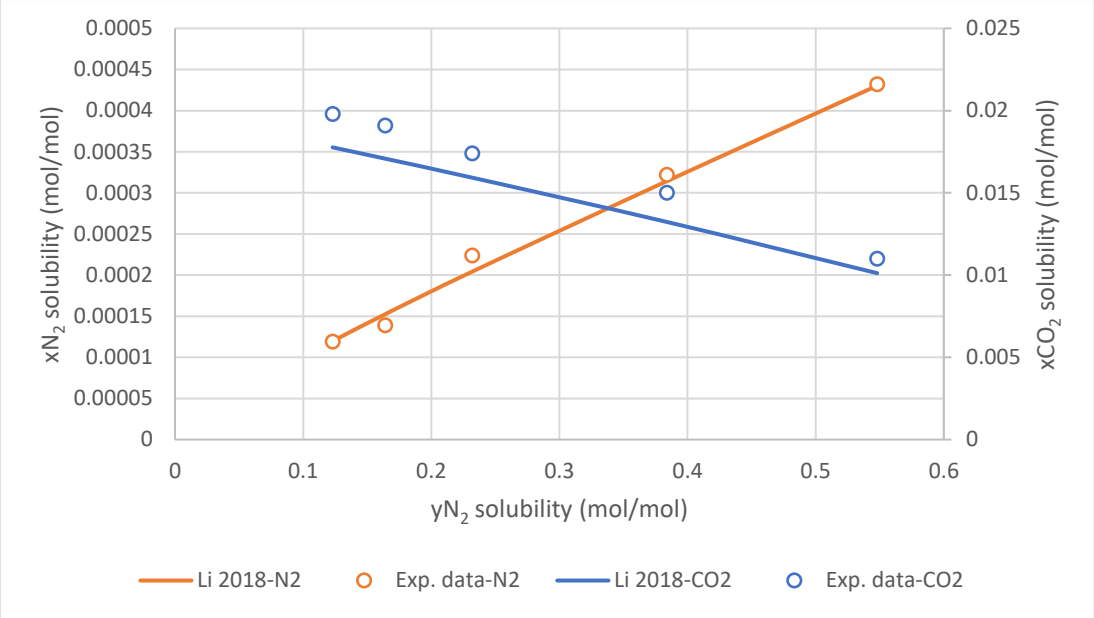

Figure 3.4 Comparison of Li et al. (2018) model's predictions with the experimental data of Liu et al. (2012) (T=308.15 K, P=80 bar, S=0 molality) as a function of pressure

4 Development of Thermodynamic Model

4.1 The equilibrium model

In this work, the equilibrium model is proposed. This model is based on the methodology followed by Pappa (2019, pers. comm., 1 October). The basic idea is the calculation of CO_2 solubility via the equality of fugacities of CO_2 and water in the vapor and liquid phase.

The vapor phase is described by the equation of state t-mPeng-Robinson:

$$P = \frac{RT}{V + t - b} - \frac{\alpha_c a(T)}{(V + t)(V + t + b) + b(V + t - b)}$$

where P is the pressure, T is the temperature, V is the volume, t is the translation factor correcting the volume in a cubic EoS, b is the EoS covolume parameter and α is the EoS attractive term (cohesion) parameter.

The expressions for the calculation of its parameter values are:

$$a=[1 + m(1 - \sqrt{T_r})]^2$$

$$m=0.384401+1.52276\omega-0.213808\omega^2+0.034616\omega^3-0.001976\omega^4$$

$$t=t_o+(t_c-t_o)\exp(\beta|1 - T_r|)$$

$$t_o=\frac{RT_c}{P_c}(-0.014471+0.067498\omega-0.084852\omega^2+0.067298\omega^3-0.017366\omega^4)$$

$$\beta=-10.2447-28.6312\omega$$

$$t_c=\frac{RT_c}{P_c}(0.3074 - Z_c)$$

The EoS has a cubic form with respect to the compressibility factor as follows:

$$Z^3-(1-B)Z^2+(A-3B^2-2B)Z-(AB-B^2-B^3)=0$$

where:

$$Z=\frac{PV}{RT}\ ;\ A=\frac{aP}{R^2T^2}\ ;\ B=\frac{bP}{RT}$$

For the calculation of the critical compressibility factor Z_c the following expression has been assumed (Czerwienski et al., 1988):

$$Z_c=0.289-0.0701\omega-0.0207\omega^2$$

For the calculation of the parameters a_m, b_m and the translation factor t_m of the t-mPR EoS for binary mixtures, the following mixing rules have been assumed:

- for the a_m parameter:

$$a_m = x_1^2 a_1 + x_2^2 a_2 + 2x_1 x_2 a_{12}$$

where a_1 and a_2 are the pure component "energy parameters" of the t-mPR EoS and a_{12} is defined through the following expression:

$$a_{12} = \sqrt{a_1 a_2}(1 - k_{12})$$

where k_{12} is the binary interaction coefficient ($k_{H_2O-CO_2}$=0.2);

- for the b_m parameter the following linear expression is used:

$$b_m=x_1b_1+x_2b_2$$

A similar linear expression is also used for the translation factor of the binary mixture, t_m:

$$t_m=x_1t_1+x_2t_2$$

The fugacity coefficients of CO_2 and H_2O in the vapor phase are calculated by the following equation:

$$\ln\widehat{\varphi_i}=\frac{B_i}{B}(z-1)-\ln(z-B)-\frac{A}{2B\sqrt{2}}\left(\frac{2\sum x_iA_{ij}}{A}-\frac{B_i}{B}\right)\ln\left(\frac{z+2.414B}{z-0.414B}\right)$$

The fugacities of each component are calculated by the following equation:

$$f_i^v=y_iP\phi_i$$

The asymmetric convention is used for the aqueous phase. The fugacity of CO_2 ($f_{CO_2}^l$) in the liquid phase is described by the Henry Law:

$$f_{CO_2}^l = x_{CO_2}H_{CO_2}$$

where x_{CO_2} is the mole fraction of CO_2 in the liquid phase and H_{CO_2} is the Henry's constant of CO_2 in the liquid phase.

The fugacity of H_2O (f_w^l) in the liquid phase is described as presented by Prausnitz, Lichtenthaler, and Azevedo (1999):

$$f_w^l = x_w\varphi_w^{sat}P_w^{sat}exp\left[\int_{P_w^{sat}}^{P}\frac{V_w}{RT}dp\right]$$

where x_w is the mole fraction of H_2O in the liquid phase, φ_w^{sat} and P_w^{sat} is the fugacity coefficient and the vapor pressure of saturated water in the temperature of the mixture respectively and V_w is the molar volume of pure water.

The fugacity coefficient of saturated water is calculated from the following equation (Canjar and Manning, 1967):

$$\begin{aligned}\varphi_w^{sat} &= 0.9958 + 9.68330\cdot10^{-5}\,T' - 6{,}17050\cdot10^{-7}\,T'^2 \\ &\quad -3.08333\cdot10^{-10}\,T'^3 && T' > 90 \\ \varphi_w^{sat} &= 1 && T' \le 90\end{aligned}$$

where *T'* is the temperature in F.

Both the vapor pressure of saturated water and the molar volume of pure water is calculated from the DIPPR equations:

$$P_w^{sat} = \exp\left((7.3649E{+}1) - \frac{7.2582E{+}3}{T} - 7.3037\ln(T) + (4.1653E{-}6)T^2\right)$$

$$V_w = \frac{1}{Liquid\ Density} = \frac{0.26214^{\left(1+\left(1-\frac{T}{647.29}\right)^{0.23072}\right)}}{4.6137}$$

where P_w^{sat} is in Pa and V_w is in lit/mol.

The dependence of Henry's constant (H_{CO_2}) from pressure and temperature is expressed through the Henry's reference constant ($H^*_{CO_2}$) and the molar volume of CO_2 in infinite dilution ($\bar{v}^{\infty}_{CO_2}$) by the equation:

$$\ln H_{CO_2} = \ln H^*_{CO_2} + \frac{\bar{v}^{\infty}_{CO_2} P}{RT}$$

In this master thesis, Henry's reference constant ($H^*_{CO_2}$) and molar volume of CO_2 in infinite dilution ($\bar{v}^{\infty}_{CO_2}$) are expressed as a function of temperature and salinity through correlation of their values to solubility data of CO_2 in pure water and NaCl solutions. The aforementioned values are calculated by minimizing the error in the calculated bubble point pressure.

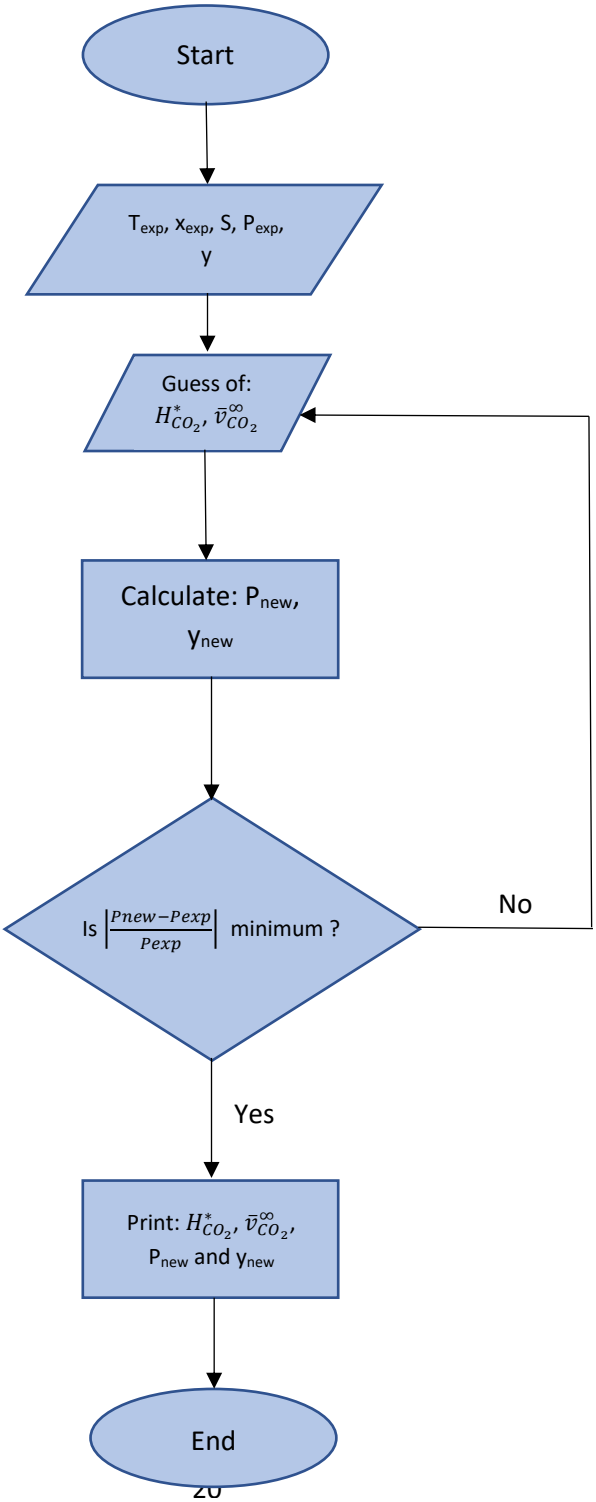

Figure 4.1 Algorithm Flowchart

The data used for the model development are presented in Table 3.1.

The expressions that occurred for $H^*_{CO_2}$ and $\bar{v}^{\infty}_{CO_2}$ are the following:

$$\boldsymbol{H^*_{CO_2}} = a_1 + a_2 * \mathbf{T} + a_3 * \mathbf{T^2} + a_4 * \mathbf{T^3} + a_5 * \mathbf{S} * \mathbf{T} + a_6 * \mathbf{S} * \mathbf{T^2} + a_7 * \mathbf{S} * \mathbf{T^3} + a_8 * \mathbf{T} * \mathbf{S^3} + a_9 * \mathbf{T} * \mathbf{ln(T)} + a_{10} * \mathbf{T} * \mathbf{exp(S)} + a_{11} * \mathbf{T} * \mathbf{S} * \mathbf{exp(S)} + a_{12} * \mathbf{exp(S)} * \mathbf{ln(T)}$$

$$\boldsymbol{\bar{v}^{\infty}_{CO_2}} = A_1 + A_2 * \mathbf{S} + A_3 * \mathbf{S^2} + A_4 * \mathbf{T} + A_5 * \mathbf{T^3} + A_6 * \mathbf{S} * \mathbf{T} + A_7 * \mathbf{S} * \mathbf{T^2} + A_8 * \mathbf{T} * \mathbf{S^2} + A_9 * \mathbf{S^2} * \mathbf{T^2}$$

where $H^*_{CO_2}$ in (bar), $\bar{v}^{\infty}_{CO_2}$ in (lt/mol), salinity (S) in (mol/kg solvent) and temperature (T) in (K).

The parameters that are used for the calculation of $H^*_{CO_2}$ and $\bar{v}^{\infty}_{CO_2}$ are presented respectively in the following tables.

Table 4.1 Parameters a_1-a_{12} for the calculation of $H^*_{CO_2}$

i	a_i
1	$54770361801.0975*10^{-5}$
2	$-23782444042.4155*10^{-6}$
3	$-10866865456.1957*10^{-9}$
4	$42624141064.4264*10^{-13}$
5	$-18605714199.0893*10^{-9}$
6	$1049242847.7532*10^{-10}$
7	$-12426802122.3715*10^{-14}$
8	$1922432361.7885*10^{-10}$
9	$43549173790.2085*10^{-7}$
10	$-48671104232.7079*10^{-11}$
11	$59301387182.4553*10^{-12}$
12	$1386735379.8785*10^{-9}$

Table 4.2 Parameters A_1-A_9 for the calculation of $\bar{v}^{\infty}_{CO_2}$

i	A_i
1	$-15975149997.2988 * 10^{-12}$
2	$10183185592.6854 * 10^{-12}$
3	$-19288680834.5857*10^{-13}$
4	$1807516897.8622*10^{-13}$
5	$-3535100035.0961 * 10^{-19}$
6	$-78753819193.9352 * 10^{-15}$
7	$14283081009.5592 * 10^{-17}$
8	$12345078510.2997*10^{-15}$
9	$-22005328591.0771 * 10^{-18}$

These expressions occurred after many tries and the conception of the more complicated terms was based on the graphical observation of the values of $H^*_{CO_2}$ as a function of temperature and salinity.

4.2 Results and discussion

In Appendix C, the errors in CO_2 solubility for each experimental point are presented. It is observed that both the Duan et al. (2006) and the equilibrium model give similar results. Based on the performance of the models in the data of Rumpf et al. (1994), it is noticed that the new

model has an advantage over the model of Duan et al. (2006) at salinities higher than 4 molality. As we can see from Appendix C, the experimental data of Takenouchi and Kennedy (1965) for S=4.2779 are not described well by both models. From the indicative figure 4.5, it is observed that the experimental data of Yan et al. (2011) don't follow a trend, so we are uncertain about their validity.

In the indicative figures 4.2-4.6 (see also Appendix C), the graphical comparison between the equilibrium model and the model of Duan et al. (2006) is presented.

Due to the fact that the inclusion of the impurities' effect on the CO_2 solubility is considered of first priority, from this point on, the model of Li et al. (2018) is used for the extraction of the rest of the results.

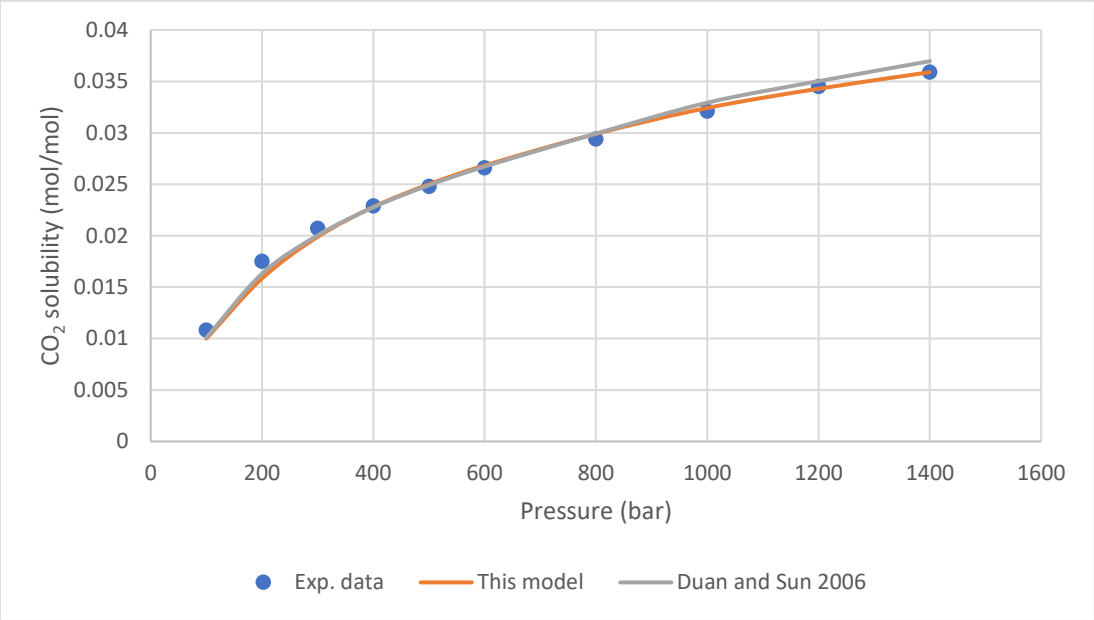

Figure 4.2 Comparison of models' predictions with the experimental data of Takenouchi and Kennedy (1965) (T=423.15 K, S=1.0922 molality) as a function of pressure

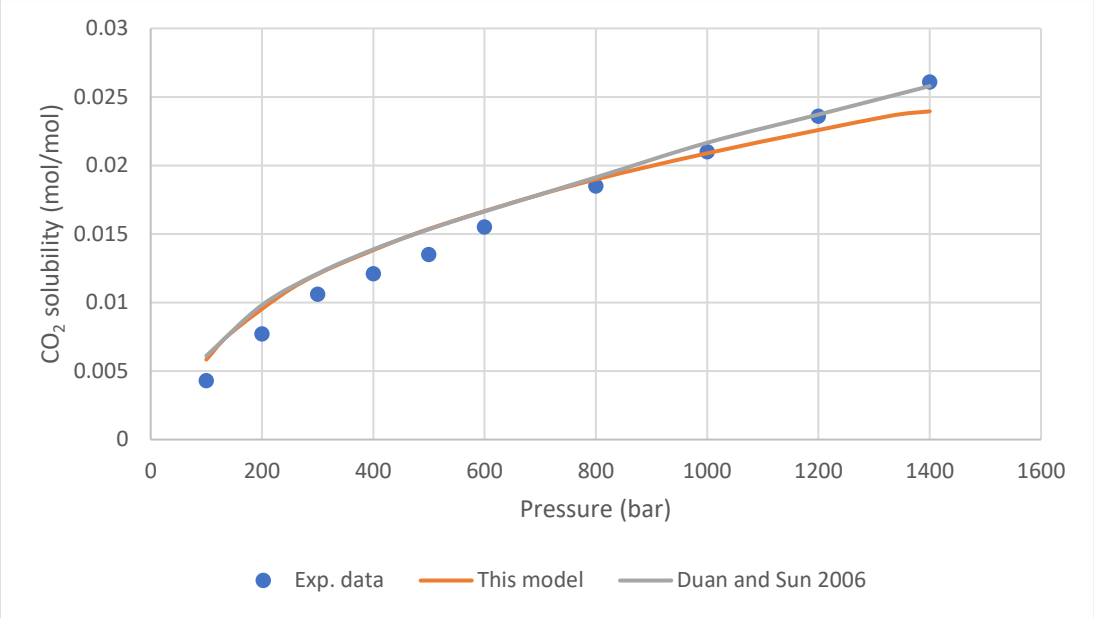

Figure 4.3 Comparison of models' predictions with the experimental data of Takenouchi and Kennedy (1965) (T=423.15 K, S=4.2779 molality) as a function of pressure

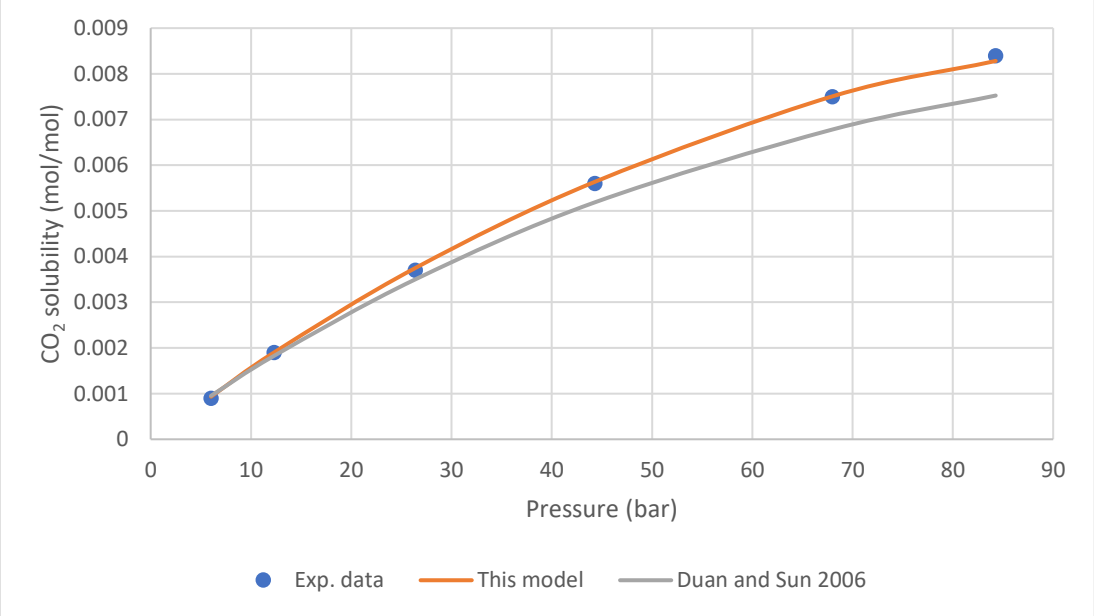

Figure 4.4 Comparison of models' predictions with the experimental data of Rumpf et al. (1994) (T=313.25 K, S=5.999 molality) as a function of pressure

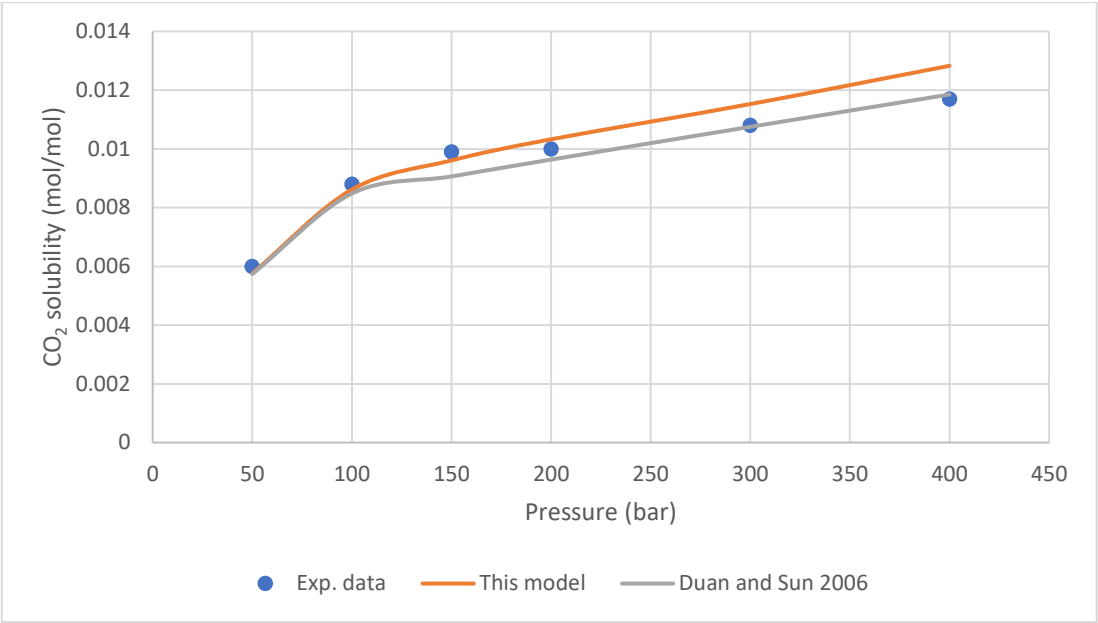

Figure 4.5 Comparison of models' predictions with the experimental data of Yan et al. (2011) (T=323.2 K, S=5 molality) as a function of pressure

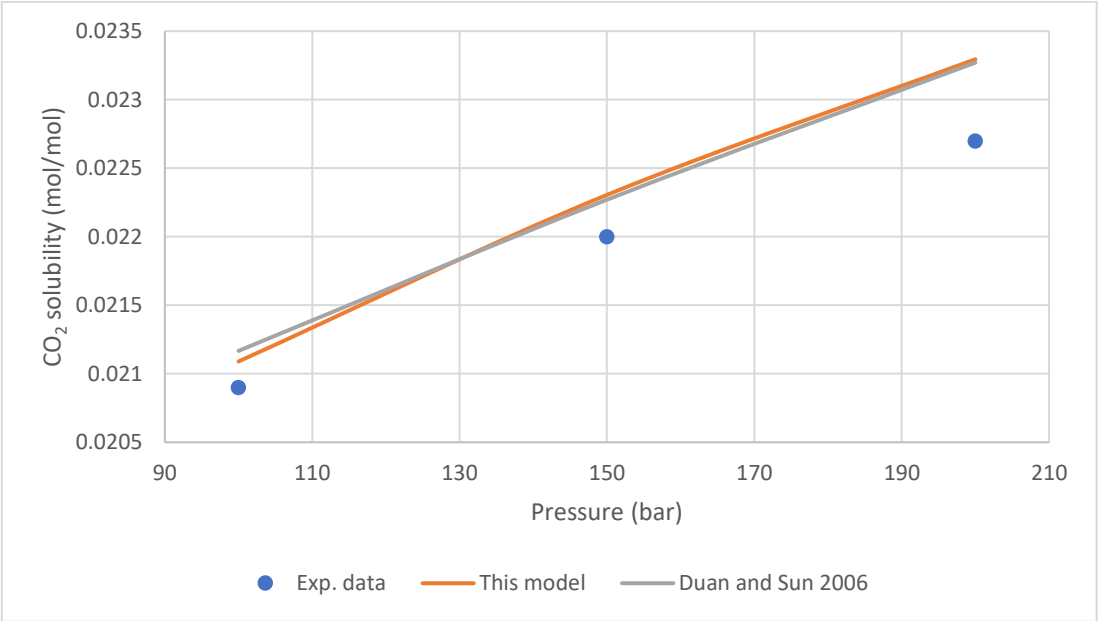

Figure 4.6 Comparison of models' predictions with the experimental data of Bando et al. (2003) (T=303.15 K, S=0.5292 molality) as a function of pressure

5 Model implementation in Unisim

As it is also mentioned in Chapter 2, the standard equations of state cannot be used for the thermodynamic description of the O_2-N_2-CO_2-H_2O-NaCl brines system. The main reasons for that is that they can neither describe the hydrogen bonding that characterizes the equilibrium nor the effect of polar molecules, like the inorganic salts (NaCl) that are present. As a result, it is necessary that the model of Li et al. (2018) is implemented in Unisim via CAPE-OPEN.

5.1 Unisim

Unisim is an intuitive process modeling software that is used for the creation of steady-state and dynamic models for plant design, performance monitoring, troubleshooting, business planning and asset management. In this work, the version R460.1 is used.

5.2 CAPE-OPEN

For the implementation of the thermodynamic model in Unisim, as mentioned above, CAPE-OPEN is used. It is a free available set of standards for communication between chemical engineering software components. There are many facets to the CAPE-OPEN standards, but the most important ones focus on thermodynamics and unit operations.

An application can access thermodynamics that are implemented and served by third party software, by using the CAPE-OPEN thermodynamic standards. Similarly, flowsheet simulation environments can use unit operations served and implemented by third party software via the CAPE-OPEN Unit Operation interfaces (Van Baten, 2020).

5.3 NeqSim

NeqSim (Non-Equilibrium Simulator) was developed by Even Solbraa at the Department of Refrigeration and Air Conditioning, NTNU (NeqSim, 2020). It is a library for estimation of fluid behavior for oil and gas production. It can also be used as a stand-alone tool via Excel or a web interface. It can easily be integrated in computer programs via available interfaces in Java, Python, .NET and Matlab. The basis for NeqSim is fundamental mathematical models related to phase behavior and physical properties of oil and gas.

In this master thesis, the model of Li et al. (2018) is written in Java code (see Appendix D) and then, by creating a dynamic link library (DLL) in Visual Studio 2019 written in C++, the model is imported in NeqSim Excel.

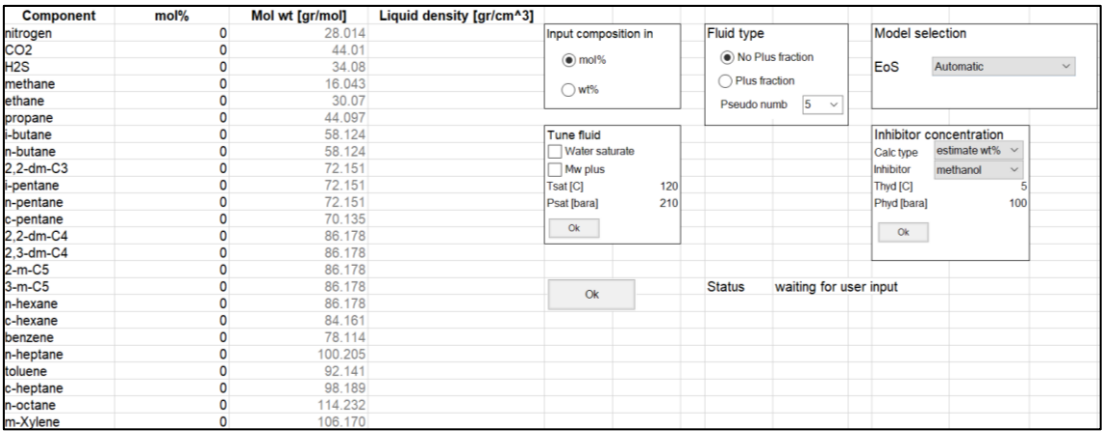

Figure 5.1 Creation of fluid-NeqSim Excel

For the creation of the fluid, the following steps are followed:

1. Go to ‘fluid’ tab
2. Select the mol% composition of the fluid
3. Select in the ‘Model selection’ the model of Li et al. 2018
4. Press ‘Ok’

After creating the fluid, the tab ‘Startup’ is selected and then the Import/Export button is selected. The user, finally, saves the fluid, which is ready for use. NeqSim Excel is linked to Unisim via the CAPE-OPEN option in the fluid packages.

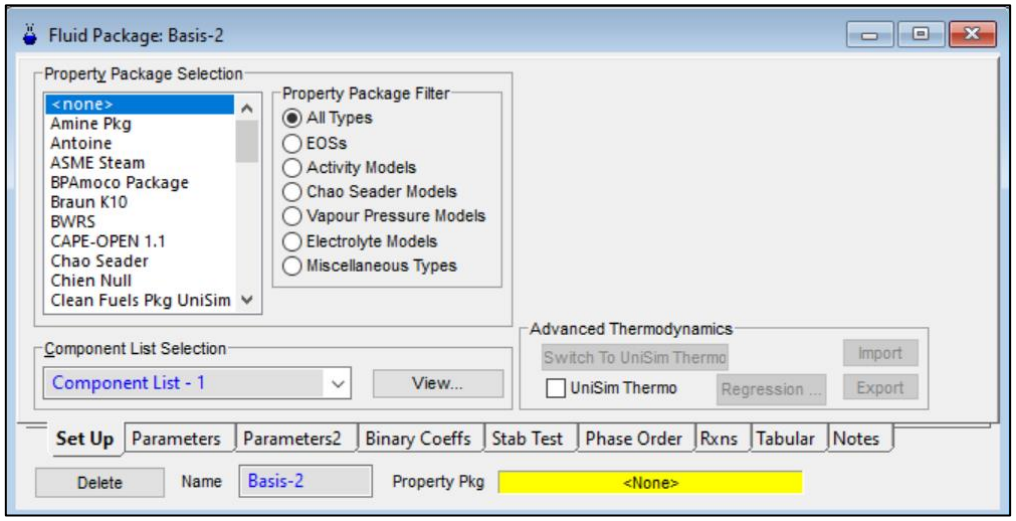

Figure 5.2 CAPE-OPEN option in Unisim

After selecting CAPE-OPEN 1.1, the created fluid is selected. CAPE-OPEN 1.1 is used for both the liquid and the vapor phase. For the liquid phase, the eThermoFlash option is chosen and the extended PropPkg Setup.

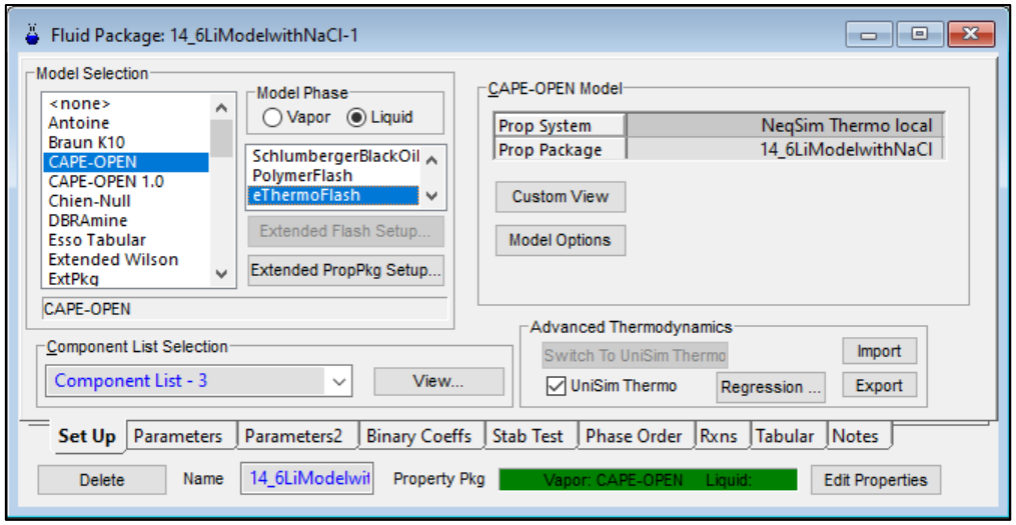

Figure 5.3 Options: eThermoFlash-Extended PropPkg Setup

5.4 Thermodynamic Model used in Unisim

It is very important to be clarified that a model, in order to be implemented in Unisim through CAPE-OPEN, must provide the properties presented in the following figure.

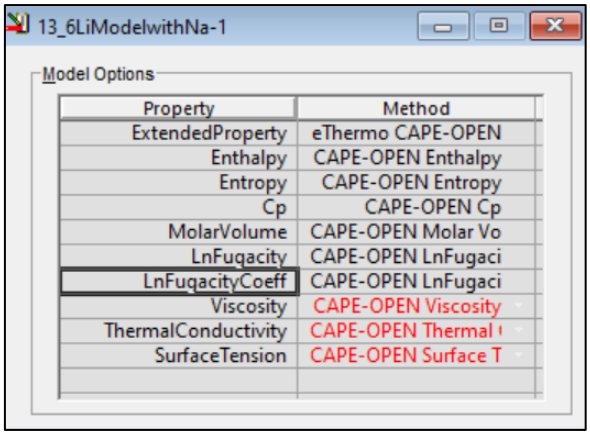

Figure 5.4 Properties provided by implemented model

Since, the model of Li et al. (2018) is only used for the calculation of the CO_2 solubility in a flash separator, all these properties except LnFugacity and LnFugacityCoeff, are calculated by default expressions. The way of calculating the fugacity-fugacity coefficients through the Li et al. 2018 model is presented in Appendix E.

The model of Li et al. (2018) is not able to calculate the thermodynamic properties of the fluid, such as the heat capacity, liquid density and others. In order to run the simulation and be able to calculate the different variables, like the compression, cooling and pumping duties, a more complete model should be used. Therefore, the comparison between the model of Li et al. and some already existing models, such as Peng-Robinson and Soave-Redlich-Kwong, is made.

The comparison lies on the results of the CO_2 solubilities that are produced in a flash separator. The first stream that enters the flash and is studied, is the following:

Table 5.1 Composition of stream 1 for the comparison of Li et al. (2018) model with Peng-Robinson and Soave-Redlich-Kwong

	Composition (mol/mol)
H_2O	0.25
CO_2	0.25
N_2	0.25
O_2	0.25

The results, concerning the CO_2 solubility, are presented in the respective tables (Appendix F):

The second stream that enters the flash and is studied, is the following:

Table 5.2 Composition of stream 2 for the comparison of Li et al. (2018) model with Peng-Robinson and Soave-Redlich-Kwong

	Composition (mol/mol)
H_2O	9.94E-01
CO_2	5.74E-03
N_2	2.87E-06
O_2	2.87E-07

The results, concerning the CO_2 solubility, are presented in the respective tables (Appendix F):

The graphical comparison of Peng-Robinson and Soave-Redlich-Kwong with the model of Li et al. (2018) is presented in the following diagrams.

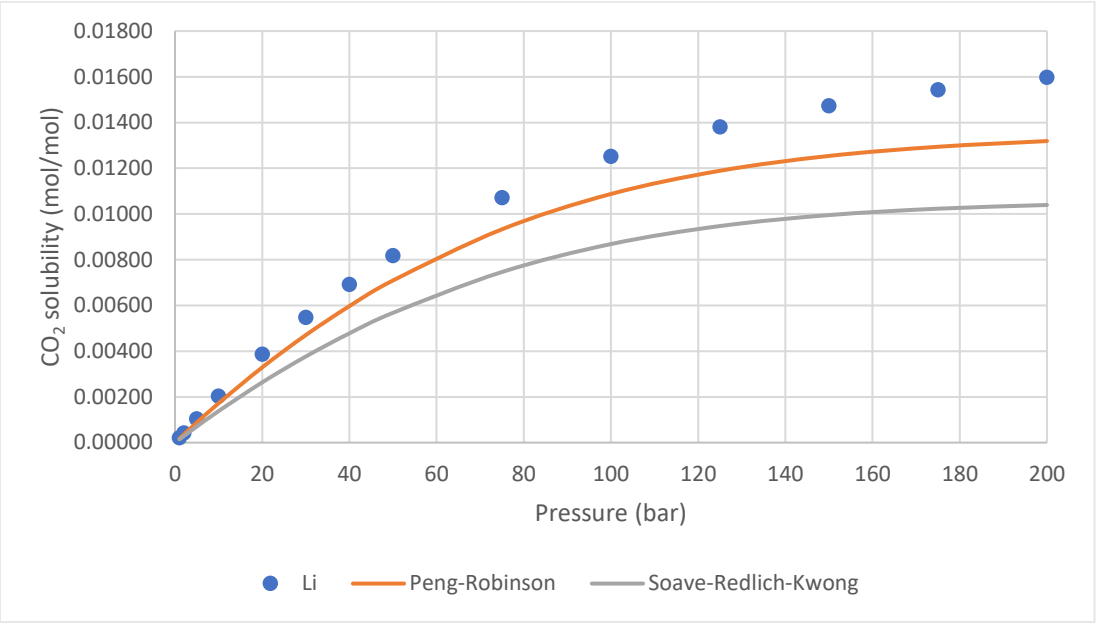

Figure 5.5 Comparison of PR's and SRK's predictions with the model of Li et al. (2018) (T=293.15 K, S=0 molality) as a function of pressure

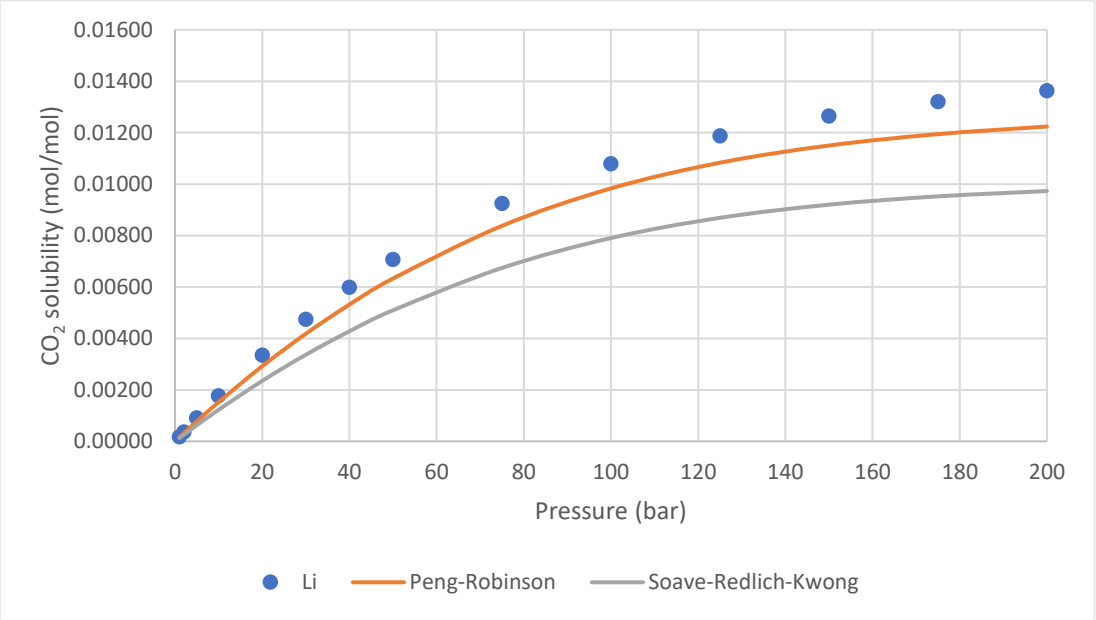

Figure 5.6 Comparison of PR's and SRK's predictions with the model of Li et al. (2018) (T=298.15 K, S=0 molality) as a function of pressure

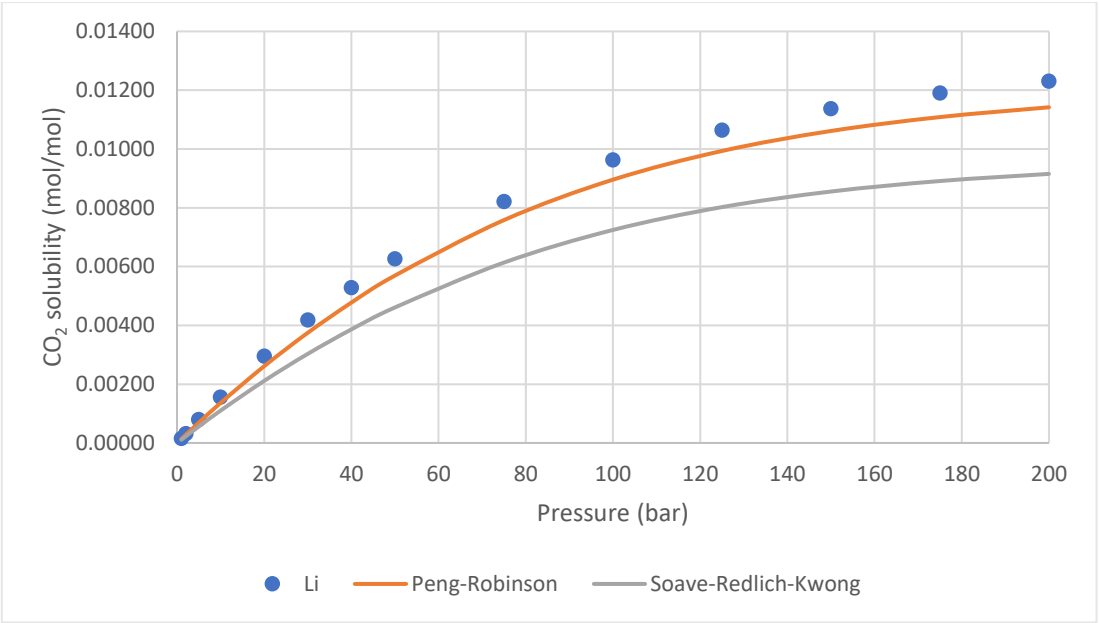

Figure 5.7 Comparison of PR's and SRK's predictions with the model of Li et al. (2018) (T=303.15 K, S=0 molality) as a function of pressure

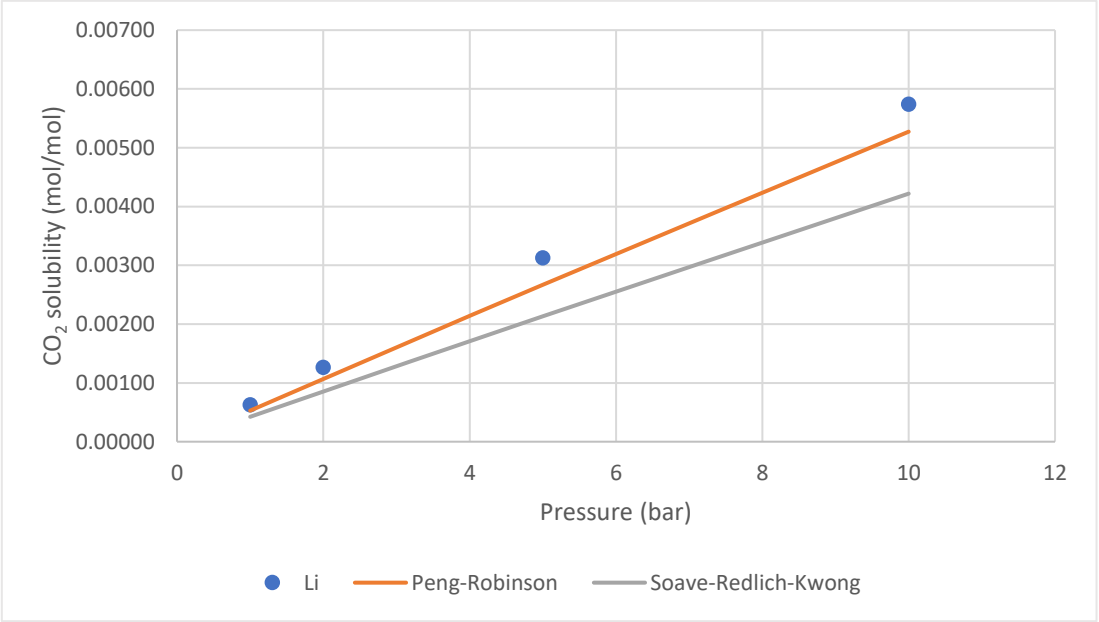

Figure 5.8 Comparison of PR's and SRK's predictions with the model of Li et al. (2018) (T=293.15 K, S=0 molality) as a function of pressure

As it is observed from the previous tables and diagrams, both models underestimate the CO_2 solubility. The Peng-Robinson model, though, approaches in better way the Li et al. (2018) model. The setup that the fluid package of Peng-Robinson uses is presented in the following figure.

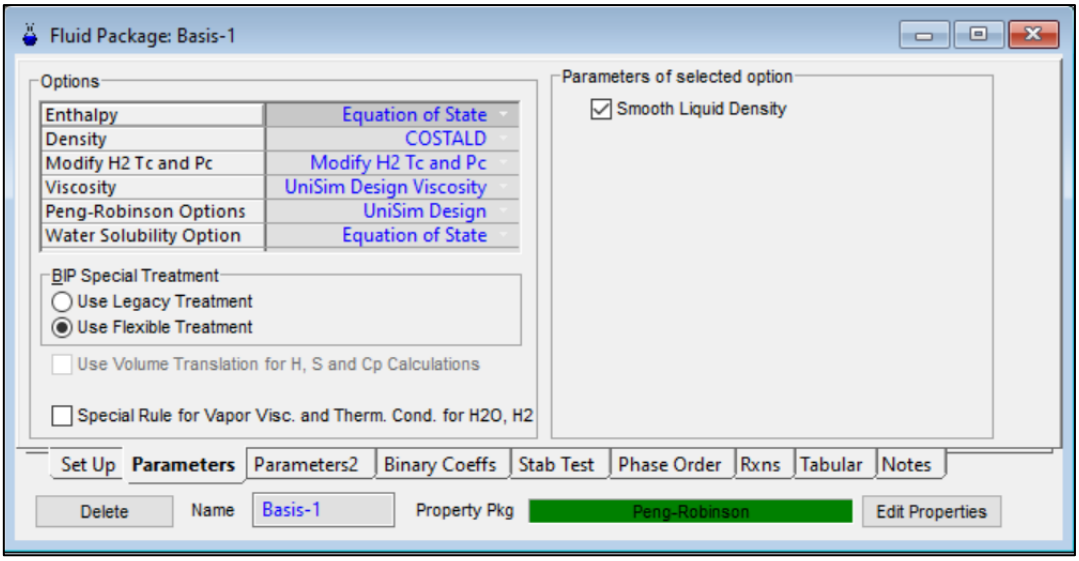

Figure 5.9 Setup for the fluid package of Peng-Robinson

At this point, it is worth noting that the salinity is introduced in Unisim through a pseudocomponent by the name of 'Na+*', which represents the sodium chloride. The properties of this pseudocomponent are presented in the following table.

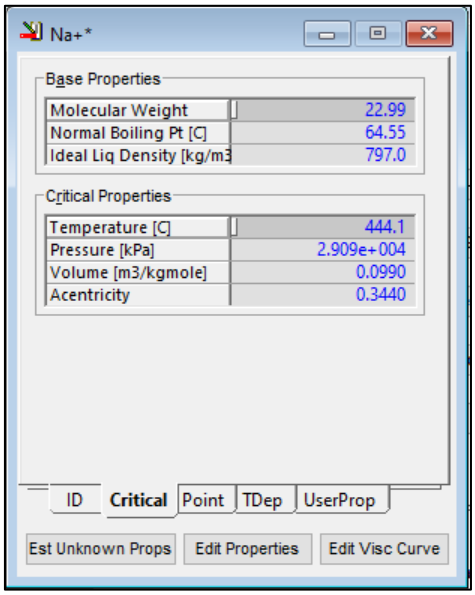

*Figure 5.10 Properties of pseudocomponent Na+**

Particular attention needs to be paid in the fact that this pseudocomponent should follow the water in a flash separator and have similar behavior to it.

6 Carbonated Water Injection Process

Some of the most important operational parameters of the carbonated water injection process are presented in this Chapter. As a process it consists of mixing a water-brine with a CO_2 stream. The water-brine stream is a mixture of sea water and produced water from the well. Its quantity is defined by the mass balance of water between the offshore installation and the well. Hydrocarbons are less dense than water, so as the drilling takes place, the gas, the oil and the water are extracted in this order. This results in a pressure drop in the well. In order to maintain the well's pressure constant, so that the flow assurance is accomplished, the necessary amount of water is injected in each life stage of the well. As its life is advancing, the amount of saline water mixed with hydrocarbons that are produced come to the surface. As a result, the amount of the produced water increases.

The CO_2 stream contains some amount of water and impurities like O_2 and N_2. It comes as a flue gas out of a turbine after combusting hydrocarbons with air and it goes through CO_2 conventional capture processes, like amine scrubbing. Even though the impurities exist in a ppm level, they play an important role. O_2 specifically is considered as a very contaminant gas. Its allowable composition limit varies globally and some indicative values range from 10 ppm to <1% by volume. The commercially available technologies for oxygen removal are catalytic oxidation and solid scavengers. The catalytic removal of oxygen from a natural gas stream is achieved by passing the gas at an elevated temperature over a catalyst bed where the oxygen reacts with a portion of the natural gas to form CO_2 and water (Oxygen Measurement in Natural Gas, 2016; Jones, McIntush, and Wallace, 2010).

6.1 Process Flow Diagram

The usual method, for the process design, includes injection of compressed CO_2 in the water-brine stream (Eke et al., 2011). Since, the ranges of temperature, salinity and impurities' content remain pretty much standard, the most critical design variable is the pressure. The value of the pressure is set so as the whole quantity of the CO_2 is dissolved in the water-brine stream. The desired pressure is reached by pumping the water-brine stream and compressing the CO_2 stream.

In order to compress the stream of carbon dioxide, the scheme of multistage compression is used. This offers serious advantages over single-stage compression. Intercooling is used between each compression stage. By cooling the gas between stages, the process reduces the gas volume, and, thus, the compression duties. Furthermore, by multistage compression, the temperature of the gas stream is not so high, so there are not any problems faced with material limitations. On the other hand, it should be noted that the intercoolers will have a pressure drop that will increase the compression work, but this effect is usually small compared with the reduction in work from gas cooling. A general process flow diagram of the process is presented in the following figure.

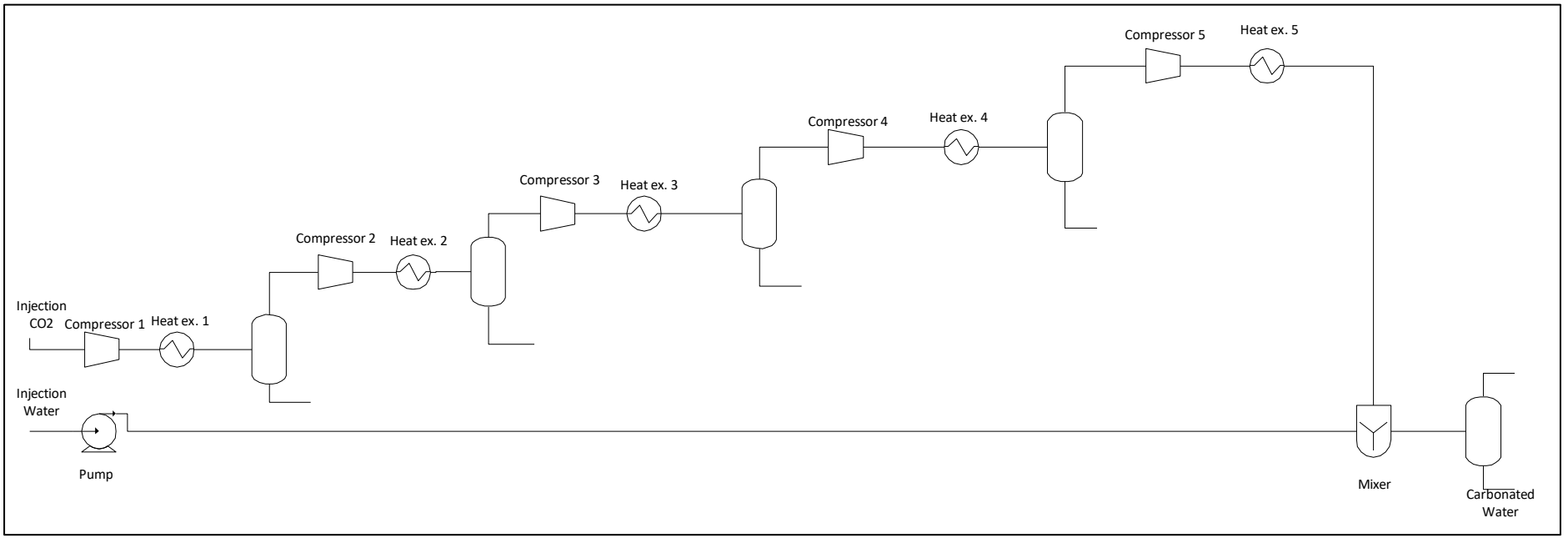

Figure 6.1 General Process Flow Diagram

Instead of the final compression stage, a pump is used, if the fluid in these conditions is liquid. In the final separation process, when the production of the carbonated water takes place, a recycling of the gas stream can be done, if the pressure is not enough for the complete dissolution of the carbon dioxide. Else, the gas stream is led to the flare system.

6.2 Pressure for complete CO_2 dissolution

The relation between the injection rate of water and the dissolution pressure is presented in the following figures, for standard quantities of CO_2 and different values of salinity.

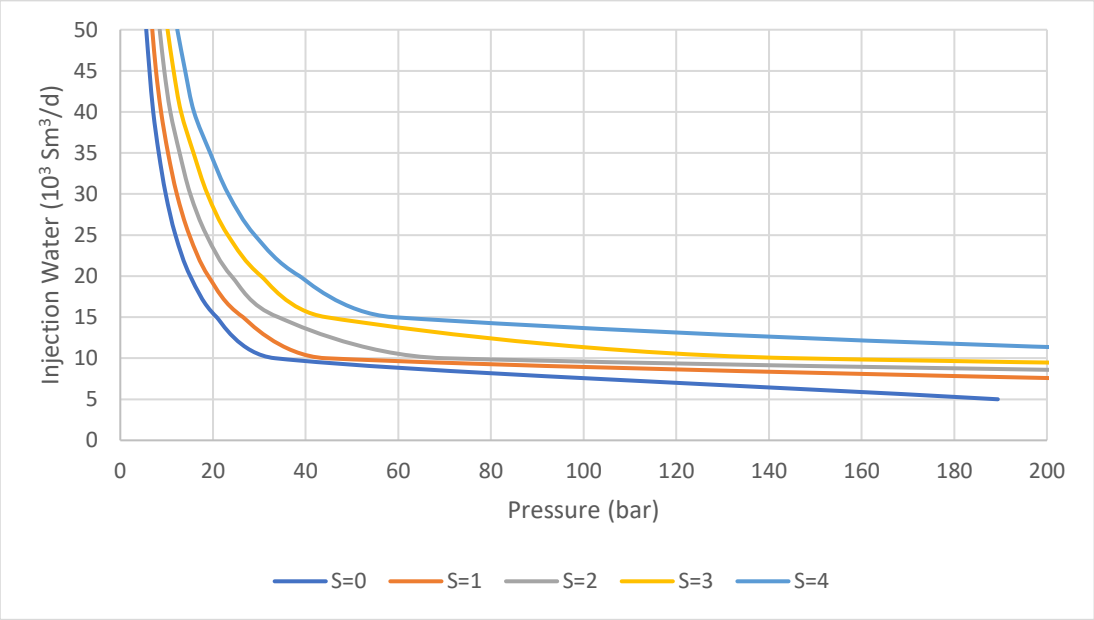

Figure 6.2 Needed amount of injection water for the dissolution of 14 t/hr CO_2 as a function of pressure for different salinities (mol/kg solvent)-(T=303.15 K)

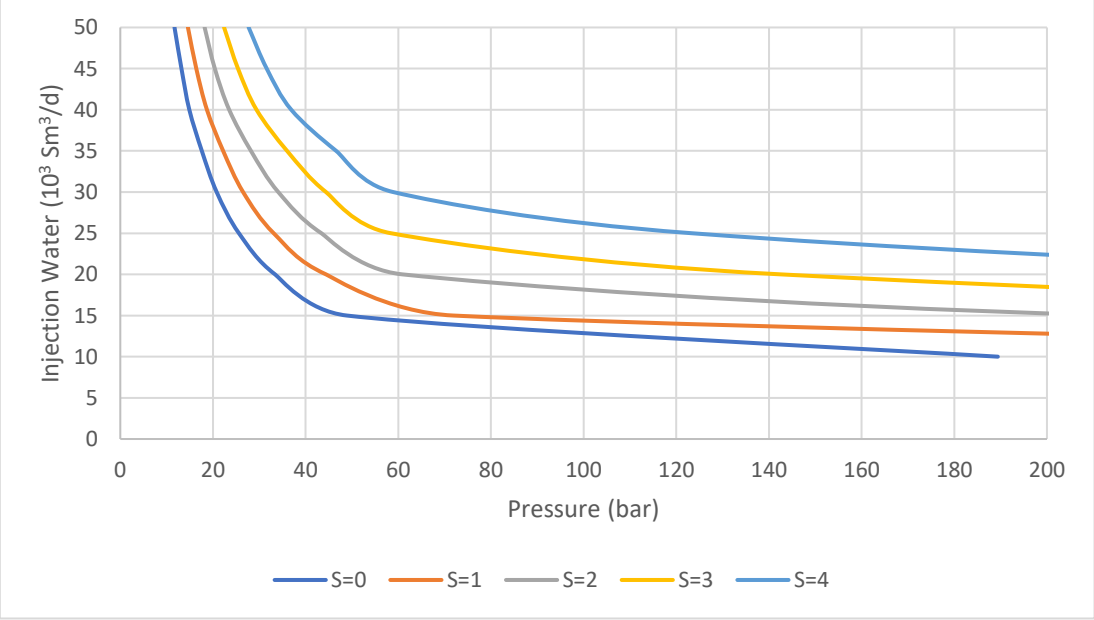

Figure 6.3 Needed amount of injection water for the dissolution of 28 t/hr CO_2 as a function of pressure for different salinities (mol/kg solvent)-(T=303.15 K)

As it can be observed from these figures, at some point, the curves become asymptotic. This means that, for standard quantities of water-brine and CO_2, the raise of pressure doesn't not

have the same impact on the increase of the CO_2 solubility. As a result, the unnecessary compression to a higher pressure should be avoided.

In the following figures, the relation between the injection water quantity and the dissolution pressure is presented, for standard salinities and different quantities of CO_2. These salinities are selected, because they represent the range of the salinities, that are studied in the case study.

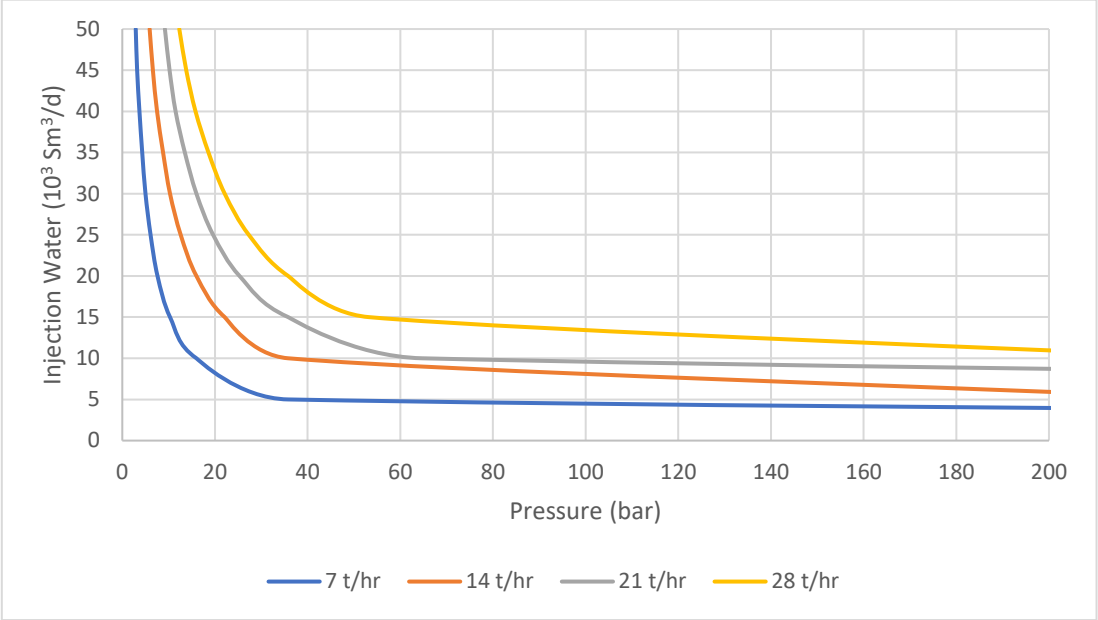

Figure 6.4 Needed amount of injection water for the dissolution of different quantities of CO_2 as a function of pressure (S=0.25 mol/kg solvent)-(T=303.15 K)

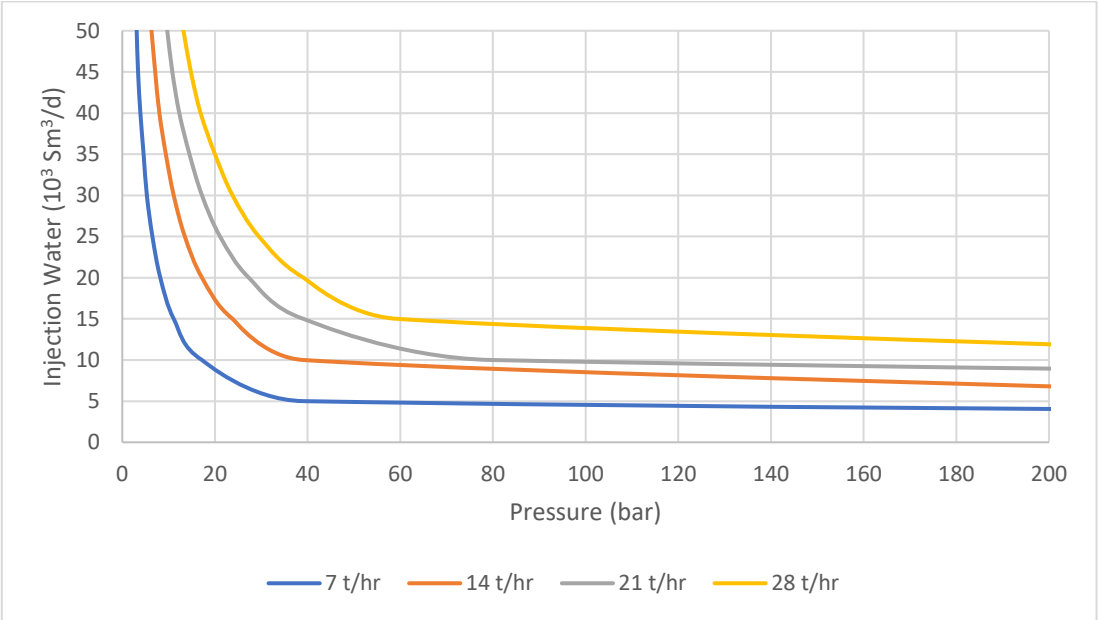

Figure 6.5 Needed amount of injection water for the dissolution of different quantities of CO_2 as a function of pressure (S=0.56 mol/kg solvent)-(T=303.15 K)

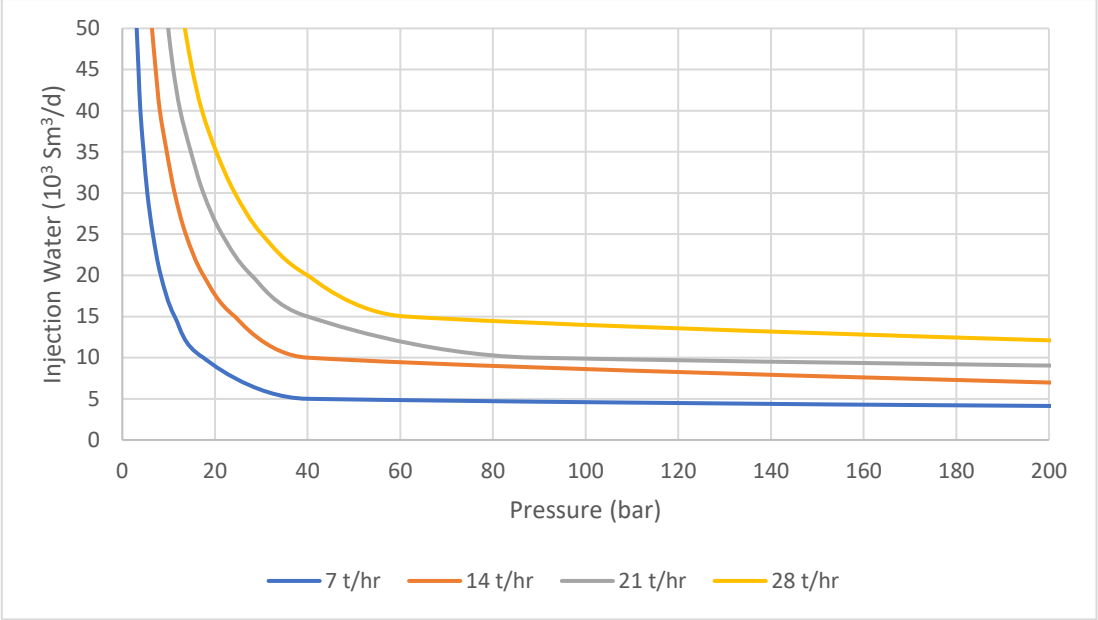

Figure 6.6 Needed amount of injection water for the dissolution of different quantities of CO_2 as a function of pressure (S=0.64 mol/kg solvent)-(T=303.15 K)

As it can be observed from these figures, as the salinity and the amount of injection water remain constant, the dissolution pressure increases with the amount of CO_2.

6.3 Compression Work

Considering that this process is an offshore one, the access to sea water for cooling is way easier than this to the power needed for the compression. As a result, the compression duties are of greater importance. In the following diagram, the compression work is presented as a function of pressure, for the different amounts of CO_2.

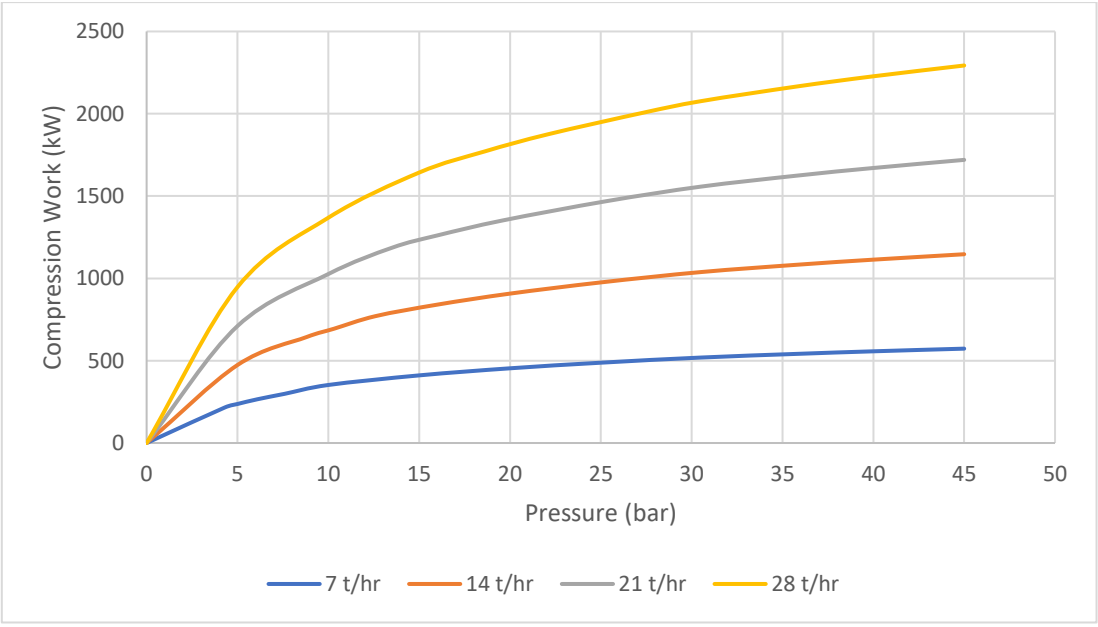

Figure 6.7 Compression work as a function of dissolution pressure (T=303.15 K)

From these figures, it is observed that as the compression pressure remains constant and the CO_2 quantity increases, the compression work increases.

6.4 Pressure Ratio in Compression Stage

A very significant design parameter is the pressure ratio of each compression stage. The minimum work is obtained when each stage of a multistage unit does the same amount of work (Appendix G), and, thus, most compressors will have approximately the same pressure ratio for each stage. In this case, the pressure ratio for m stages is computed by:

$$PR=(P2/P1)^{(1/m)}$$

where P2: the outlet and P1: the inlet pressure (Kidnay and Parrish, 2006, p. 68).

As also stated before, with an increasing compression ratio, compression efficiency decreases and mechanical stress as well as temperature problems become more severe. Speaking of an offshore process, the space is limited, so this should be taken into consideration for the needed space for the compressors. As a result, the value of the pressure ratio should be taken between 2 and 3 (El-Suleiman et al., 2016; Witkowski and Majkut, 2012; and Bahadori, 2014, p. 225).

7 Case Study

In this Chapter the case study provided by Equinor for the carbonated water injection is presented.

7.1 Case Study description

The pressure needed for the carbonated water to be injected in the well is 180 bar. The injection water (H_2O) has a temperature of 20-30 °C and an inlet pressure of 3.5 bar. The injection carbon dioxide (CO_2) has a temperature of 30 °C and a pressure of 1.5 bar. The composition of the CO_2 stream, coming from the capture plant, is presented in the following table:

Table 7.1 Composition of injection CO_2 stream

Water	Saturated at 30°C and 1.5 bar
Nitrogen	500 ppmv
Oxygen	50 ppmv

Injection water is a mix of produced water and sea water. More sea water is injected at the beginning of the field lifetime, while produced water will increase at later stages. Table 7.2 shows the relative rates of sea water and produced water at different stages of the field lifetime.

Table 7.2 Composition of injection water stream

	Early life	**Max injection**	**Late life**
Sea water (Sm^3/d)	23 850	27 030	1 450
Produced water (Sm^3/d)	0	6 360	19 700
Injection water (Sm^3/d)	***23 850***	***33 390***	***21 147***

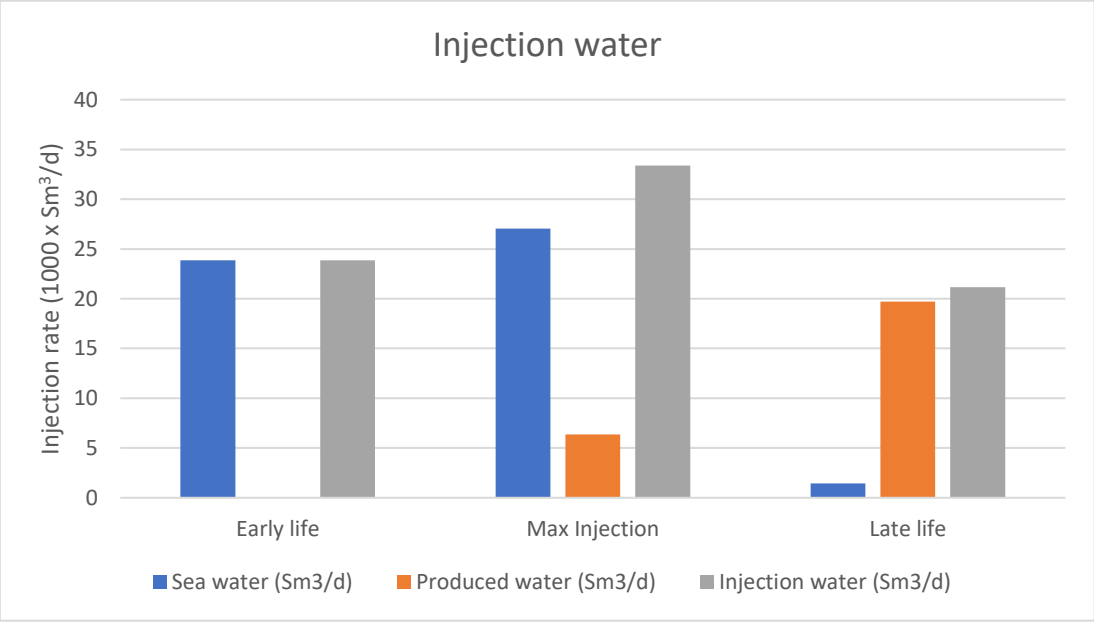

Figure 7.1 Composition of injection water stream

Table 7.3 Case studies: injection CO_2

	Injection carbon dioxide (t/hr)
Case 1	14
Case 2	28

For this specific field, the formation water has a salinity of ~13 g/litre, while sea water has a salinity of ~36 g/litre. The salinity of injection water will also change during the field lifetime since the relative rates of sea water and produced water change. Table 7.4 shows the salinity of injection water, in terms of molality ≡ mol/kg solvent, at different stages of the field lifetime.

Table 7.4 Salinity in each stage of the life of the field

	Early life	**Max injection**	**Late life**
Salinity (mol/kg solvent)	0.64	0.56	0.25

Two cases are studied in order to reach the pressure of 180 bar. The first one is by immediately pumping the water and compressing the carbon dioxide in the pressure of 180 bar. The second one is by pumping the water and compressing the carbon dioxide in an intermediate pressure and then pumping the carbonated water in the pressure of 180 bar. The criterion, on which the selection between these two cases is based, is the comparison of the required duties for the whole process. As it can be noticed from Figure 6.1 (see Chapter 6), the duties are separated into three categories: the compression, the cooling and the water pumping duties. In the following analysis (see Chapter 8), these duties are thoroughly examined.

7.2 Process Flow Diagram in Unisim

The overall process flow diagram that is made in Unisim is presented in Appendix H. Its parts are going to be explained more specifically. In the following figure, the unit operation Saturate is presented, that contributes to the making of the initial stream, in which the water is saturated.

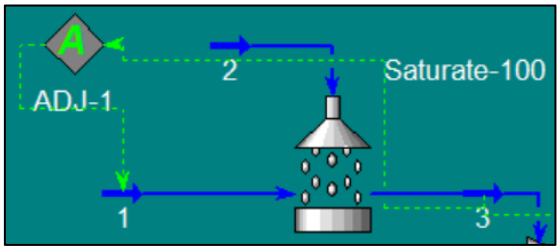

Figure 7.2 Saturate-100

ADJ-1 is used to adjust the mass flow of stream 1 so that stream 3 has the mass flow of either 14 t/hr or 28 t/hr. In the following figure, the SETs in the multistage compression are explained.

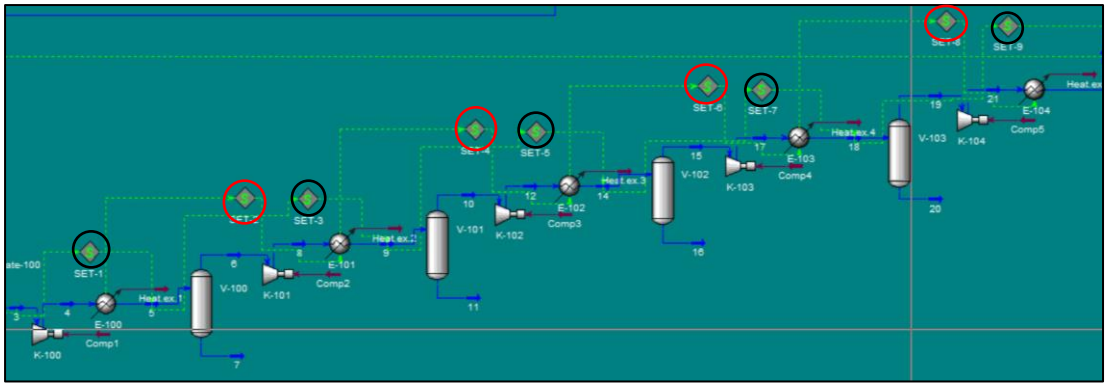

Figure 7.3 Explanation of SETs-Multistage Compression

SETs 1,3,5,7,9 (black circles) are used for defining the temperature in the outlet of the heat exchanger. SETs 2,4,6,8 (red circles) are used for defining the pressure drop in the heat exchangers.

For the compressors K100-K104, the adiabatic efficiencies of the compressors are considered to be 75% and, as mentioned before, the pressure ratios are equal. In the following diagram, the pump that is needed for the pumping of water in an intermediate or in the pressure of 180 bar is presented.

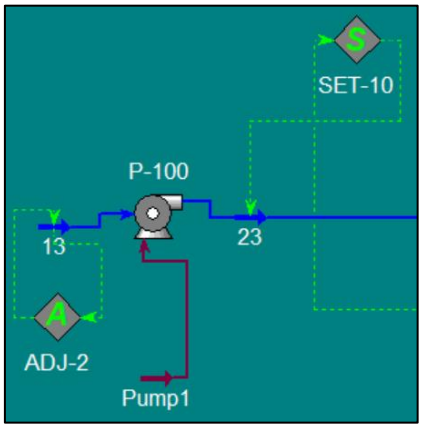

Figure 7.4 P-100

For the pump P-100, the adiabatic efficiency is considered to be 75%. ADJ-2 is used to adjust the mass flow of stream 13 so that its actual liquid flow becomes 23850 (Sm^3/d), 33390 (Sm^3/d) or 21147 (Sm^3/d). SET-10 is used so that the pressure before the mixing become equal. In the following figure, the part of the process after the mixing of the two streams is presented.

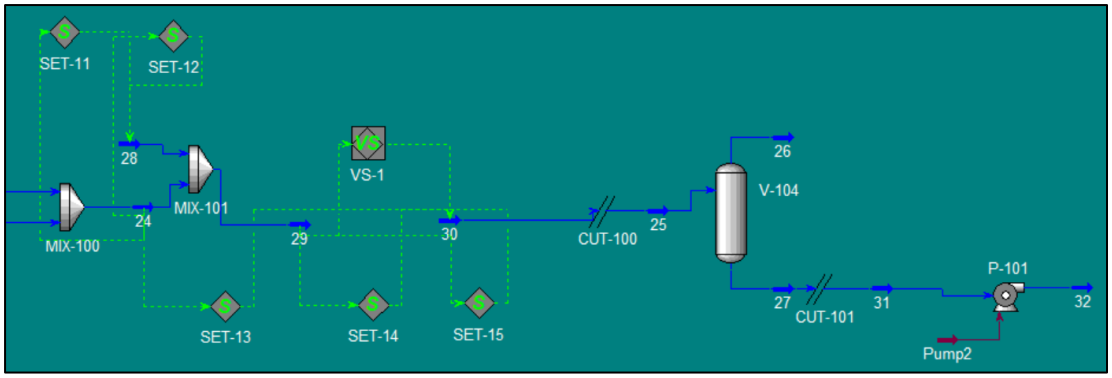

Figure 7.5 Part of the process after the mixing of the two streams

Most of this part of the process is artificial. Normally, the stream 24, after MIX-100, would enter the flash separator and then the carbonated water would be produced. Now, though, the simulation previous to MIX-100 contains traces of Na+*. As a result, the artificial stream 28 is used for fixing the salinity at the right level, through a simple mass balance (Appendix I). The visual stream (VS-1) option is used so that stream 30 has the following properties.

Table 7.5 Properties of Stream 30

	Stream 30
Temperature	T_{24}
Pressure	$P_{29} - \Delta P_{mixer}$
Mole Composition	Mole Composition$_{29}$
Overall Mole flow	Overall Mole flow$_{24}$

Then, CUT-100 is used for the transition from the Peng-Robinson to Li et al. (2018) model. After the production of the carbonated water is done, the Li et al. (2018) model is transitioned back to the model of Peng-Robinson, so that the duty Pump2 is calculated. For the pump P-101, the adiabatic efficiency is considered to be 75% and its delta P is defined so that the pressure of stream 32 is 180 bar.

8 Simulation Results

As also mentioned in Chapter 7, the criterion, on which the selection between the intermediate and the high pressure cases is based, is the requirement of duties for the whole process. As a result, in this Chapter, the behavior of the compression, cooling and water pumping duties of the aforementioned Case Study-Unisim simulation, is presented.

Four cases are taken into consideration, for this case study. These cases are presented in the following table.

Table 8.1 Cases of the case study

	Injection carbon dioxide (t/hr)	Pressure (bar)
HP-14	14	180
IP-14	14	Intermediate Pressure
HP-28	28	180
IP-28	28	Intermediate Pressure

It is known that the pressure of 180 bar is high enough, so that the carbon dioxide is dissolved in the injection water stream. For the intermediate pressure cases, the pressure through the model of Li et al. (2018) is calculated so that all carbon dioxide is dissolved. Considering the worst case, which is that the mixing takes place at 30^{o} C, the pressure is calculated for each life-stage of the well. The results are presented in the following table.

Table 8.2 IP cases: pressures for complete CO_2 dissolution

	Pressure(bar) Early life	Pressure(bar) Max injection	Pressure(bar) Late life
IP-14	15	11	16
IP-28	35	23	37

For the dissolution to take place in each life-stage of the field, the compression pressure is set to the highest value. In case IP-14, the selected compression pressure is 16 bar and in case IP-28, the selected compression pressure is 37 bar.

8.1 Case HP-14

Considering the analysis made on the pressure ratio in Chapter 6, in order to reach the pressure of 180 bar, it is set to 2.605. The compression stages that are needed are 5. The process flow diagram is presented in the following figure.

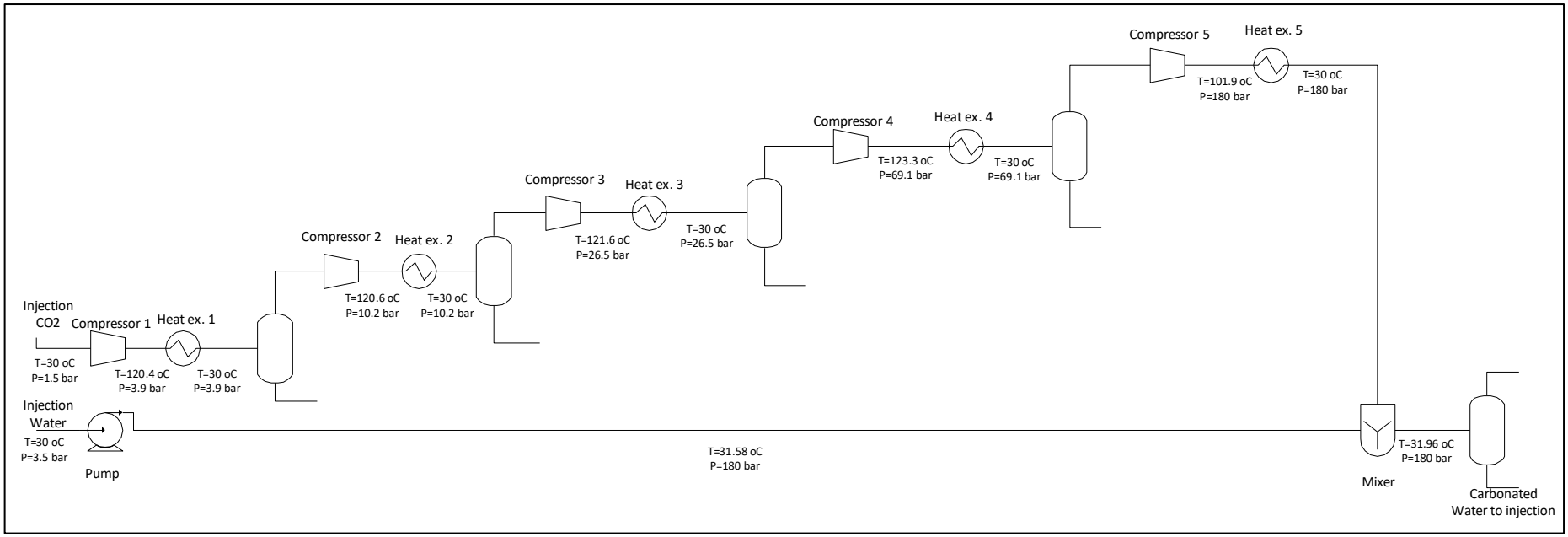

Figure 8.1 Process Flow Diagram (HP-14)

The required compression, cooling and water pumping duties for this simulation are presented in the following table.

Table 8.3 Required Duties for case (HP-14)

	HP-14		
Compression Duties (kW)	1354		
Cooling Duties (kW)	2449		
	Early life	**Max Injection**	**Late life**
Water Pumping Duties (kW)	6496	9095	5760

The amount of seawater that is used for the cooling of the CO_2 stream is estimated. It is calculated through the following equation:

$$\dot{m} = \frac{Q}{C_p * \Delta T}$$

where $\dot{m}$=mass flow rate (kg/s), Q=duty of each heat exchanger (kW), C_p=specific heat capacity of seawater (=4 kJ/kg/^{o}C) and ΔT=temperature difference between the inlet and the outlet of the seawater stream (^{o}C).

The countercurrent scheme is used and the temperature differences ($T_{h,in} - T_{c,out}$) and ($T_{h,out} - T_{c,in}$) are set to the typical value 10 ^{o}C.

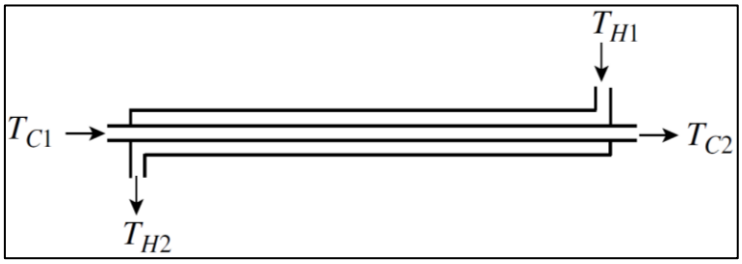

Figure 8.2 Countercurrent flow - Heat Exchanger

The needed mass flow of water for the cooling duties is estimated to be 7.51 kg/s.

8.2 Case IP-14

Considering the analysis made on the pressure ratio in Chapter 6, in order to reach the pressure of 16 bar, it is set to 2.201. The compression stages that are needed are 3. The process flow diagram is presented in the following figure.

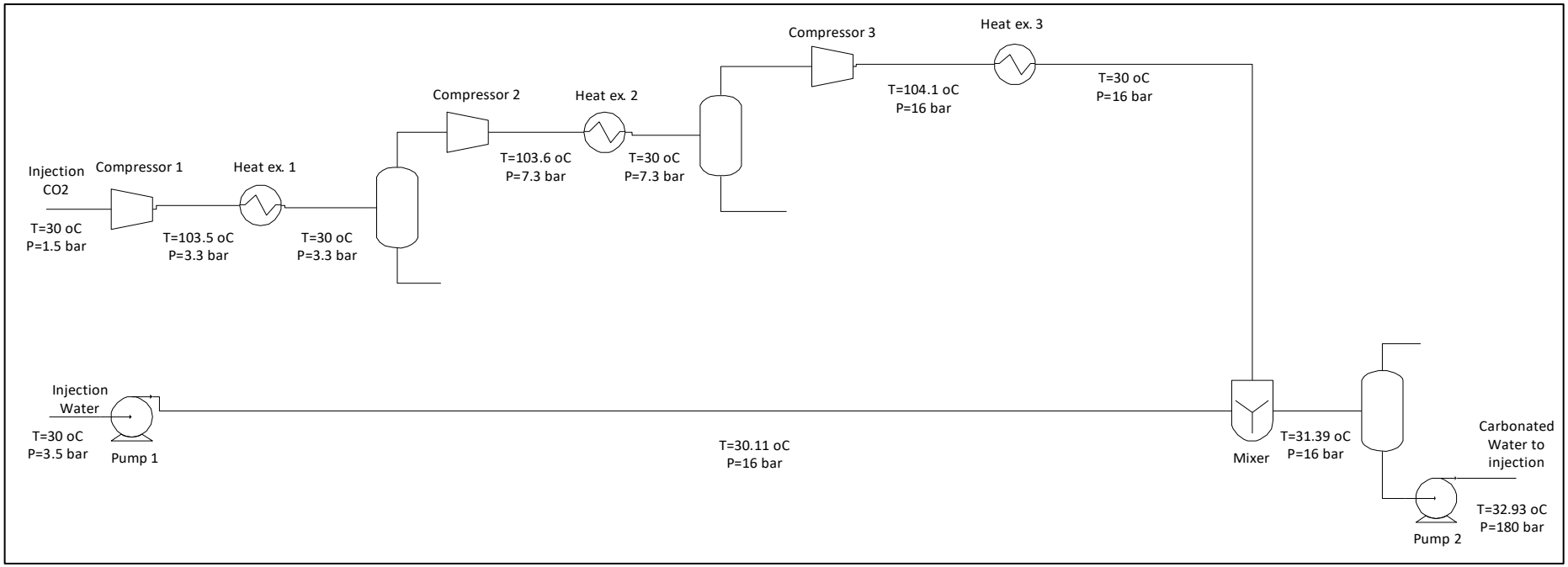

Figure 8.3 Process Flow Diagram (IP-14)

The required compression, cooling and water pumping duties for this simulation are presented in the following table.

Table 8.4 Required Duties for case (IP-14)

	IP-14		
Compression Duties (kW)	752		
Cooling Duties (kW)	907		
	Early life	**Max Injection**	**Late life**
Water Pumping Duties (kW)	6570	9167	5832

The needed mass flow of water for the cooling duties is estimated to be 3.71 kg/s.

8.3 Case HP-28

Considering the analysis made on the pressure ratio in Chapter 6, in order to reach the pressure of 180 bar, it is set to 2.605. The compression stages that are needed are 5. The process flow diagram is presented in the following figure.

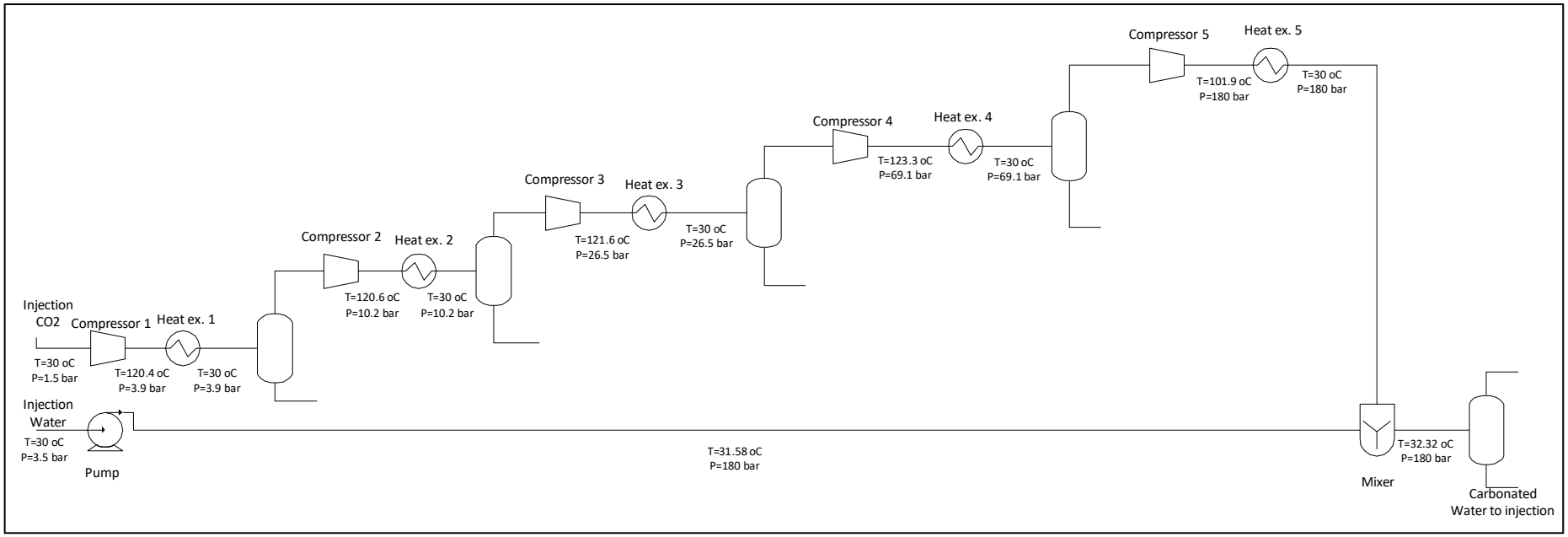

Figure 8.4 Process Flow Diagram (HP-28)

The required compression, cooling and water pumping duties for this simulation are presented in the following table.

Table 8.5 Required Duties for case (HP-28)

	HP-28		
Compression Duties (kW)	2707		
Cooling Duties (kW)	4897		
	Early life	**Max Injection**	**Late life**
Water Pumping Duties (kW)	6496	9095	5760

The needed mass flow of water for the cooling duties is estimated to be 14.37 kg/s.

8.4 Case IP-28

Considering the analysis made on the pressure ratio in Chapter 6, in order to reach the pressure of 37 bar, it is set to 2.229. The compression stages that are needed are 4. The process flow diagram is presented in the following figure.

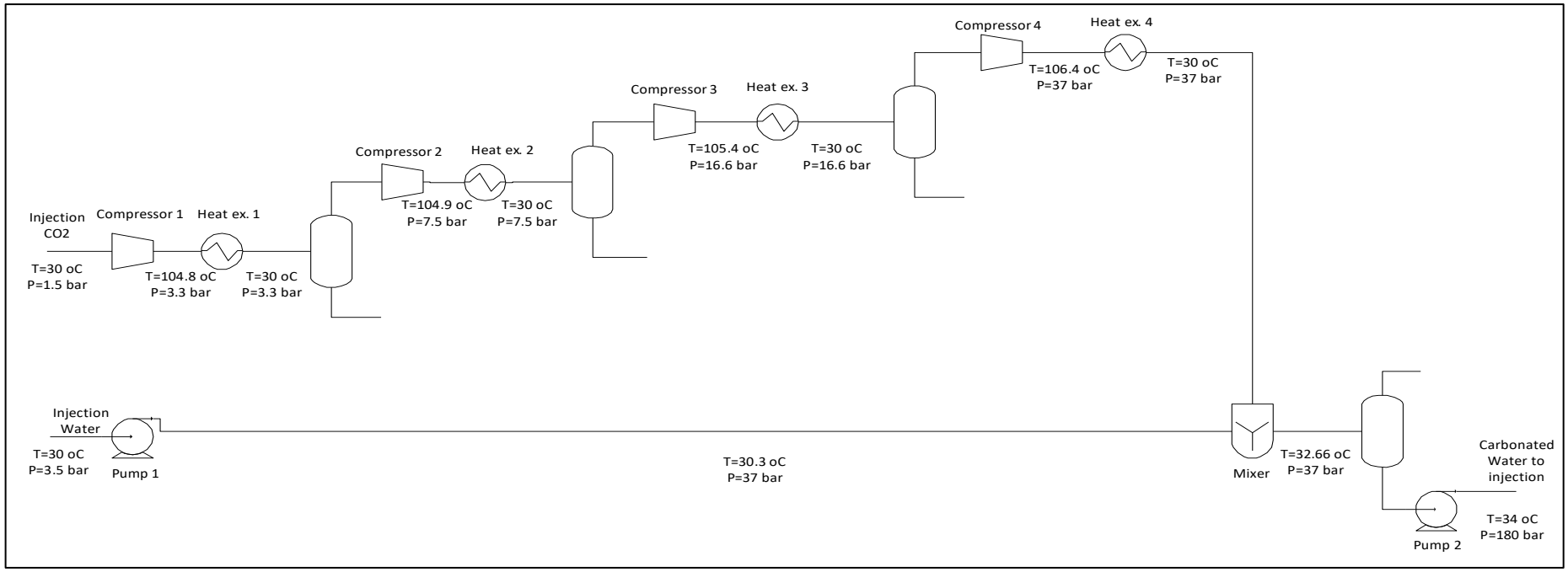

Figure 8.5 Process Flow Diagram (IP-28)

The required compression, cooling and water pumping duties for this simulation are presented in the following table.

Table 8.6 Required Duties for case (IP-28)

	IP-28		
Compression Duties (kW)	1996		
Cooling Duties (kW)	2506		
	Early life	**Max Injection**	**Late life**
Water Pumping Duties (kW)	6623	9219	5887

The needed mass flow of water for the cooling duties is estimated to be 9.35 kg/s.

8.5 Discussion

The simulation results of the case study indicate that the needed duties, for the production of carbonated water, in terms of values, are sorted as following: water pumping duties > cooling duties > compression duties. It is observed that the cooling and the compression duties in the intermediate pressure cases are lower in comparison with the high pressure ones. The pumping duties, though, are of similar values in both intermediate and high pressure cases. In the intermediate pressure cases, they are a little bit greater because the volume that has to be pumped is greater than the high pressure ones. As a result, in terms of energy the compression of the CO_2 stream in an intermediate pressure has the advantage over the immediate compression at 180 bar.

An overview table of the compression and the cooling duties for all the cases, supposing that the mixing temperature is 30°C, is presented.

Table 8.7 Overview of compression and cooling duties for IP and HP cases

	HP-14	IP-14	HP-28	IP-28
Compression Duties (kW)	1354	752	2707	1996
Cooling Duties (kW)	2449	907	4897	2506

The energy savings on these duties are calculated from the following equation:

$$Energy\ savings = \frac{Duty_{HP} - Duty_{IP}}{Duty_{HP}}$$

They are presented in the following table.

Table 8.8 Percentage Energy Savings (%) for IP compared to HP cases: Compression and Cooling Duties

CO_2 injection: 14 t/hr – Energy Savings	
Compression	44.4%
Cooling	63.0%
CO_2 injection: 28 t/hr – Energy Savings	
Compression	26.2%
Cooling	48.8%

An overview table of the water pumping duties for all the cases, supposing that the mixing temperature is 30°C, is presented.

Table 8.9 Overview of water pumping duties for IP and HP cases

Water Pumping Duties (kW)	HP-14	IP-14	HP-28	IP-28
Early life	6496	6570	6496	6623
Max Injection	9095	9167	9095	9219
Late life	5760	5832	5760	5887

The energy losses on these duties are calculated from the following equation.

$$Energy\ Losses = \frac{Duty_{IP} - Duty_{HP}}{Duty_{IP}}$$

They are presented in the following table.

Table 8.10 Percentage Energy Losses (%) for IP compared to HP cases: Water Pumping Duties

CO_2 injection: 14 t/hr – Energy Savings			
	Early life	**Max Injection**	**Late life**
Pumping	1.1%	0.8%	1.3%
CO_2 injection: 28 t/hr – Energy Savings			
	Early life	**Max Injection**	**Late life**
Pumping	2.0%	1.4%	2.2%

From these tables, it is noticed that the smaller the quantity of CO_2 that is about to be dissolved and as a result the compression pressure, the larger are the energy savings on the compression and cooling duties. These energy savings of the latter are higher.

At this point, is should be noticed that the intermediate pressure cases require a second pump, so they present less flexibility than the high pressure ones. On the other hand, though, the compressors that are needed are smaller in size.

Moreover, in the intermediate pressure cases, taking into consideration the possibility that the model doesn't predict accurately the pressure needed for the dissolution of CO_2 in the water stream, there is the possibility of vapor CO_2 entering the second pump and therefore leading to cavitation.

9 Sensitivity Analysis

In this Chapter, a sensitivity analysis is made to estimate the effect of some of the most important parameters in the behavior of the duties studied in Chapter 8. These parameters are the type of compression (one vs multi-stage), the thermodynamic approach to equilibrium, the pressure drops in the mixer and the heat exchanger, and the pressure ratio.

9.1 One vs multi-stage compression

The multi-stage is selected over the one-stage compression, as the requirements that are needed for compression are lower and the temperature of the stream doesn't become prohibitive. This phenomenon is shown in the following tables.

Table 9.1 Compression Duties: one vs multi-stage compression

	Compression Duties (kW) Multi-stage	**Compression Duties (kW) One-stage**
HP-14	1354	2423
IP-14	752	916
HP-28	2707	4847
IP-28	1996	2716

The energy savings on the compression duties are presented in the following table.

Table 9.2 One vs multi-stage compression: Percentage energy savings

CO_2 injection: 14 t/hr – Energy Savings	
HP	44.1%
IP	17.9%
CO_2 injection: 28 t/hr – Energy Savings	
HP	44.2%
IP	26.5%

It is observed that the higher the pressure the higher are the energy savings on the compression duties.

Table 9.3 Outlet Temperature: one vs multi-stage compression

	Outlet Temperature (°C) Multi-stage (Highest)	**Outlet Temperature (°C) One-stage**
HP-14	123.3	625.7
IP-14	104.1	277.4
HP-28	123.3	625.7
IP-28	106.4	385.8

Due to material limitations, the outlet temperatures in the one-stage compression are considered prohibitive.

9.2 Effect of Thermodynamic Approach to Equilibrium

The results for the duties, that are presented in Chapter 8, are calculated having made the assumption, that the thermodynamic equilibrium in the mixing process between the carbon dioxide and the water is 100% percent. In reality, in order to be sure that the dissolution of carbon dioxide will take place, lower values of thermodynamic approach to equilibrium should be considered. In this study, the thermodynamic approach to equilibrium is defined as follows:

$$Thermodynamic\ Approach\ to\ Equilibrium = \frac{CO_2\ quantity\ in\ real\ mixing}{CO_2\ quantity\ in\ ideal\ mixing}$$

The cases of 85%, 90% and 95% approach to equilibrium are studied. The quantity of CO_2 in real mixing is set to the quantity of CO_2 of the case study. Considering, for example, that the approach is 95% and the CO_2 injection rate is 14 t/hr, the quantity of CO_2 before the mixer is 13.8 t/hr (real mixing) and as a result the respective one in ideal mixing would be 14.5 t/hr (=13.8/0.95). For this greater amount, the new pressure for the complete CO_2 dissolution is estimated.

These values of approach to equilibrium are consistent with the ones proposed by Meijer et al. 2011. In their work, the mixing measure is based on the intensity of segregation I. It is a first-order statistic moment that quantifies the deviation of the composition of the mixture to the ideal case. Its value is scaled such that it ranks from 1 (poor mixing) < I < 0 (ideal mixing). It is connected with the thermodynamic approach to equilibrium as follows:

$$I = 1 - Thermodynamic\ Approach\ to\ Equilibrium$$

Since, the pressure of 180 bar is high enough for the dissolution to happen, no matter the aforementioned approaches, the effect of it is studied on the intermediate pressure cases. The pressure, for the dissolution of carbon dioxide in ideal mixing in the water stream, is calculated from the Li et al. (2018) model. These pressures are presented in the following table.

Table 9.4 Pressures for the dissolution of CO_2 for the different thermodynamic approaches to equilibrium

Thermodynamic approach to equilibrium	Pressure (bar) IP-14	Pressure (bar) IP-28
100%	16	37
95%	17	40
90%	18	43
85%	19	46

In Appendix J, the pressure ratios, for each value of approach to equilibrium, and the necessary compression stages are presented.

For each thermodynamic approach to equilibrium, the behavior of the compression, cooling and water pumping duties is studied. In the following tables, a comparison is made between each level of approach to equilibrium for all the cases.

Table 9.5 Compression Duties (kW) - Thermodynamic Approach to Equilibrium

Compression Duties (kW)		
Approach to Equilibrium	Cases	
	IP-14	IP-28

100%	752	1996
95%	772	2045
90%	792	2090
85%	810	2131

Table 9.6 Cooling Duties (kW) - Thermodynamic Approach to Equilibrium

Cooling Duties (kW)		
Approach to Equilibrium	**Cases**	
	IP-14	**IP-28**
100%	907	2506
95%	932	2587
90%	956	2665
85%	978	2742

As it can be observed, for both cases, from these tables, the compression and the cooling duties are becoming greater, in a similar trend, as the thermodynamic approach to equilibrium lowers. The approach to equilibrium doesn't have any significant effect on the water pumping duties. The energy losses, for the compression and the cooling duties, according to the thermodynamic approach to equilibrium are presented in the following table.

Table 9.7 Percentage Energy Losses: Compression and Cooling Duties – Thermodynamic Approach to Equilibrium

Energy Losses				
Approach to Equilibrium	**Compression Duties**		**Cooling Duties**	
	IP-14	**IP-28**	**IP-14**	**IP-28**
95%	2.7	2.4	2.8	3.2
90%	5.2	4.7	5.4	6.3
85%	7.7	6.8	7.9	9.4

It is noticed that the intermediate cases, with 85% approach to equilibrium, are still more profitable, in terms of the duties' requirements, than the high-pressure ones (Tables 9.5, 9.6, 8.3 and 8.5).

9.3 Effect of Pressure Drop

Another factor that should be examined is the effect of the pressure drops in the intercoolers and the mixer.

9.3.1 Pressure Drop in Heat Exchanger

Considering that we have shell and tube heat exchangers, in the absence of a specific retrofit constraint for pressure drop, for gases, the maximum allowable pressure drop varies typically between 1 bar for high-pressure gases (10 bar and above) down to 0.01 bar for gases under vacuum conditions (Smith, 2005, p. 321)**.**

Following the procedure that is presented in Appendix K and assuming that the fluid velocity for the tube-side is 5 m/s, the number of tube passes is 2 and that the heat transfer area is 5 m^2, the pressure drop in the tubes is estimated to be 0.003 bar. Considering that the tube pitch is 0.025 m, the baffle cut is 0.25 m and the pitch configuration factor is 1 m, the pressure drop in the tubes is estimated to be 0.102 bar. Since the estimated pressure drop is 0.105 bar,

the case studies from to 0.1 to 0.5 bar are studied. Some other typical values for the pressure drop in the cooler have been presented by El-Suleiman et al. (2016); and Witkowski and Majkut (2012).

9.3.2 Pressure Drop in Mixer

The pressure drop in the mixer is calculated by the following formula:

$$\Delta P=(f/2)*\rho*(v^2)*(L/D)$$

where f/2=the friction factor, ρ=density of the fluid (kg/m^3), v=superficial velocity (m/s), L=mixer length (m) and D=inner pipe diameter (m) (Yang and Park, 2004).

The Reynold's number is calculated, as follows:

$$Re=\frac{3157*Q*SG}{\mu*D}$$

where Q=flow rate (m^3/s), SG=specific gravity, μ=absolute viscosity (kg/m/s) and D=pipe inside diameter (m) (Sizing the Admixer™ Static Mixer and Sanitary Static Blender, 1998).

The friction fanning factor f/2 is correlated to the Reynold's number by the following expression:

$$f/2=0.4+110/Re^{0.8}$$ (Li et al., 1996)

Considering that the superficial velocity is 3 m/s and the length:diameter ratio is 4 m, the estimated pressure drop in the mixer is 3.76 bar. Since the estimated pressure drop is 3.76 bar, the case studies from to 1 to 5 bar are studied.

9.3.3 Pressure Drop - Results

Taking into consideration these pressure drops, the compression's pressures that are studied are presented in Appendix L. The values of the pressure ratios and the necessary compression stages are also presented, for each case.

The following table represents the compression duties for all the cases, considering that the mixing temperature is 30° C.

Table 9.8 Compression Duties (kW) – Pressure Drop

HP-14					
Pressure Drop Mixer (bar)	**Pressure Drop Heat Exchanger (bar)**				
	0.5	**0.4**	**0.3**	**0.2**	**0.1**
5	1442	1424	1406	1387	1369
3	1442	1424	1406	1388	1370
1	1442	1424	1406	1388	1371
IP-14					
Pressure Drop Mixer (bar)	**Pressure Drop Heat Exchanger (bar)**				
	0.5	**0.4**	**0.3**	**0.2**	**0.1**
5	922	907	890	875	859
3	892	875	859	842	826
1	859	841	824	807	789
HP-28					
Pressure Drop Mixer (bar)	**Pressure Drop Heat Exchanger (bar)**				
	0.5	**0.4**	**0.3**	**0.2**	**0.1**
5	2884	2848	2811	2775	2738

3	2884	2848	2812	2776	2740
1	2884	2848	2812	2777	2741
IP-28					
Pressure Drop Mixer (bar)	**Pressure Drop Heat Exchanger (bar)**				
	0.5	**0.4**	**0.3**	**0.2**	**0.1**
5	2255	2218	2182	2146	2110
3	2228	2190	2153	2117	2081
1	2199	2161	2123	2086	2049

The effect of the pressure drops in the mixer and in each heat exchanger is studied. This effect is calculated through this type:

$$\frac{Comp.Duty_{0,0} - Comp.Duty_{i,j}}{Comp.Duty_{i,j}}$$

where i: pressure drop in the mixer and j: pressure drop in the heat exchanger.

Table 9.9 Percentage Energy Losses: Compression Duties – Pressure Drop

HP-14					
Pressure Drop Mixer (bar)	**Pressure Drop Heat Exchanger (bar)**				
	0.5	**0.4**	**0.3**	**0.2**	**0.1**
5	6.5	5.2	3.8	2.4	1.1
3	6.5	5.2	3.8	2.5	1.2
1	6.5	5.2	3.8	2.5	1.3
IP-14					
Pressure Drop Mixer (bar)	**Pressure Drop Heat Exchanger (bar)**				
	0.5	**0.4**	**0.3**	**0.2**	**0.1**
5	22.6	20.6	18.4	16.4	14.2
3	18.6	16.4	14.2	12.0	9.8
1	14.2	11.8	9.6	7.3	4.9
HP-28					
Pressure Drop Mixer (bar)	**Pressure Drop Heat Exchanger (bar)**				
	0.5	**0.4**	**0.3**	**0.2**	**0.1**
5	6.5	5.2	3.8	2.5	1.1
3	6.5	5.2	3.9	2.5	1.2
1	6.5	5.2	3.9	2.6	1.3
IP-28					
Pressure Drop Mixer (bar)	**Pressure Drop Heat Exchanger (bar)**				
	0.5	**0.4**	**0.3**	**0.2**	**0.1**
5	13.0	11.1	9.3	7.5	5.7
3	11.6	9.7	7.9	6.1	4.3
1	10.2	8.3	6.4	4.5	2.7

Thus, the pressure drops in the mixer and in each heat exchanger can have some important effect on the compression duties in the intermediate pressure cases. In the high pressure ones, their effect is not so important.

The following table represents the cooling duties for all the cases, considering that the mixing temperature is 30^{o} C.

Table 9.10 Cooling Duties (kW) – Pressure Drop

HP-14					
Pressure Drop Mixer (bar)	**Pressure Drop Heat Exchanger (bar)**				
	0.5	**0.4**	**0.3**	**0.2**	**0.1**
5	2540	2522	2503	2485	2467
3	2539	2521	2503	2485	2467
1	2538	2520	2502	2484	2466
IP-14					
Pressure Drop Mixer (bar)	**Pressure Drop Heat Exchanger (bar)**				
	0.5	**0.4**	**0.3**	**0.2**	**0.1**
5	1100	1084	1068	1053	1037
3	1061	1044	1027	1011	995
1	1018	1001	983	966	949
HP-28					
Pressure Drop Mixer (bar)	**Pressure Drop Heat Exchanger (bar)**				
	0.5	**0.4**	**0.3**	**0.2**	**0.1**
5	5080	5044	5007	4970	4933
3	5078	5041	5006	4970	4934
1	5075	5039	5003	4967	4933
IP-28					
Pressure Drop Mixer (bar)	**Pressure Drop Heat Exchanger (bar)**				
	0.5	**0.4**	**0.3**	**0.2**	**0.1**
5	2819	2782	2746	2710	2675
3	2770	2732	2695	2659	2622
1	2719	2681	2644	2607	2570

The effect of the pressure drops in the mixer and in each heat exchanger is studied. This effect is calculated through this type:

$$\frac{Cool.Duty_{0,0} - Cool.Duty_{i,j}}{Cool.Duty_{i,j}}$$

where i: pressure drop in the mixer and j: pressure drop in the heat exchanger.

Table 9.11 Percentage Energy Losses: Cooling Duties – Pressure Drop

HP-14					
Pressure Drop Mixer (bar)	**Pressure Drop Heat Exchanger (bar)**				
	0.5	**0.4**	**0.3**	**0.2**	**0.1**
5	3.7	3.0	2.2	1.5	0.7
3	3.7	2.9	2.2	1.5	0.7
1	3.6	2.9	2.2	1.4	0.7
IP-14					
Pressure Drop Mixer (bar)	**Pressure Drop Heat Exchanger (bar)**				
	0.5	**0.4**	**0.3**	**0.2**	**0.1**
5	21.3	19.5	17.8	16.1	14.3
3	17.0	15.1	13.2	11.5	9.7
1	12.2	10.4	8.4	6.5	4.6
HP-28					
	Pressure Drop Heat Exchanger (bar)				

Pressure Drop Mixer (bar)	0.5	0.4	0.3	0.2	0.1
5	3.7	3.0	2.2	1.5	0.7
3	3.7	2.9	2.2	1.5	0.8
1	3.6	2.9	2.2	1.4	0.7
IP-28					
Pressure Drop Mixer (bar)	**Pressure Drop Heat Exchanger (bar)**				
	0.5	**0.4**	**0.3**	**0.2**	**0.1**
5	12.5	11.0	9.6	8.1	6.7
3	10.5	9.0	7.5	6.1	4.6
1	8.5	7.0	5.5	4.0	2.6

Thus, the pressure drops in the mixer and in each heat exchanger can have some important effect on the cooling duties in the intermediate pressure cases. In the high pressure ones, their effect is not so important.

In the following table, the water pumping duties for all the cases, considering that the mixing temperature is 30° C, are presented.

Table 9.12 Water Pumping Duties (kW) – Pressure Drop

HP-14/HP-28			
Pressure Drop Mixer (bar)	**Life-stages of the well**		
	Early life	**Max injection**	**Late life**
5	6681	9353	5923
3	6601	9241	5853
1	6535	9149	5794
IP-14			
Pressure Drop Mixer (bar)	**Life-stages of the well**		
	Early life	**Max injection**	**Late life**
5	6755	9425	6032
3	6681	9322	5966
1	6607	9219	5901
IP-28			
Pressure Drop Mixer (bar)	**Life-stages of the well**		
	Early life	**Max injection**	**Late life**
5	6807	9477	6050
3	6733	9374	5985
1	6660	9271	5920

From this table, it can be observed that, in all the cases, the effect of the pressure drop in the mixer is minimal. In the intermediate pressure cases the water pumping duties are greater because the volume that has to be pumped is greater than this in the high pressure ones.

9.4 Effect of Pressure Ratio

The minimum compression work is obtained when each stage of a multistage unit does the same amount of work, and, thus, most compressors will have approximately the same pressure ratio for each stage. Some alternative cases for case HP-14 are presented, assuming that the mixing temperature is 30° C.

Table 9.13 Alternative Case 1 for pressure ratios

Compression Stage	Pressure Ratios – Alternative Case 1
1	2.809
2	2.709
3	2.709
4	2.209
5	2.635

Table 9.14 Alternative Case 2 for pressure ratios

Compression Stage	Pressure Ratios – Alternative Case 2
1	2.554
2	2.754
3	2.254
4	2.854
5	2.654

The compression and cooling duties for these cases are presented in the following table.

Table 9.15 Compression and Cooling Duties – Alternative Cases for pressure ratios

Cases	Compression Duties (kW)	Cooling Duties (kW)
	HP-14	HP-14
1	1356	2451
2	1362	2457

It is observed that the compression and the cooling duties are greater when the pressure ratio is not the same in each compression stage. Its effect though, comparing Tables 9.16 and 8.3, is not important.

10 Discussion

The Duan and Sun 2003, Duan et al. 2006 and equilibrium model describe the CO_2 solubility in systems like water-CO_2 and water-NaCl brines-CO_2. The advantage of the first two models is that the fugacity coefficient of CO_2 in the liquid phase is calculated with a non-iterative method and as a result the calculation of the CO_2 solubility requires much less computational time. Their main disadvantage is that they are only able to calculate this solubility and not to describe the equilibrium in the system CO_2-water-NaCl. The equilibrium model, though, is able to predict the fugacities of both components (CO_2 and H_2O), in both the liquid and the vapor phase. The latter is also more accurate in the prediction of CO_2's solubility in higher salinities, more than 4 molality.

The inclusion of the impurities' effect on CO_2 solubility is considered of first priority and, thus, the model of Li et al. 2018 is studied and used for the simulation. After comparing it with both binary and ternary systems, it is shown that its main disadvantage is that it underestimates the CO_2 solubility.

The most important factors that affect the latter are the pressure, the temperature, the salinity and the impurities' content. It is observed that the solubility increases with pressure, decreases with salinity and impurities' content. The influence of the temperature is more complex. Its effect varies according to the values of the aforementioned factors. In general, in temperatures below 100^o C the solubility decreases, whereas over 100^{o}C it increases with it.

The model of Li et al. 2018 is implemented in Unisim for the thermodynamic description of the system CO_2-N_2-O_2-water-NaCl brines in the carbonated water injection process, because of the incapability of the already existing thermodynamic models to predict the effect of salinity and hydrogen bonding. The salinity is introduced in the simulator through the addition of a pseudocomponent that represents the concentration of ions that form NaCl. NaCl is considered to be the salt that has the greater influence on the CO_2 solubility. It should be noted that, despite that the model of Li et al. 2018 predicts the equilibrium in the aforementioned system, it is not able to calculate the thermodynamic properties of the fluid and therefore Peng-Robinson is used. It is proven that Peng-Robinson simulates in a better way the behavior of Li et al.'s model than the other available models, like Soave-Redlich-Kwong. The parameters used by its fluid package are not analyzed in this master thesis.

The modelling of the carbonated water injection process that is proposed consists of mixing a water-brine with a CO_2 stream. The CO_2 stream is compressed through a multi-stage compression with intercooling scheme and the water is pumped in the same pressure. This takes place, so that the whole amount of CO_2 is dissolved. Then, the final stream enters through a flash separator and the liquid product of it is the carbonated water.

One of the most important characteristics of the CWI process is that, for standard quantities of water-brine and CO_2, the raise of pressure doesn't not have the same impact on the increase of the CO_2 solubility (Figures 6.2-6.6). As a result, since the access to compression's power in an offshore installation is difficult, the unnecessary compression to a higher pressure needs to be avoided.

The simulation results of the case study indicate that the needed duties, for the production of carbonated water, in terms of values, are sorted as following: water pumping duties > cooling duties > compression duties. The pumping duties, though, are of similar values in both intermediate and high pressure cases. The comparison of the compression and cooling duties

suggests that the compression of the CO_2 stream in an intermediate pressure has the advantage over the immediate compression at 180 bar.

More specifically, the energy savings on the cooling and the compression duties are presented in Table 8.8 and could reach 25-45% for the compression and 49-63% for the cooling ones. It is observed that the lower the CO_2 quantity that is about to be dissolved the greater are the energy savings on the compression and the cooling duties. More savings are noticed in the cooling duties.

It should be noted, though, that the intermediate pressure cases require a second pump, which increases the CAPEX of the process. As a result, they offer less flexibility. In terms of cost, despite the fact that the compressors in the high pressure cases are larger in size, the cost of the second pump in the intermediate pressure ones plays a critical role. The most important costs of a pump are the maintenance and the energy ones. In this work, it is shown that the energy costs of the intermediate and the high pressure cases are of similar values. The maintenance costs, though, play an important role, since a possible inaccuracy of the model in the calculation of the intermediate pressure could lead to vapor CO_2 at pump inlet and, therefore, to cavitation.

The sensitivity analysis indicates that the type of compression (one vs multi-stage) is very crucial, since 18-27 and 44% savings on the compression duties can be achieved in the intermediate and high pressure cases respectively. Moreover, the outlet temperature, in the one-stage compression, is very high and can lead to the degradation of the materials used.

The thermodynamic approach to equilibrium in the mixing process plays an important role in the intermediate pressure cases, since 2-8 and 3-9% losses on the compression and the cooling duties can take place, as it ranges from 95 to 85%, which are typical values as mixing measures.

The pressure drops in each heat exchanger and the mixer are considered to be the most critical factor on the compression and the cooling duties. Their effect on the first can be up to 13-23% in the intermediate pressure cases and up to 7% in the high pressure ones. On the latter it can reach the level of 13-21% and 4% in the intermediate and high pressure ones respectively. Despite their influence, in terms of energy, the intermediate pressure cases are still more profitable.

Knowing that the minimum work is achieved when each compression stage has the same pressure ratio, diverse pressure ratios are tested. It is noticed that they have minimal effect on the compression and cooling duties.

Even after the study of the effect of these factors, in terms of energy requirements, the intermediate pressure cases remain more profitable than the high pressure ones.

11 Conclusions and Future Work

In this work, an evaluation of the models that accurately predict the solubility of CO_2 in saline aqueous solutions for a wide range of pressures, temperatures and salinities was studied. A model based on the methodology followed by Pappa (2019, pers. comm., 1 October) was developed for this purpose and also the model proposed by Duan and Sun (2003) was studied. In conclusion, the equilibrium model presented and the model of Duan and Sun (2003) are similar. The equilibrium model has an advantage over the Duan and Sun's (2003) model at salinities higher than 4 molality.

The need for the inclusion of impurities' content, such as O_2 and N_2, led to the evaluation of models that give accurate predictions for the solubility of CO_2 in the system: CO_2-N_2-O_2-H_2O-NaCl. The model of Li et al. (2018), as a result, was studied. The basic advantage over the Duan and Sun (2003) and the equilibrium model is that the effect of impurities (N_2 and O_2) is implemented. On the other hand, the main disadvantage is that it is not so accurate in the prediction of the CO_2 solubility in the system: CO_2-H_2O-NaCl.

Despite the fact that the equilibrium model predicts the solubility of carbon dioxide accurately, there is some room for improvement. A future work that is suggested is that, for the correlations of $H^*_{CO_2}$ and $\bar{v}^{\infty}_{CO_2}$, only experimental data should be used and not generated ones like those of Duan and Sun (2003). The same work could be done by using a wider variety of experimental data of binary and ternary systems, in order to predict the solubility of carbon dioxide in the system CO_2-N_2-O_2-H_2O-NaCl.

The model of Li et al. 2018 was implemented in Unisim via CAPE-OPEN, because the already existing thermodynamic models don't include the effect of the hydrogen bonding and the salinity. The effect of the latter was introduced through the creation of a pseudocomponent "Na+*", representing this way the concentration of inorganic salt NaCl. For the rest of the thermodynamic properties the model of Peng-Robinson is used.

For the implementation of the thermodynamic model in the process simulation, further work should be done. Based on experimental data, correlations could be made for the liquid phase, in order to estimate more accurately some of the most important properties of the system CO_2-N_2-O_2-H_2O-NaCl, like the density or the heat capacity.

Another point that could be tested more is the setup of the fluid package Peng-Robinson. The effect of the different combinations of the options: Enthalpy, Density, Modify H2 Tc and Pc, Viscosity, Peng-Robinson Options and Water Solubility Option, could be tested. Moreover, a more detailed analysis on the introduction of the salinity in Unisim could be done. More specifically, the selection of the pseudocomponent's properties could be investigated more.

For the process simulation that is used for the carbonated water injection, the scheme of multistaging compression with intercooling is considered. As it is already mentioned, the pressure of the carbonated water should be 180 bar. Two cases were studied in order to reach this pressure: a) the pumping of water and the compression of carbon dioxide in an intermediate pressure and then the final pumping in the pressure of 180 bar and b) the immediate pumping of the water and the compression of the carbon dioxide.

The intermediate pressures were calculated so that the whole quantity of carbon dioxide is dissolved in the water injection stream. The comparison of these two cases consisted of comparing the compression, cooling and water pumping duties that are consumed. It is

concluded that the first case is more advantageous than the later one, since the compression and the cooling duties are considerably lower and the water pumping ones have a similar value.

In the sensitivity analysis, the effect on the duties of the most important factors that affect the dissolution pressure was studied. It was proven that the multi-stage compression is far more advantageous than the one-stage one. It was, also, observed that the compression and the cooling duties raise as the thermodynamic approach to equilibrium lowers. They, moreover, raise with the pressure drops in each heat exchanger and the mixer and as the pressure ratios are different in each compression stage. The water pumping duties are of similar value in all the cases. None of these factors, alternated the initial selection of the intermediate pressure case.

A more thorough analysis could be done for the selection between the intermediate and the high pressure case. The cost of the whole offshore installation could be also examined. The combination of these two factors would completely describe the process of the carbonated water injection.

References

1. Tassios, D.P. (2001) Applied Chemical Engineering Thermodynamics. Athens: N.T.U.A. University Press.(in Greek)

2. Søreide, I.; Whitson, C.H. (1992) Peng-Robinson predictions for hydrocarbons, CO_2, N_2 and H_2S with pure water and NaCl brine, *Fluid Phase Equilibria,* 77, pp. 217-240. Available at: http://www.ipt.ntnu.no/~curtis/courses/PhD-PVT/PVT-HOT-Vienna-May-2016x/e-course/Papers/misc/FPE-water-HC-paper-Soreide-Whitson.pdf

3. Firoozabadi, A.; Nutakki, R.; Wong, T.W.; Aziz, K. (1988) EOS Predictions of Compressibility and Phase Behavior in Systems Containing Water, Hydrocarbons, and CO_2, *SPE Reservoir Engineering,* 3(2), pp. 673-684. doi: 10.2118/15674-PA

4. Peng, D.Y.; Robinson, D.B. (1980) Two- and Three-Phase Equilibrium Calculations for Coal Gasification and Related Processes. *Thermodynamics of Aqueous Systems with Industrial Applications,* pp. 393-414. doi: 10.1021/bk-1980-0133.ch020

5. Pappa, G.D.; Perakis, C.; Tsimpanogiannis, I.N.; Voutsas, E.C. (2009) Thermodynamic Modeling of the Vapor-Liquid Equilibrium of the CO_2/H_2O mixture, *Fluid Phase Equilibria,* 284, pp. 56-63. doi: 10.1016/j.fluid.2009.06.011

6. Ji, X.; Tan, S.P.; Adidharma, H.; Radosz, M. (2005) SAFT1-RPM Approximation Extended to Phase Equilibria and Densities of CO_2-H_2O and CO_2-H_2O-NaCl Systems, *Industrial Engineering Chemical Research,* 44, pp. 8419-8427. doi: 10.1021/ie050725h

7. Li, Y.K.; Nghiem, L.X. (1986) Phase Equilibria of Oil, Gas and Water/Brine Mixtures from a Cubic Equation of State and Henry's Law, *The Canadian Journal of Chemical Engineering,* 64, pp. 486-496. doi: 10.1002/cjce.5450640319

8. Enick, R.M.; Klara, S.M. (1990) CO_2 Solubility in Water and Brine under Reservoir Conditions, *Chemical Engineering Communications,* 90(1), pp. 23-33. doi: 10.1080/00986449008940574

9. Diamond, L.W.; Akinfiev, N.N. (2003) Solubility of CO_2 in Water from -1.5 to 100 °C and from 0.1 to 100 MPa: evaluation of literature data and thermodynamic modelling, *Fluid Phase Equilibria,* 208, pp. 265-290. doi: 10.1016/S0378-3812(03)00041-4

10. Spycher, N.; Pruess, K.; Ennis-King, J. (2003) CO_2-H_2O mixtures in the geological sequestration of CO_2. I. Assessment and Calculation of Mutual Solubilities from 12 to 100 °C and up to 600 bar, *Geochimica and Cosmochimica Arta,* 67(16), pp. 3015-3031. doi: 10.1016/S0016-7037(03)00273-4

11. Nighswander, J.A.; Kalogerakis, N.; Mehrotra, A.K. (1989) Solubilities of Carbon Dioxide in Water and 1 wt% NaCl Solution at Pressures up to 10 MPa and Temperatures from 80 to 200 °C, *Journal of Chemical and Engineering Data,* 34(3), pp. 355-360. doi: 10.1021/je00057a027

12. Duan, Z.; Sun, R. (2003) An Improved Model Calculating CO_2 Solubility in Pure Water and Aqueous NaCl Solutions from 273 to 533 K and from 0 to 2000 bar, *Chemical Geology,* 193, pp. 257-271. doi: 10.1016/S0009-2541(02)00263-2

13. Duan, Z.; Sun, R.; Zhu, C.; Chou, I.-M. (2006) An Improved Model for the Calculation of CO_2 Solubility in Aqueous Solutions Containing Na^+, K^+, Ca^{2+}, Mg^{2+}, Cl^-, SO_4^{2-}, *Marine Chemistry,* 98, pp. 131-139. doi: 10.1016/j.marchem.2005.09.001

14. Sørensen, H.; Pedersen, K.S.; Christensen P.L. (2002) Modeling of gas solubility in brine, *Organic Geochemistry,* 33, pp. 635-642. doi: 10.1016/S0146-6380(02)00022-0

15. Li, J.; Ahmed, R.; Li, X. (2018) Thermodynamic Modeling of CO_2-N_2-O_2-Brine-Carbonates in Conditions from Surface to High Temperature and Pressure, *Energies,* 11, pp. 2627-2645. doi: 10.3390/en11102627

16. Duan, Z.; Moller, N.; Greenberg, J.; Weare, J.H. (1992) The Prediction of Methane Solubility in Natural Waters to High Ionic Strength from 0 to 25 °C and from 0 to 1600 bar, *Geochimica et Cosmochima Acta,* 56, pp. 1451-1460. doi: 10.1016/0016-7037(92)90215-5

17. Duan, Z.; Moller, N.; Weare, J.H. (1992) An Equation of State for the–CO_2–H_2O System: Pure Systems for 0 to 1000 °C and 0 to 8000 bar, *Geochimica et Cosmochimica Acta,* 56, pp. 2605-2617. doi: 10.1016/0016-7037(92)90347-L

18. Pitzer, K.S (1973) Thermodynamics of Electrolytes. I. Theoretical Basis and General Equations, *The Journal of Physical Chemistry,* 77(2), pp. 268-277. doi: 10.1021/j100621a026

19. Pitzer, K.S.; Pelper, J.C.; Busey, R.H. (1984) Thermodynamic Properties of Aqueous Sodium Chloride Solutions, *J. Phys. Chem. Ref. Data,* 13(1). doi: 10.1063/1.555709

20. Helgeson, H.C.; Kirkham, D.H.; Flowers, G.C. (1981) Theoretical Prediction of the Thermodynamic Behavior of Aqueous Electrolytes at High Pressures and Temperatures: IV. Calculation of Activity Coefficients, and Apparent Molal and Standard and Relative Partial Molal Properties to 600° C and 5 KB, *American Journal of Science,* 281(10), pp. 1249-1516. doi: 10.2475/ajs.281.10.1249

21. Bradley, D.J.; Pitzer, K.S. (1979) Thermodynamics of Electrolytes. 12. Dielectric Properties of Water and Debye-H*ü*ckel Parameters to 350° C and 1 kbar, *The Journal of Physical Chemistry,* 83(12), pp. 1599. doi: 10.1021/j100475a009

22. Takenouchi, S.; Kennedy, G.C. (1965) The Solubility of Carbon Dioxide in NaCl Solutions at High Temperatures and Pressures, *American Journal of Science,* 263, pp. 445-454. doi: 10.2475/ajs.263.5.445

23. Rumpf, B.; Nicolaisen, H.; Ocal, C.; Maurer, G. (1994) Solubility of Carbon Dioxide in Aqueous Solutions of Sodium Chloride: Experimental Results and Correlation, *Journal of Solution Chemistry,* 23(3), pp. 431-448. doi: 10.1007/BF00973113

24. Yan, W.; Huang, S.; Stenby, E.H. (2011) Measurement and Modeling of CO_2 Solubility in NaCl Brine and CO_2-saturated NaCl Brine Density, *International Journal of Greenhouse Gas Control,* 5, pp. 1460-1477. doi: 10.1016/j.ijggc.2011.08.004

25. Bando, S.; Takemura, F.; Nishio, M.; Hihara, E.; Akai, M. (2003) Solubility of CO_2 in Aqueous Solutions of NaCl at (30 to 60) °C and (10 to 20) MPa, *J. Chem. Eng. Data,* 48, pp. 576-579. doi: 10.1021/je0255832

26. King, M.B.; Mubarak, A.; Kim, J.D.; Bott, T.R. (1992) The Mutual Solubilities of Water with Supercritical and Liquid Carbon Dioxide, *The Journal of Supercritical Fluids,* 5, pp. 296-302. doi: 10.1016/0896-8446(92)90021-B

27. Wiebe, R; Gaddy, V.L. (1940) The Solubility of Carbon Dioxide in Water at Various Temperatures from 12 to 40 °C and at Pressures to 500 Atmospheres. Critical Phenomena*, J. Am. Chem. Soc.,* 62(4), pp. 815-817. doi: 10.1021/ja01861a033

28. Geng, M.; Duan, Z. (2010) Prediction of oxygen solubility in pure water and brines up to high temperatures and pressures, *Geochimica et Cosmochimica Acta,* 74, pp. 5631-5640. doi: 10.1016/j.gca.2010.06.034

29. Mao, S.; Duan, Z. (2006) A thermodynamic model for calculating nitrogen solubility, gas phase composition and density of the N_2-H_2O-NaCl system, *Fluid Phase Equilibria,* 248, pp. 103-114. doi: 10.1016/j.fluid.2006.07.020

30. Liu, Y.; Hou, M.; Ning, H.; Yang, D.; Yang, G.; Han, B. (2012) Phase Equilibria of CO_2+N_2+H_2O and N_2+CO_2+H_2O+NaCl+KCl+$CaCl_2$ Systems at Different Temperatures and Pressures, *Journal of Chemical & Engineering data,* 57, pp. 1928-1932. doi: 10.1021/je3000958

31. Czerwienski, G.J; Tomasula, P.; Tassios, D. (1988) Vapor-Liquid Equilibria with the vdW-711 Equation of state, *Fluid Phase Equilibria,* 42, pp. 63-83. doi: 10.1016/0378-3812(88)80050-5

32. Prausnitz, J. M.; Lichtenthaler, R.N.; Azevedo E.G. (1999) *Molecular Thermodynamics of Fluid-Phase Equilibria.* 3rd edn. New Jersey: Prentice-Hall.

33. Canjar, L.N.; Manning, F.S. (1967) *Thermodynamic Properties and Reduced Correlations for Gases*. Texas: Gulf Publishing Co.

34. Liu, Y.; Hou, M.; Yang, G.; Han, B. (2011) Solubility of CO_2 in Aqueous Solutions of NaCl, KCl, $CaCl_2$ and their Mixed Salts at Different Temperatures and Pressures, *J. of Supercritical Fluids,* 56, pp. 125-129. doi: 10.1016/j.supflu.2010.12.003

35. Koschel, D.; Coxam, J.Y.; Rodier, L.; Majer, V. (2006) Enthalpy and Solubility Data of CO_2 in Water and NaCl(aq) at Conditions of Interest for Geological Sequestration, *Fluid Phase Equilibria,* 247, pp. 107-120. doi: 10.1016/j.fluid.2006.06.006

36. Hangx, S.J.T. (2005) Subsurface Mineralisation: Rate of CO_2 Mineralisation and Geomechanical Effects on Host and Seal Formations. Behavior of the CO_2-H_2O System and Preliminary Mineralization Model and Experiments, *CATO Workpackage WP,* 4(1), pp. 1-43.

37. Esene, C.; Rezaei N.; Aborig, A.; Zendehboudi, S. (2019) Comprehensive Review of Carbonated Water Injection for Enhanced Oil Recovery, *Fuel,* 237, pp. 1086-1107. doi: 10.1016/j.fuel.2018.08.106

38. Ervik, A.; Westman, S.F.; Hammer, M.; Skaugen, G.; Lilliestrale, (2012) *A Review of Experimental Data for CO_2 Solubility in NaCl Brine. For Temperatures 273-373 K and Pressure 10-120 bar*. Internal SINTEF Energy Research Report.

39. Boström, M.; Ninham, B.W. (2004) Contributions from Dispersion and Born Self-Free Energies to the Solvation Energies of Salt Solutions, *J. Phys. Chem. B,* 108(33), pp. 12593-12595. doi: 10.1021/jp048517a

40. Wang, J.; Ryan D.; Anthony, E.J.; Wigston, A. (2011) *Effects of Impurities on Geological Storage of CO_2*. (IEAGHG-2011/04). Available at: https://ieaghg.org/docs/General_Docs/Reports/2011-04.pdf (Accessed: June 23, 2020).

41. Nguyen, T.A.; Ali, F. (1998) Effect of Nitrogen on the Solubility and Diffusivity of Carbon Dioxide into Oil and Oil Recovery by the Immiscible WAG Process, *The Journal of Canadian Petroleum Technology,* 37(2), pp. 24-31. doi: 10.2118/98-02-02

42. *NeqSim* (2020) Available at: https://equinor.github.io/neqsimhome/ (Accessed: June 24, 2020).

43. Witkowski, A.; Majkut, M. (2012) The Impact of CO_2 Compression Systems on the Compressor Power Required for a Pulverized Cola-Fired Power Plant in Post-Combustion Carbon Dioxide Sequestration, *The Archive of Mechanical Enginnering,* LIX(3), pp. 343-360. doi: 10.2478/v10180-012-0018-x

44. El-Suleiman, A.; Anosike, N.B; Pilidis P. (2016) A Preliminary Assessment of the Initial Compression Power Requirement in CO_2 Pipeline "Carbon Capture and Storage (CCS) Technologies", *Technologies,* 4(15), pp. 1-9. doi: 10.3390/technologies4020015

45. Yang, H.C.; Park, S.K. (2004) Pressure Drop in Motionless Mixers, *KSME International Journal,* 18(3), pp. 526-532. doi: 10.1007/BF02996117

46. Li, H.Z.; Fasol, Ch.; Choplin, L. (1996) Hydrodynamics and Heat Transfer of Rheologically Complex Fluids in a Sultzer SMX Statix Mixer, *Chemical Engineering Science,* 51(10), pp. 1947-1955. doi: 10.1016/0009-2509(96)00052-8

47. Bahadori, A. (2014) *Natural Gas Processing Technology and Engineering Design.* Waltham: Gulf Professional Publishing.

48. Smith, R. (2005) *Chemical Process Design and Integration.* Chichester: John Wiley and Sons.

49. Kidnay, A.J.; Parrish, W.R. (2006) *Fundamentals of Natural Gas Processing.* Boca Raton: Taylor and Francis Group.

50. Eke, P.E.; Naylor, M.; Haszeldine, S.; Curtis, A. (2011) CO_2/Brine Surface Dissolution and Injection: CO_2 Storage Enhancement, *SPE Projects, Facilities & Construction,* 6(1), pp. 41-53. doi: 10.2118/124711-PA

51. *Sizing the Admixer™ Static Mixer and Sanitary Static Blender* (1998) Available at: https://www.admix.com/pdfs/admixer-tech102.pdf (Accessed: July 2, 2020)

52. Jones, R.A.; McIntush, K.E.; Wallace, C.B. (2010) Oxygen Removal from Natural Gas, *Proceedings of 89th Annual GPA convention*. Austin, March 21-24, 2010. Available at: http://trimeric.com/assets/oxygen-removal-in-natural-gas-systems-lrgcc-paper.pdf (Accessed: July 2, 2020)

53. *Oxygen Measurement in Natural Gas* (2016) Available at: http://www.michell.com/uk/documents/appnotes/Oxygen_Measurement_in_Natural_Gas.pdf (Accessed: 25 June 2020)

54. Van Baten, J. (2020) *CAPE-OPEN software design and development.* Available at: https://www.amsterchem.com/capeopen.html (Accessed: July 2, 2020)

55. Meijer, H.E.H.; Singh, M.K.; Anderson, P.D. (2011) On the performance of static mixers: A quantitative comparison, *Progress in Polymer Science,* 37, pp. 1333-1349. doi: 10.1016/j.progpolymsci.2011.12.004

Appendices

Appendix A

In this appendix, some more figures concerning the effect of pressure, temperature and salinity on the CO_2 solubility from Chapter 2, are presented.

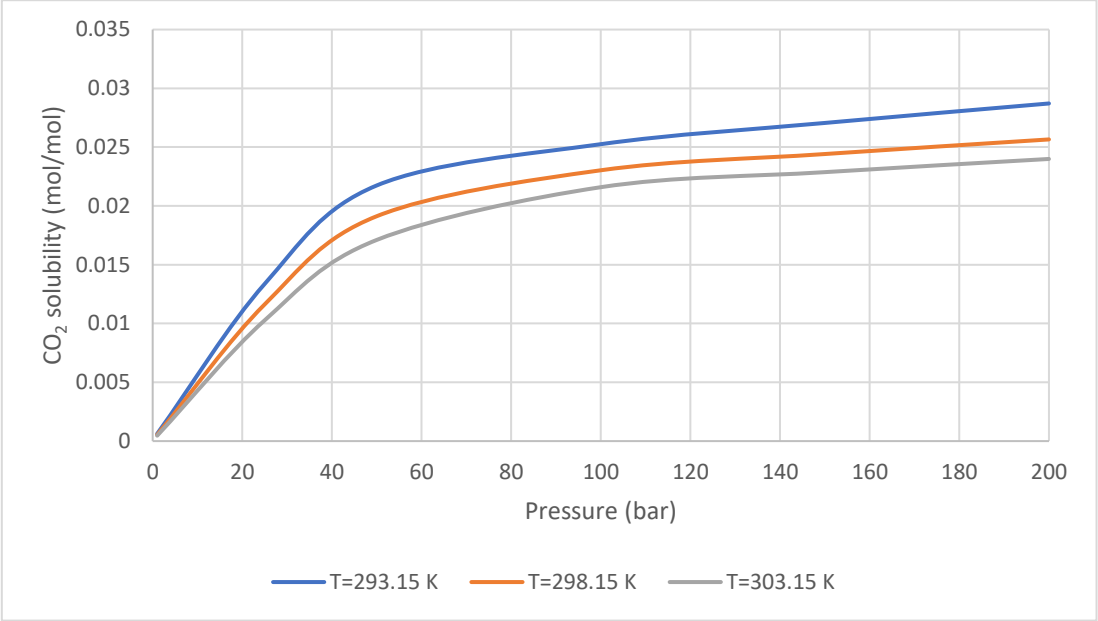

Figure A.1 CO_2 solubility using Li et al.'s 2018 model for the different temperatures (S=0 mol/kg solvent) as a function of pressure

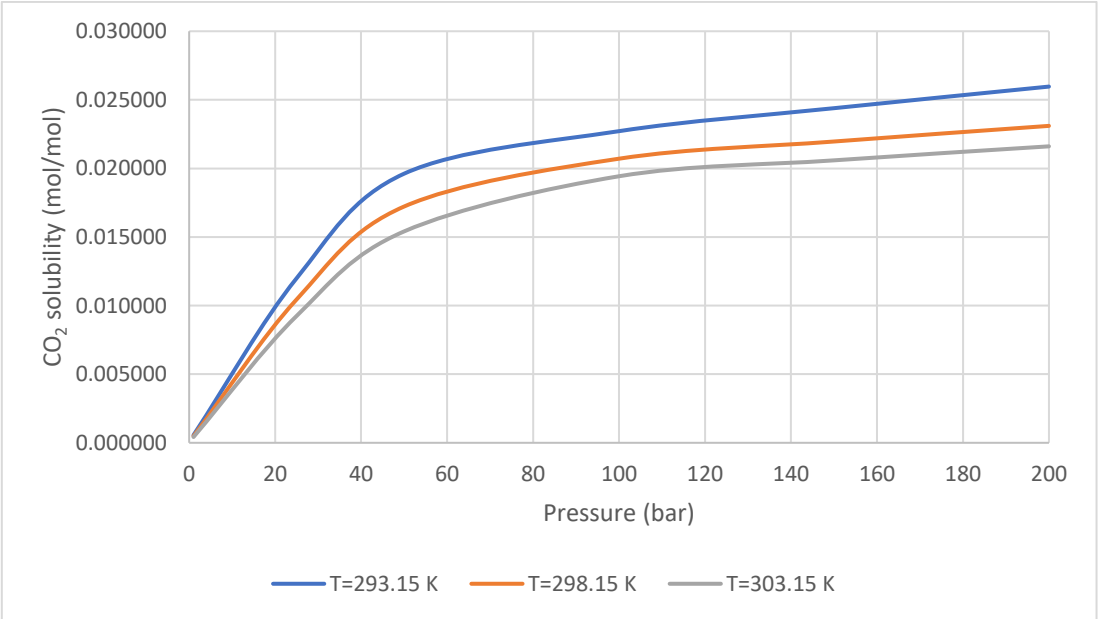

Figure A.2 CO_2 solubility using Li et al.'s 2018 model for the different temperatures (S=0.5 mol/kg solvent) as a function of pressure

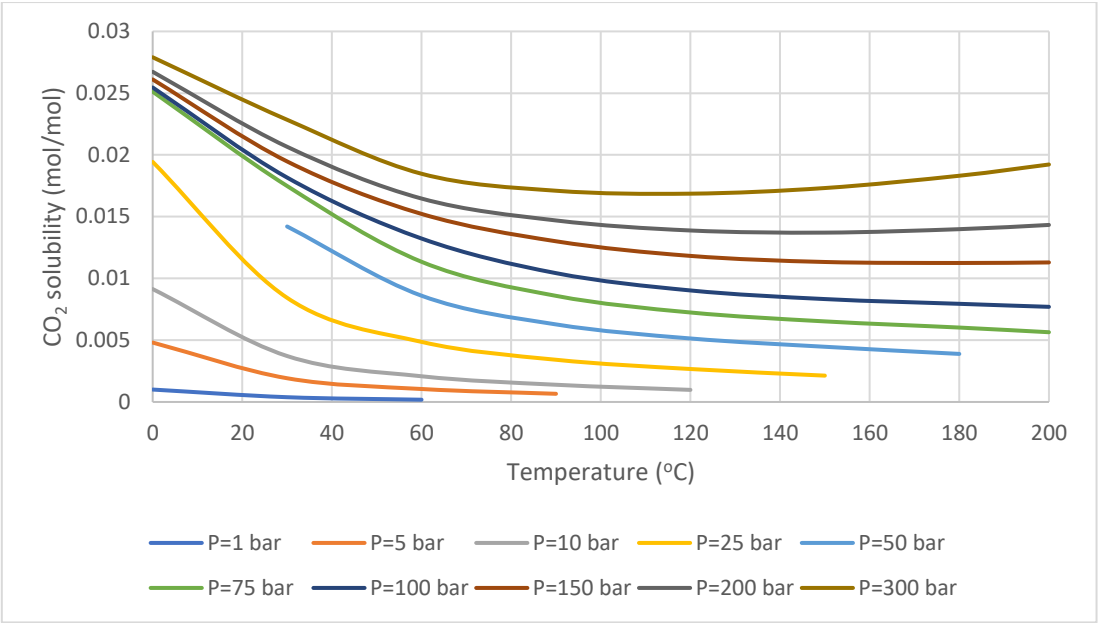

Figure A.3 CO_2 solubility using Li et al.'s 2018 model for the different pressures (S=0.5 mol/kg solvent) as a function of temperature

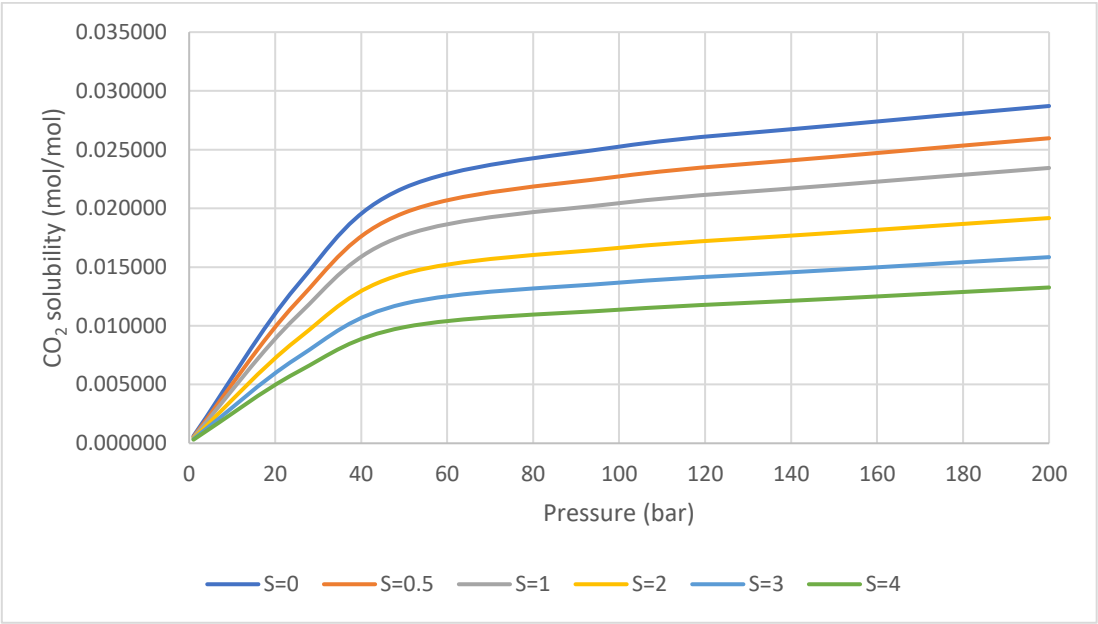

Figure A.4 CO_2 solubility using Li et al.'s 2018 model for the different salinities (T=293.15 K) as a function of pressure

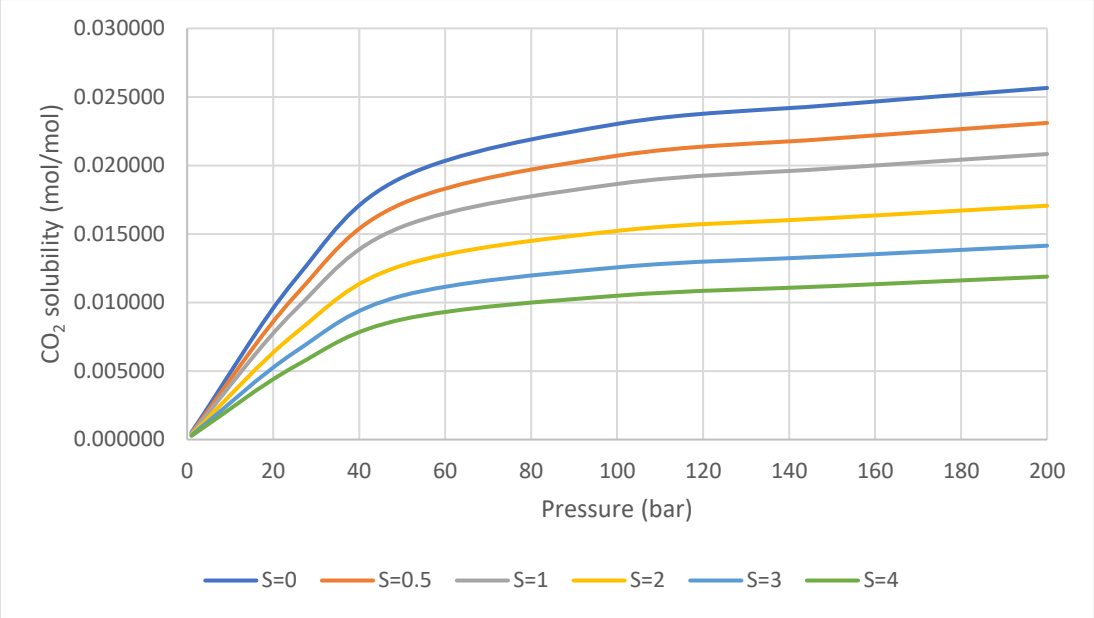

Figure A.5 CO_2 solubility using Li et al.'s 2018 model for the different salinities (T=298.15 K) as a function of pressure

Appendix B

The following tables and figures refer to the comparison of the model of Li et al. (2018) with experimental and generated data in both binary and ternary systems.

Table B.1 Errors % in CO_2 solubility in binary system: Model of Li et al. 2018

Salinity (mol/kg solvent)	T(K)	P(bar)	Model of Li et al. 2018	Bando et al. 2003	% error
0.1711	303.15	100	0.020922	0.02270	7.83
		150	0.022217	0.02350	5.46
		200	0.023337	0.02460	5.14
Average (%) error					**6.14**
Salinity (mol/kg solvent)	T(K)	P(bar)	Model of Li et al. 2018	Bando et al. 2003	% error
0.3492	303.15	100	0.02008	0.02150	6.63
		150	0.02132	0.02230	4.42
		200	0.02239	0.02320	3.48
Average (%) error					**4.84**
Salinity (mol/kg solvent	T(K)	P(bar)	Model of Li et al. 2018	Bando et al. 2003	% error
0.5292	303.15	100	0.01926	0.02090	7.86
		150	0.02044	0.02200	7.08
		200	0.02148	0.02270	5.37
Average (%) error					**6.77**

Table B.2 Errors % in CO_2 solubility in binary system: Model of Li et al. 2018

CO_2 solubility (mol/kg solvent)					
Salinity (mol/kg solvent)	T(K)	P(bar)	Model of Li et al. 2018	Duan and Sun 2003	% error
0	303.15	10	0.25728	0.28090	8.41
		50	0.98339	1.08110	9.04
		100	1.23938	1.36110	8.94
		200	1.38708	1.48890	6.84
1	303.15	10	0.21010	0.22940	8.41
		50	0.79400	0.87290	9.04
		100	0.99783	1.09580	8.94
		200	1.11697	1.19900	6.84
Average (%) error					**8.31**

Table B.3 Errors % in CO_2 solubility in ternary system: Model of Li et al. 2018

CO_2 solubility (mol/mol) in the ternary system (CO_2-N_2-H_2O)					
Salinity (mol/kg solvent)	T(K)	P(bar)	Model of Li et al. 2018	Liu et al. 2012	% error
0	308.15	160	0.01998	0.02290	12.76
			0.01938	0.02180	11.12
			0.01862	0.02040	8.71
			0.01626	0.01790	9.16
			0.01421	0.01570	9.51

Average (%) error	10.65

Table B.4 Errors % in CO_2 solubility in ternary system: Model of Li et al. 2018

N_2 solubility (mol/mol) in the ternary system (CO_2-N_2-H_2O)					
Salinity (mol/kg solvent)	T(K)	P(bar)	Model of Li et al. 2018	Liu et al. 2012	% error
0	308.15	160	0.00035	0.00033	7.13
			0.00042	0.00040	5.14
			0.00049	0.00049	0.41
			0.00066	0.00063	4.70
			0.00078	0.00079	1.01
Average (%) error					**3.68**

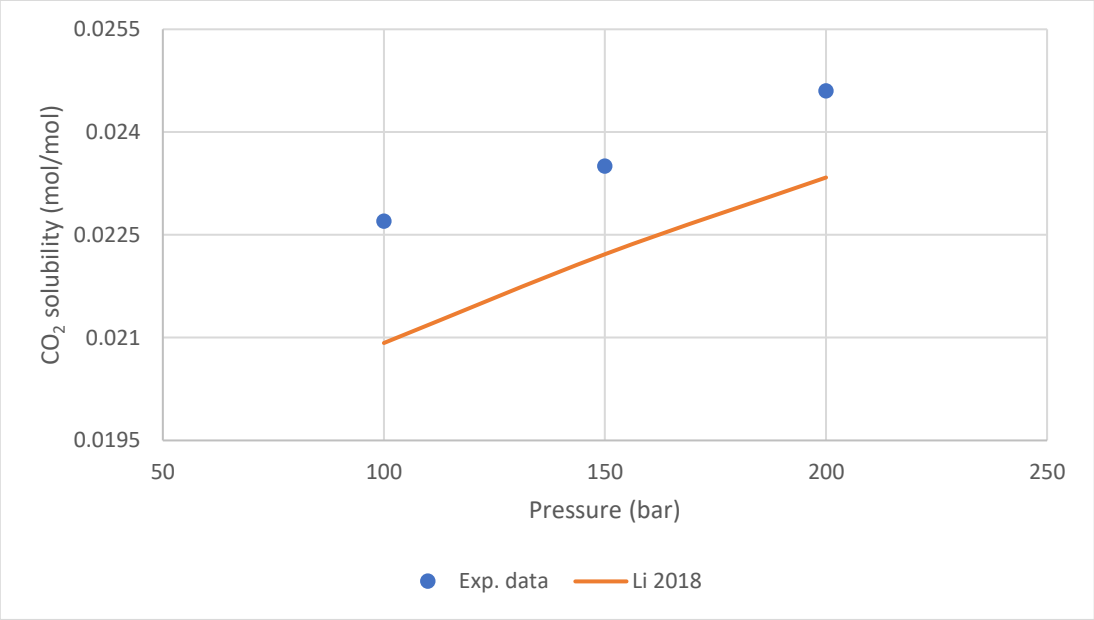

Figure B.1 Comparison of Li et al. 2018 model's predictions with the experimental data of Bando et al. 2003 (T=303.15 K, S=0.1711 molality) as a function of pressure

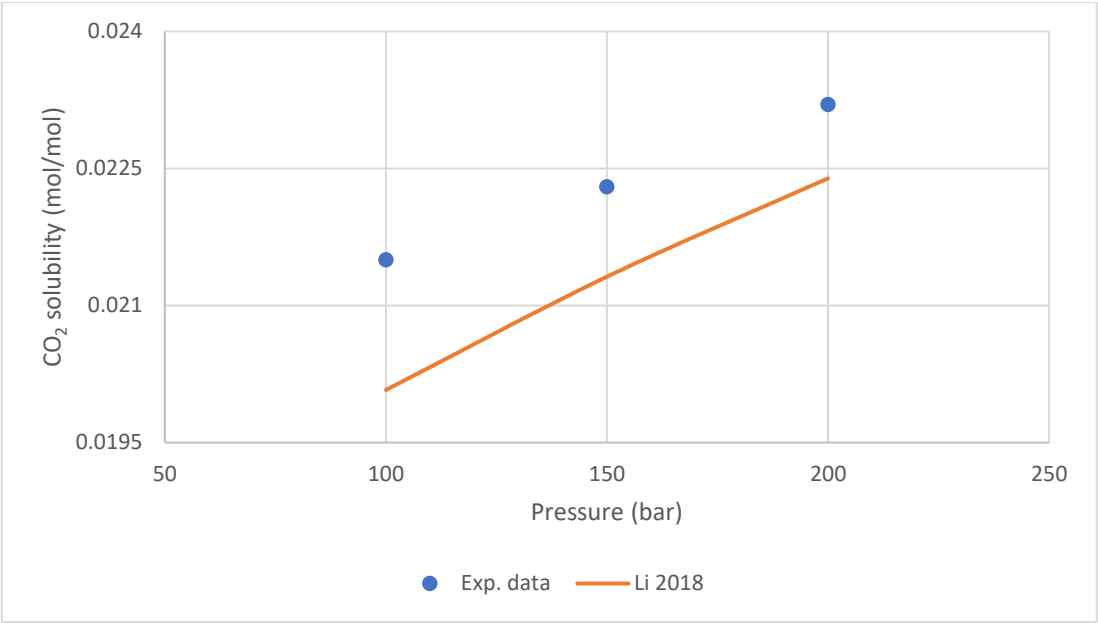

Figure B.2 Comparison of Li et al. 2018 model's predictions with the experimental data of Bando et al. 2003 (T=303.15 K, S=0.3492 molality) as a function of pressure

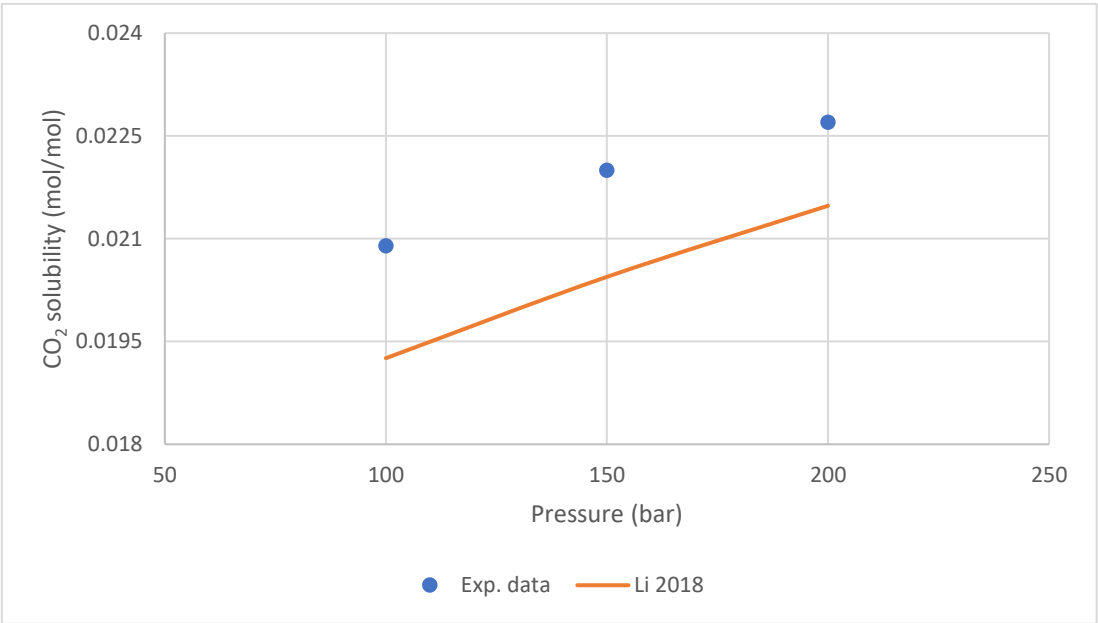

Figure B.3 Comparison of Li et al. 2018 model's predictions with the experimental data of Bando et al. 2003 (T=303.15 K, S=0.5292 molality) as a function of pressure

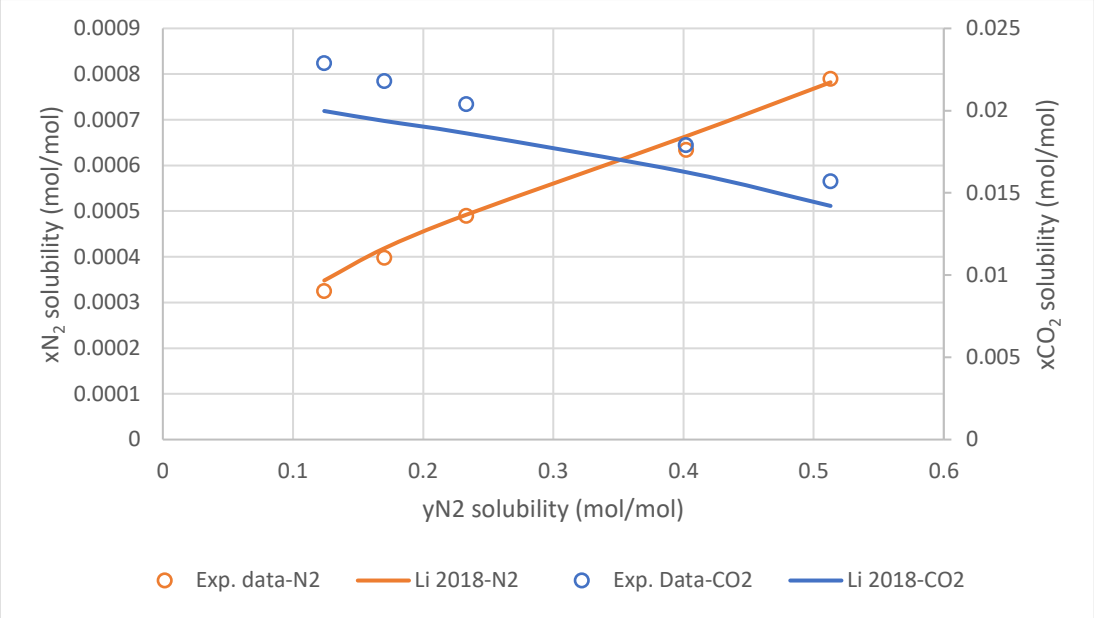

Figure B.4 Comparison of Li et al. 2018 model's predictions with the experimental data of Liu et al. 2012 (T=308.15 K, P=160 bar, S=0 molality) as a function of pressure

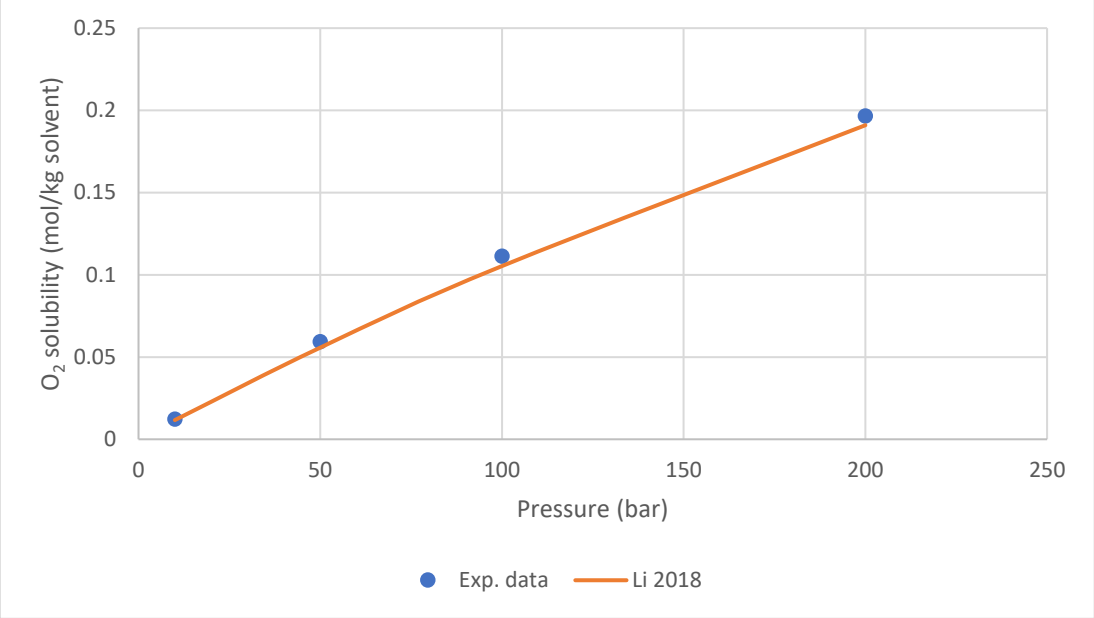

Figure B.5 Comparison of Li et al. 2018 model's predictions with the generated data of Geng and Duan 2010 (T=303 K, S=0 molality) as a function of pressure

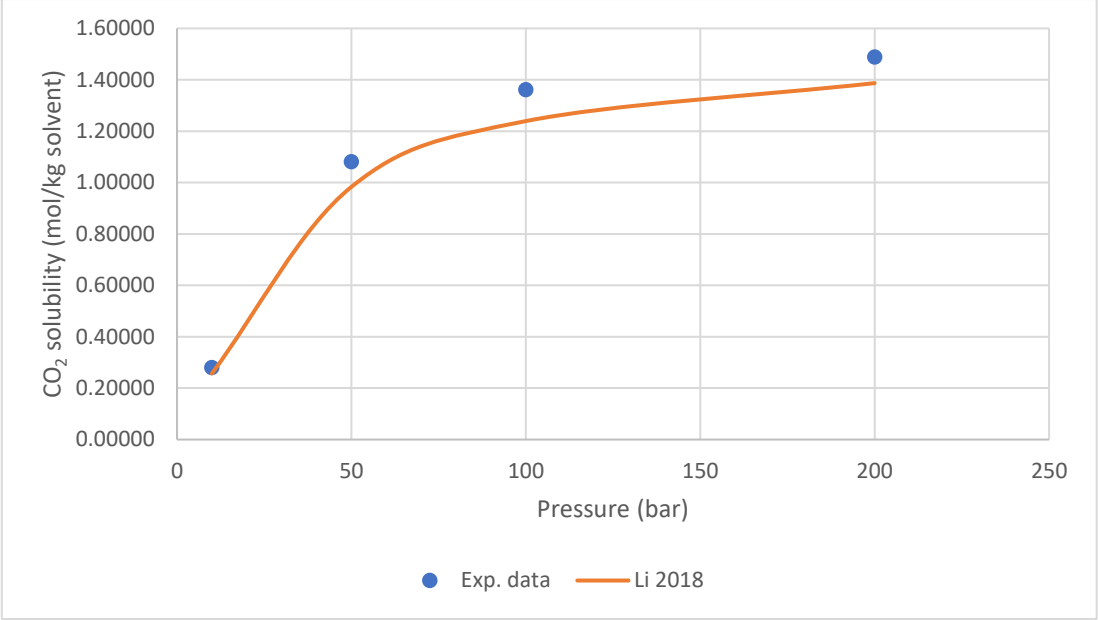

Figure B.6 Comparison of Li et al. 2018 model's predictions with the generated data of Duan and Sun 2003 (T=303.15 K, S=0 molality) as a function of pressure

Appendix C

The comparison of the equilibrium model and the model of Duan et al. (2006) with experimental data takes place in the following table and figures.

Table C.1 Errors % in CO_2 solubility: Model of Duan et al. 2006-Equilibrium Model

Salinity (mol/kg solvent)	T (K)	P (bar)	%Error in CO_2 solubility this work	Duan et al. 2006
Experimental Data by Takenouchi and Kennedy 1965				
0	423.15	100	3.26	2.84
		200	6.79	4.72
		300	2.54	2.08
		400	1.33	1.34
		500	0.40	0.61
		600	0.63	0.28
		800	0.22	0.08
		1000	1.46	2.46
		1200	1.55	2.99
		1400	3.55	4.18
average % error			**2.17**	**2.16**
0	473.15	100	2.31	3.16
		200	8.67	7.06
		300	5.53	5.81
		400	5.99	6.37
		500	6.17	6.36
		600	5.39	5.36
		800	1.75	1.65
		1000	2.88	2.68
		1200	6.10	6.83
		1400	4.85	11.09
average % error			**4.96**	**5.64**
1.0922	423.15	100	7.42	6.68
		200	9.47	6.86
		300	3.92	3.24
		400	0.48	0.57
		500	0.82	0.43
		600	0.86	0.45
		800	1.70	1.78
		1000	1.01	2.59
		1200	0.61	1.52
		1400	0.01	2.96
average % error			**2.63**	**2.71**
1.0922	473.15	100	6.37	6.44
		200	6.04	3.77
		300	2.12	1.95
		400	0.46	0.48
		500	2.27	2.55
		600	1.68	2.29
		800	2.77	3.64
		1000	5.50	6.18

		1200	6.10	7.96
		1400	1.10	9.31
average % error			**3.44**	**4.46**
4.2779	423.15	100	35.67	41.95
		200	23.59	27.47
		300	13.97	14.25
		400	15.18	14.69
		500	13.94	13.61
		600	7.20	7.40
		800	1.97	3.41
		1000	0.14	3.12
		1200	3.70	0.48
		1400	8.24	1.18
average % error			**12.36**	**12.76**
overall % error			**5.11**	**5.54**
Experimental data by Rumpf et al. 1994				
3.997	313.16	4.67	0.01	9.56
	313.14	9.11	6.10	2.67
	313.14	19	7.82	0.86
	313.19	31.47	7.03	1.58
	313.19	51.23	8.93	4.77
	313.19	69.17	9.98	5.87
average % error			**6.65**	**4.22**
	333.13	6.25	7.31	6.44
	333.16	11.41	4.88	5.81
	333.16	13.28	7.22	2.47
	333.15	25.14	6.18	0.88
	333.16	28.71	8.05	1.64
	333.14	35.21	7.18	1.43
	333.17	47.37	8.13	3.44
	333.15	73.03	8.28	4.65
	333.16	96.42	9.13	5.90
average % error			**7.37**	**3.63**
	353.12	8.17	2.68	7.78
	353.12	16.42	4.76	5.17
	353.1	33.87	7.38	0.11
	353.1	55.92	7.58	2.58
	353.12	69.4	6.43	2.30
	353.11	83.37	8.17	4.70
	353.11	96.37	9.44	6.24
average % error			**6.63**	**4.13**
	393.07	12.04	7.11	7.44
	393.19	23.31	3.77	1.37
	393.1	47.42	5.30	0.32
	393.19	76.5	6.19	2.09
	393.12	93.28	5.52	2.31
average % error			**5.58**	**2.71**
	413.07	13.93	6.41	3.44
	413.08	25.5	5.77	3.56

	413.09	50.42	5.61	0.78
	413.07	86.71	6.09	2.63
average % error			**5.97**	**2.60**
	432.86	16.62	9.03	1.78
	432.96	28.58	6.20	3.17
	432.95	59.12	4.87	1.49
	432.98	90.48	5.37	0.45
average % error			**6.37**	**1.72**
5.999	313.31	6.02	3.67	5.78
	313.22	12.32	0.15	3.74
	313.28	26.4	1.35	5.35
	313.27	44.3	0.64	7.37
	313.31	67.99	0.09	9.59
	313.19	84.27	1.41	10.43
average % error			**1.22**	**7.04**
	333.12	8.2	2.64	7.78
	333.12	16.78	0.18	2.05
	333.1	36.57	1.03	5.76
	333	68.44	0.26	8.03
	333.05	86.7	1.07	9.46
average % error			**1.03**	**6.62**
	353.12	9.97	0.70	4.33
	353.11	20.32	0.76	0.67
	353.08	43.94	0.32	6.03
	353.1	76.1	1.33	5.64
	353.08	90.44	1.61	9.58
average % error			**0.94**	**5.25**
	393.17	14.21	1.59	4.56
	393.14	27.78	0.54	3.47
	393.13	59.37	1.61	3.32
	393.12	91.35	2.39	9.29
average % error			**1.53**	**5.16**
	413.09	16.61	1.00	4.33
	413.09	31.95	5.39	5.06
	413.09	62.91	0.63	4.68
	413.12	92.01	0.18	7.46
average % error			**1.80**	**5.38**
	433.07	18.98	3.97	0.33
	433.05	34.06	0.53	1.00
	433.08	65.78	0.04	5.68
	433.05	89.81	0.19	6.45
average % error			**1.18**	**3.36**
overall % error			**4.21**	**4.36**
Experimental data by Yan et al. 2011				
0	323.2	50	7.30	7.34
		100	11.64	5.38
		150	3.18	2.53
		200	0.74	0.50
		300	1.09	1.00

		400	0.20	2.42
average % error			**4.02**	**3.20**
	373.2	50	0.49	0.88
		100	3.38	3.09
		150	3.65	3.30
		200	3.68	3.88
		300	1.60	1.74
		400	0.83	1.79
average % error			**2.27**	**2.45**
	413.2	50	2.46	1.63
		100	1.10	0.06
		150	2.87	1.99
		200	2.20	1.64
		300	1.08	0.75
		400	1.76	1.42
average % error			**1.91**	**1.25**
1	323.2	50	7.20	6.14
		100	6.81	2.60
		150	2.13	2.24
		200	3.98	4.49
		300	0.17	1.66
		400	2.18	0.11
average % error			**3.74**	**2.87**
	373.2	50	11.55	11.27
		100	6.73	6.22
		150	2.96	2.55
		200	5.51	5.82
		300	1.35	2.15
		400	1.64	3.71
average % error			**4.96**	**5.29**
	413.2	50	2.26	3.98
		100	0.44	0.34
		150	8.11	6.98
		200	5.34	3.98
		300	10.02	9.49
		400	0.99	1.06
average % error			**4.53**	**4.30**
5	323.2	50	3.99	4.38
		100	2.10	3.64
		150	2.96	8.47
		200	3.27	3.65
		300	6.73	0.45
		400	9.64	1.29
average % error			**4.78**	**3.65**
	373.2	50	1.14	0.32
		100	2.38	3.43
		150	5.46	8.55
		200	9.31	13.71
		300	3.92	8.45
		400	15.13	3.14

average % error			**6.22**	**6.27**
	413.2	50	8.42	6.12
		100	1.57	2.12
		150	7.20	9.16
		200	12.94	15.48
		300	2.81	0.86
		400	4.96	0.65
average % error			**6.32**	**5.73**
overall % error			**4.31**	**3.89**
Experimental data by Liu et al. 2011				
0	308.15	21	10.89	9.07
		40.9	9.45	7.83
		60.8	9.77	7.74
		80.9	7.34	5.35
		100.8	5.52	6.15
		120.5	6.12	6.52
		140.1	8.11	7.64
		158.3	8.28	7.46
average % error			**8.18**	**7.22**
	318.15	20.8	8.10	6.98
		41	8.60	6.53
		60.9	7.96	6.23
		81.1	9.89	7.11
		100.8	9.85	7.49
		120.6	8.99	7.78
		141.1	7.95	7.02
		158.6	7.11	6.51
average % error			**8.56**	**6.96**
	323.15	21	7.04	5.41
		41.1	5.19	3.39
		61.2	6.42	4.58
		81	5.61	3.00
		101	6.65	2.87
		120.4	6.20	4.53
		159.9	4.01	3.44
average % error			**5.87**	**3.89**
	328.15	28.6	7.29	6.24
		43.7	8.79	7.21
		61.1	8.34	6.79
		84.8	7.64	5.55
		99.9	7.25	4.59
		122	7.99	5.57
		131.9	8.37	6.54
		152.3	6.55	5.38
average % error			**7.78**	**5.99**
1.9013	318.15	21	4.00	1.92
		40.9	0.90	0.91
		60.6	1.10	0.03
		81	0.86	1.29

		100.9	0.25	1.35
		121	0.33	0.32
		140.8	1.50	0.57
		158.3	1.79	0.49
average % error			**1.34**	**0.86**
overall % error			**6.36**	**5.01**
Experimental data by Bando et al. 2003				
0	303.15	100	1.41	0.35
		150	0.12	0.63
		200	0.76	1.44
average % error			**0.76**	**0.81**
	313.15	100	2.75	4.97
		150	2.70	3.09
		200	1.99	3.04
average % error			**2.48**	**3.70**
	323.15	100	1.00	2.81
		150	2.55	3.10
		200	0.82	0.91
average % error			**1.46**	**2.27**
	333.15	100	3.19	1.65
		150	1.10	0.63
		200	2.10	2.89
average % error			**2.13**	**1.72**
0.1711	303.15	100	0.36	0.67
		150	1.71	2.32
		200	1.50	2.11
average % error			**1.19**	**1.70**
	313.15	100	1.26	3.24
		150	2.18	2.64
		200	1.79	2.43
average % error			**1.74**	**2.77**
	323.15	100	0.20	3.99
		150	2.87	3.45
		200	0.18	0.44
average % error			**1.08**	**2.63**
	333.15	100	2.90	1.28
		150	1.27	0.61
		200	0.95	0.68
average % error			**1.71**	**0.86**
0.3492	303.15	100	1.51	2.30
		150	3.47	3.77
		200	3.57	4.21
average % error			**2.85**	**3.43**
	313.15	100	1.06	0.45
		150	0.38	0.74
		200	2.04	2.28
average % error			**1.16**	**1.16**
	323.15	100	0.45	3.58
		150	1.67	2.27

		200	0.40	0.44
average % error			**0.84**	**2.10**
	333.15	100	0.38	2.13
		150	1.84	0.09
		200	0.66	0.43
average % error			**0.96**	**0.89**
0.5292	303.15	100	0.91	1.28
		150	1.39	1.23
		200	2.62	2.51
average % error			**1.64**	**1.67**
	313.15	100	0.07	1.31
		150	0.80	0.84
		200	0.97	0.83
average % error			**0.61**	**1.00**
	323.15	100	0.97	2.70
		150	0.67	1.18
		200	0.33	0.24
average % error			**0.66**	**1.37**
	333.15	100	2.59	0.85
		150	0.85	0.78
		200	1.53	2.07
average % error			**1.66**	**1.23**
overall % error			**1.08**	**1.83**
Experimental Data by King et al. 1992				
0	288.15	60.8	1.50	1.13
		70.9	2.48	0.00
		76	2.27	0.00
		101.3	0.83	1.45
		121.6	1.48	0.71
		131.7	0.96	1.41
		152	1.00	1.04
		157.1	0.93	1.38
		177.3	1.38	0.68
		202.7	1.20	1.00
		243.2	0.30	1.63
average % error			**1.30**	**0.95**
	293.15	65.9	1.26	0.40
		76	1.33	0.39
		96.3	0.73	1.15
		101.3	0.98	0.76
		136.8	0.16	1.49
		146.9	0.71	0.73
		152	0.62	0.73
		177.3	0.96	0.36
		202.7	0.34	1.05
		217.9	2.60	1.36
average % error			**0.97**	**0.84**
	298.15	76	2.79	0.41
		101.3	1.77	0.40

		136.8	0.85	0.39
		152	0.25	0.77
		177.3	0.70	0.37
		202.7	0.83	0.00
average % error			**1.20**	**0.39**
overall % error			**1.16**	**0.78**
Experimental data by Wiebe and Gaddy 1940				
0	285.15	50.6625	1.32	0.24
		75.9938	2.06	0.12
		101.325	1.53	1.40
		151.9875	1.74	1.25
		202.65	1.12	1.72
		303.975	1.48	5.17
average % error			**1.54**	**1.65**
	291.15	25.3313	0.23	1.53
		50.6625	0.03	1.56
		75.9938	0.07	0.68
		101.325	0.08	1.58
		151.9875	0.09	1.34
		202.65	0.01	1.37
		303.975	0.07	2.54
average % error			**0.08**	**1.52**
	298.15	50.6625	1.01	0.53
		75.9938	4.05	0.55
		101.325	0.66	0.49
		405.3	3.23	3.32
average % error			**2.24**	**1.22**
	304.19	25.3313	1.41	0.30
		50.6625	2.38	0.72
		75.9938	4.43	0.98
		101.325	1.78	0.72
		151.9875	0.52	0.18
		202.65	0.46	0.92
		405.3	2.56	3.11
		506.625	3.19	3.53
average % error			**2.09**	**1.31**
	308.15	25.3313	0.84	0.98
		50.6625	1.82	0.37
		75.9938	3.95	0.54
		101.325	1.18	0.75
		151.9875	0.69	0.16
		202.65	0.06	0.64
		405.3	2.66	2.83
		506.625	2.02	2.28
average % error			**1.65**	**1.07**
	313.15	25.3313	0.72	1.61
		50.6625	1.81	0.06
		75.9938	2.72	0.40
		101.325	1.06	0.27

		126.6562	1.28	0.67
		151.9875	0.23	0.02
		202.65	2.97	2.70
		405.3	2.18	1.99
		506.625	2.07	2.55
average % error			**1.67**	**1.14**
overall % error			**1.52**	**1.30**
Experimental data by Koschel et al. 2006				
1	323.1	51	0.562229	1.801802
		100.3	2.508848	1.219512
		143.8	1.108516	1.129944
		202.4	6.54861	2.762431
average % error			**2.68**	**1.73**
	373.1	50.7	13.50426	15
		104	4.137618	4.464286
		191.4	0.854152	1.863354
average % error			**6.17**	**7.11**
3	323.1	50	7.305028	6.024096
		100.4	5.282165	0.877193
		144.1	1.850364	1.612903
		202.4	5.732305	5.109489
average % error			**5.04**	**3.41**
	373.1	50.4	10.7981	16.27907
		102.9	1.806683	3.75
		190.2	0.061064	0.892857
average % error			**4.22**	**6.97**
overall % error			**4.43**	**4.48**

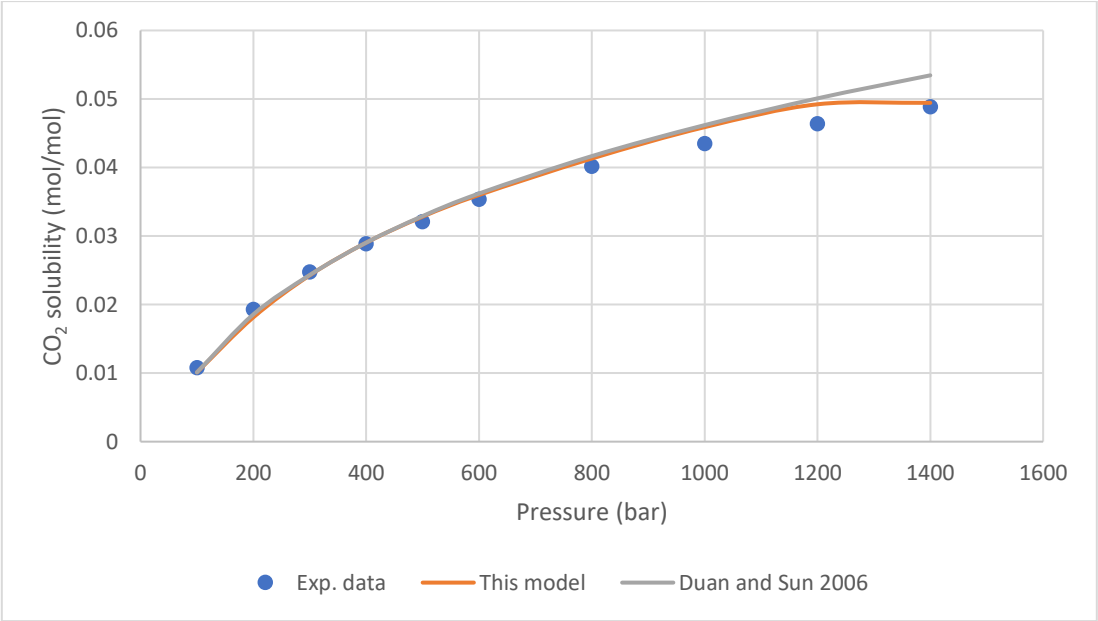

Figure C.1 Comparison of models' predictions with the experimental data of Takenouchi and Kennedy 1965 (T=473.15 K, S=1.0922 molality) as a function of pressure

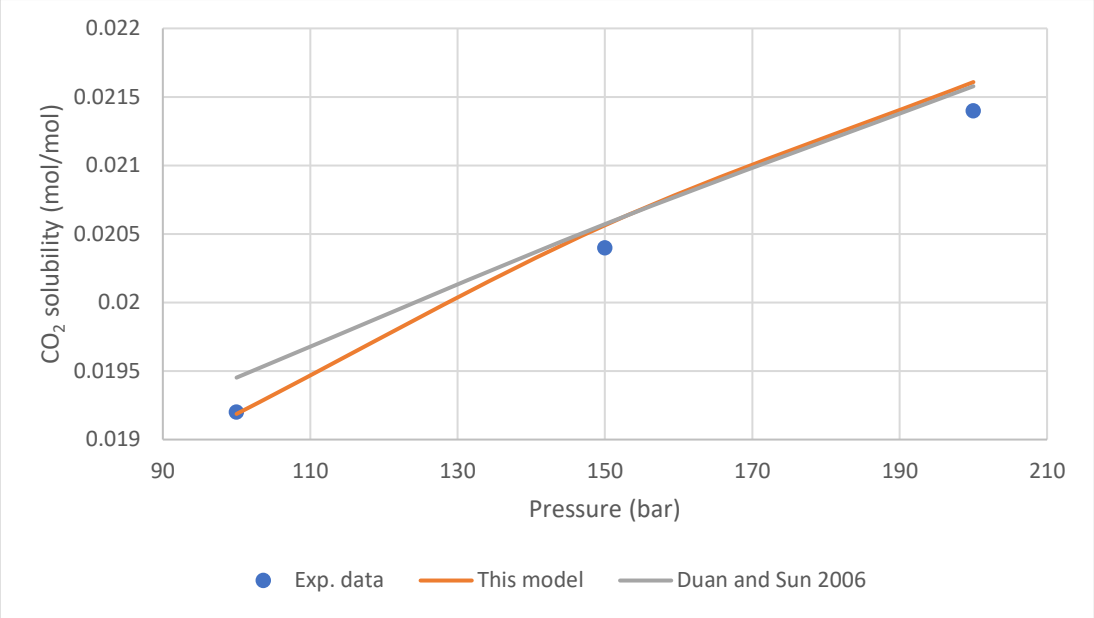

Figure C.2 Comparison of models' predictions with the experimental data of Bando et al. 2003 (T=313.15 K, S=0.5292 molality) as a function of pressure

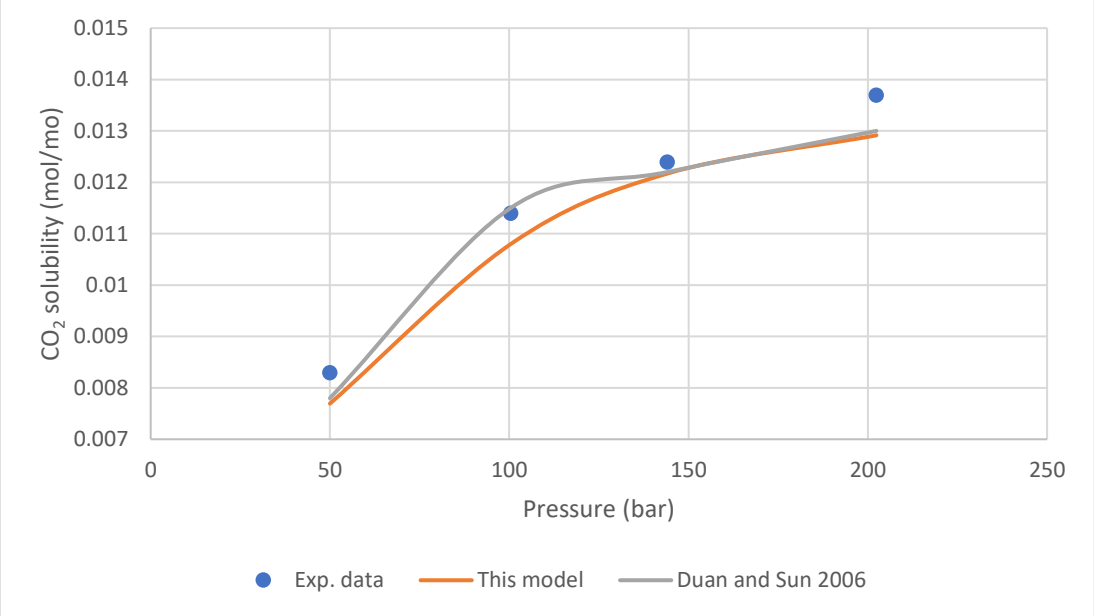

Figure C.3 Comparison of models' predictions with the experimental data of Koschel et al. 2006 (T=323.1 K, S=3 molality) as a function of pressure

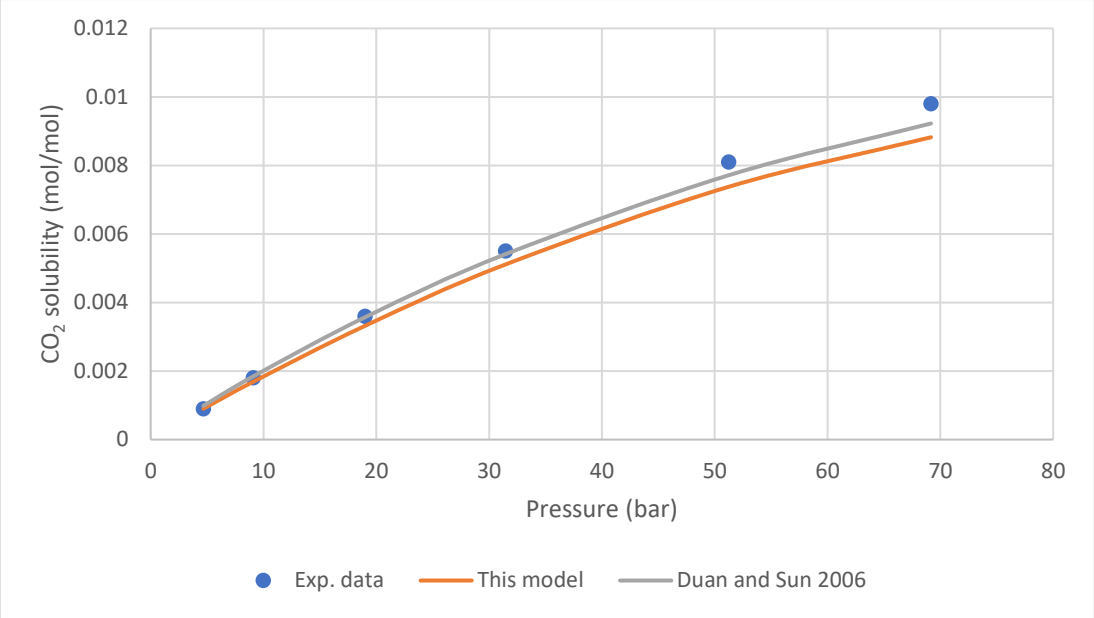

Figure C.4 Comparison of models' predictions with the experimental data of Rumpf et al. 1994 (T=313.17 K, S=3.997 molality) as a function of pressure

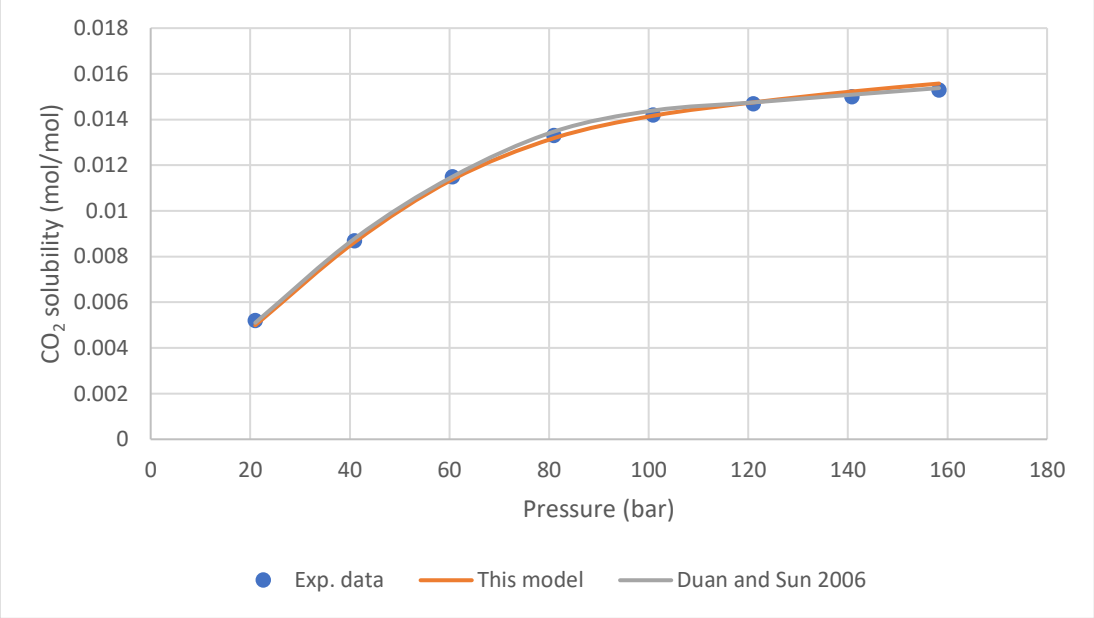

Figure C.5 Comparison of models' predictions with the experimental data of Liu et al. 2011 (T=318.15 K, S=1.9013 molality) as a function of pressure

Appendix D

The Java code of Li et al. 2018 model is presented in this Appendix.

```
public double calcCO2solubimpurities(double temperature, double pressure,
double salinity, double molefracvapCO2, double molefracvapN2, double
molefracvapO2, double molefracvapH2O) {

//0=CO2,1=N2,2=O2,3=H2O
double P=pressure;
double T=temperature;
double S=salinity;
double y []= {molefracvapCO2,molefracvapN2,molefracvapO2,molefracvapH2O};
double m []= {0.0, 0.0, 0.0};
double Tc []= {304.2, 126.2, 154.6, 647.3};
double Pc []= {72.8, 34.0, 49.8, 217.6};
double w[]= {0.2236, 0.0377, 0.021, 0.3434};
double K12[][]= {{0.0,-0.007,0.114,0.2},
                 {-0.007,0.0,-0.0119,0.32547},
                 {0.114,-0.0119,0.0,0.20863},
                 {0.2,0.32547,0.20863,0.0}};

//Normalize Y
double SUMY=0.0;
for (int i=0; i<4; i++) {
SUMY=SUMY+y[i];
}
for (int i=0; i<4; i++) {
y[i]=y[i]/SUMY;
}

double R=8.314*Math.pow(10.0,-2.0);

//Calculate A and B of pure compound
double Tr[]= {0.0,0.0,0.0,0.0};
double ac=0.45724;
double bc=0.07780;
double d[]= {0.384401,1.52276,-0.213808,0.034616,-0.001976};
double dm[]= {0.0,0.0,0.0,0.0};
double ag[]= {0.0,0.0,0.0,0.0};
double asmal[]= {0.0,0.0,0.0,0.0};
double bsmal[]= {0.0,0.0,0.0,0.0};
double a[]= {0.0,0.0,0.0,0.0};
double b[]= {0.0,0.0,0.0,0.0};

for (int i=0; i<4; i++) {
Tr[i]=T/Tc[i];dm[i]=d[0]+w[i]*(d[1]+w[i]*(d[2]+w[i]*(d[3]+w[i]*d[4])));
ag[i]=Math.pow((1.0+dm[i]*(1.0-Math.pow(Tr[i],0.5))),2.0);
asmal[i]=ag[i]*ac*((Math.pow(R*Tc[i],2.0))/Pc[i]);
bsmal[i]=bc*(R*Tc[i])/Pc[i];
a[i]=asmal[i]*P/(Math.pow(R*T,2.0));
b[i]=bsmal[i]*P/(R*T);
}

//Calculate A and B of mixture

double av=0.0;
double bv=0.0;
double sumav[]= {0.0,0.0,0.0,0.0};
```

```
double aij=0.0;

for (int i=0; i<4; i++) {
sumav[i]=0.0;
  for (int j=0; j<4; j++) {
  aij=Math.sqrt(a[i]*a[j])*(1.0-K12[i][j]);
  av=av+y[i]*y[j]*aij;
  sumav[i]=sumav[i]+y[j]*aij;
  }
bv=bv+y[i]*b[i];
}

//ZCUBIC
double c0= 0.0;
double c1= 0.0;
double c2= 0.0;
double c3= 0.0;

c0=-(av*bv-Math.pow(bv,2.0)-Math.pow(bv,3.0));
c1=av-3.0*Math.pow(bv,2.0)-2.0*bv;
c2=-(1.0-bv);
c3=1.0;

//PZEROS
double OMEGA=0.0;
double ROOT[]= {0.0,0.0,0.0};
double W[]= {0.0,0.0,0.0};
double k=0.0;
double NRR=0.0;
double PHI=0.0;
double A0=c0/c3;
double A1=c1/c3;
double A2=c2/c3;
double p=(3*A1-Math.pow(A2,2))/3.0;
double Q=(27.0*A0-9.0*A1*A2+2.0*Math.pow(A2,3.0))/27.0;
double D=(Math.pow(Q,2))/4.0+(Math.pow(p,3.0)/27.0);
double r=Math.sqrt(Math.pow(Math.abs(p),3)/27.0);
double PI=Math.acos(-1.0);

if(D<Math.pow(10.0,-16.0))
{
NRR=3.0;PHI=Math.acos(-Q/(2.0*r));
  for (int i=0; i<3; i++){
  k=i-1.0; W[i]=2.0*Math.pow(r,(1.0/3.0))*Math.cos((PHI+2.0*PI*k)/3.0);
  ROOT[i]=W[i]-A2/3.0;
  }
}else
{
NRR=1.0;
if(p<0.0)
{
OMEGA=Math.asin(2.0*r/Q);
PHI=Math.atan(Math.pow((Math.tan(Math.abs(OMEGA)/2.0)),1.0/3.0));
  if (OMEGA<0.0)
  {
  PHI=-PHI;W[0]=-2.0*Math.sqrt(-p/3.0)/Math.sin(2.0*PHI);
  }
}else
{
```

```
OMEGA=Math.atan(2.0*r/Q);
PHI=Math.atan(Math.pow((Math.tan(Math.abs(OMEGA)/2.0)),1.0/3.0));
if(OMEGA<0.0)
{
PHI=-PHI;
}
W[0]=-2.0*Math.sqrt(p/3.0)/Math.tan(2.0*PHI);
}
ROOT[0]=W[0]-A2/3.0;ROOT[1]=0.0;ROOT[2]=0.0;
}

double zv=0.0;
double IERR=0.0;

if(NRR==1.0)
{
zv=ROOT[0];
}else
{
zv=Math.max(Math.max(ROOT[0],ROOT[1]),ROOT[2]);
}

if(zv<Math.pow(10.0,-19.0))
{
IERR=1;
// System.out.println(IERR);
}

double VV=0.0;

VV=zv*R*T/P;

//Correction of volume
double trans[]= {0.0,0.0,0.0,0.0};
double bh[]= {0.0,0.0,0.0,0.0};
double t0[]= {0.0,0.0,0.0,0.0};
double ti[]= {0.0,0.0,0.0,0.0};
double zc[]= {0.0,0.0,0.0,0.0};
double TEV= 0.0;
double zceos=0.3074;
double dk0=-0.014471;
double dk1=0.067498;
double dk2=-0.084852;
double dk3=0.067298;
double dk4=-0.017366;
double dl0=-10.24470;
double dl1=-28.63120;
double dl2=0.0;

for (int i=0; i<4;i++) {
zc[i]=0.2890+w[i]*(-0.0701-0.0207*w[i]);
ti[i]=(R*Tc[i]/Pc[i])*(zceos-zc[i]);
t0[i]=(R*Tc[i]/Pc[i])*(dk0+w[i]*(dk1+w[i]*(dk2+w[i]*(dk3+w[i]*dk4))));
bh[i]=dl0+w[i]*(dl1+w[i]*dl2);
trans[i]=t0[i]+(ti[i]-t0[i])*Math.exp(bh[i]*Math.abs(1.0-Tr[i]));
TEV=TEV+y[i]*trans[i];
}
VV=VV-TEV;
```

```
//Calculate fugacity coefficient (FC) for all components and phases

double dlnfc[]= {0.0,0.0,0.0,0.0};
double fcv[]= {0.0,0.0,0.0,0.0};

for (int i=0;i<4;i++) {
dlnfc[i]=(b[i]/bv)*(zv-1.0)-Math.log(zv-bv)-
(av/(2.0*Math.sqrt(2.0)*bv))*(2.0*sumav[i]/av-
b[i]/bv)*Math.log((zv+2.414*bv)/(zv-0.414*bv));
fcv[i]=Math.exp(dlnfc[i]);
}

double fv[]= {0.0,0.0,0.0,0.0};

for (int i=0;i<4;i++) {
fv[i]=fcv[i]*y[i]*P;
}

//System.out.println(fv[0]);
//System.out.println(fv[1]);
//System.out.println(fv[2]);
//System.out.println(fv[3]);

//Born function
double BORN=0.0;
double EPS=0.0; double EPS1000=0.0;double CB=0.0;double BB=0.0;
EPS1000=3.4279*Math.pow(10.0,2.0)*Math.exp((-5.0866*Math.pow(10.0,-
3.0)*T+9.469*Math.pow(10.0,-7.0)*Math.pow(T,2.0)));
CB=-2.0525+3.1159*Math.pow(10.0,3.0)/(T-1.8289*Math.pow(10.0,2.0));
BB=-8.0325*Math.pow(10.0,-3.0)+4.21452*Math.pow(10.0,6.0)/T+2.1417*T;
EPS=EPS1000+CB*Math.log((BB+P)/BB+1000.0);
BORN=(1.0/EPS)*(CB/((P+BB)*(CB*Math.log((P+BB)/(BB+1000.0))+EPS)));

//Average partial molar volume
double Vm[]= {0.0,0.0,0.0};
Vm[0]=41.84*(0.1*7.29+(100*0.92)/(2600+P)+2.07/(T-288.0)-
1.23*Math.pow(10.0,4.0)/((2600+P)*(T-288.0))+1.6*BORN);
Vm[1]=41.84*(0.1*7.0);
Vm[2]=41.84*(0.1*5.7889+(100*6.3536)/(2600+P)+3.2528/(T-288.0)-
3.0417*Math.pow(10.0,4.0)/((2600+P)*(T-288.0))+0.3943*BORN);

//System.out.println(Vm[0]);
//System.out.println(Vm[1]);
//System.out.println(Vm[2]);

double Poynteff[]= {0.0,0.0,0.0};
Poynteff[0]=Vm[0]*(P-1.0)/(1000.0*R*T);
Poynteff[1]=Vm[1]*(P-1.0)/(1000.0*R*T);
Poynteff[2]=Vm[2]*(P-1.0)/(1000.0*R*T);

//System.out.println(Poynteff[0]);
//System.out.println(Poynteff[1]);
//System.out.println(Poynteff[2]);
//System.out.println(Math.exp(Poynteff[0]));
//System.out.println(Math.exp(Poynteff[1]));
//System.out.println(Math.exp(Poynteff[2]));

double K[]= {0.0,0.0,0.0,0.0};
```

```
double a1=0.0;double a2=0.0;double a3=0.0;double a4=0.0;double
a5=0.0;double a6=0.0;double a7=0.0;
double ACO20=-10.52624;double ACO21=2.3547*Math.pow(10.0,-2.0);double
ACO22=3972.8;double ACO23=0.0;
double ACO24=-5.8746*Math.pow(10.0,5.0);double ACO25=-
1.9194*Math.pow(10.0,-5.0);
double AN20=58.453;double AN21=-1.818*Math.pow(10.0,-3.0);double AN22=-
3199.0;double AN23=-17.909;double AN24=27460.0;double AN25=0.0;
double AO20=7.5001;double AO21=-7.8981*Math.pow(10.0,-3.0);double
AO22=0.0;double AO23=0.0;double AO24=-2.0027*Math.pow(10.0,5.0);double
AO25=0.0;

if(T<=373.15)
{
a1=9.31063597;a2=-1.892867005*Math.pow(10.0,-
1.0);a3=1.307135652*Math.pow(10.0,-3.0);a4=-3.800223763*Math.pow(10.0,-
6.0);a5=4.0091369717*Math.pow(10.0,-
9.0);a6=2.2769246863*Math.pow(10.0,1.0);a7=-1.1291330188*Math.pow(10.0,-
2.0);
}else
{
a1=-9.0283127*Math.pow(10.0,-1.0);a2=3.6492938*Math.pow(10.0,-
2.0);a3=4.3610019*Math.pow(10.0,-4.0);a4=-3.10936036*Math.pow(10.0,-
6.0);a5=4.592053*Math.pow(10.0,-
9.0);a6=1.62996873*Math.pow(10.0,1.0);a7=2.81119409*Math.pow(10.0,-2.0);
}

K[3]=(a1+a2*T+a3*Math.pow(T,2.0)+a4*Math.pow(T,3.0)+a5*Math.pow(T,4.0))*Mat
h.exp((P-1.0)*(a6+a7*T)/(1000.0*R*T));

K[0]=Math.pow(10.0,(ACO20+ACO21*T+ACO22/T+ACO23*Math.log10(T)+ACO24/(Math.p
ow(T,2.0))+ACO25*Math.pow(T,2.0)))*Math.exp(Poynteff[0]);

K[1]=Math.pow(10.0,(AN20+AN21*T+AN22/T+AN23*Math.log10(T)+AN24/(Math.pow(T,
2.0))+AN25*Math.pow(T,2.0)))*Math.exp(Poynteff[1]);

K[2]=Math.pow(10.0,(AO20+AO21*T+AO22/T+AO23*Math.log10(T)+AO24/(Math.pow(T,
2.0))+AO25*Math.pow(T,2.0)))*Math.exp(Poynteff[2]);

//System.out.println(K[0]);
//System.out.println(K[1]);
//System.out.println(K[2]);
//System.out.println(K[3]);

//double Tro=298.15;
double lamdaCO2Na=-0.411370585+0.000607632*T+97.5347708/T-
0.023762247*P/T+0.017065624*P/(630.0-T)+1.41335834*Math.pow(10.0,-
5.0)*T*Math.log(P);
//double lamdaCO2Na1=0.085;
//double lamdaN2Na1=0.1402-595.0*((1.0/T)-(1.0/Tro))-
4.025*Math.log(T/Tro)+0.01044*(T-Tro)-2.131*Math.pow(10.0,-
6.0)*(Math.pow(T,2.0)-Math.pow(Tro,2.0))+49970.0*((1.0/Math.pow(T,2.0))-
(1.0/Math.pow(Tro,2.0)));
double lamdaN2Na=-2.4434074+0.0036351795*T+447.47364/T-
0.000013711527*P+0.0000071037217*Math.pow(P,2.0)/T;
double lamdaO2Na=0.19997;
double zetaN2NaCl=-0.58071053*Math.pow(10.0,-2.0);
double zetaO2NaCl=-1.2793*Math.pow(10.0,-2.0);
```

```
double zetaCO2NaCl=0.00033639-1.9829898*Math.pow(10.0,-
5.0)*T+0.002122208*P/T-0.005248733*P/(630.-T);

double gamma[]= {0.0,0.0,0.0};

gamma[0]=Math.exp(2.0*S*lamdaCO2Na+Math.pow(S,2.0)*zetaCO2NaCl);
gamma[1]=Math.exp(2.0*S*lamdaN2Na+Math.pow(S,2.0)*zetaN2NaCl);
gamma[2]=Math.exp(2.0*S*lamdaO2Na+Math.pow(S,2.0)*zetaO2NaCl);
//gamma[3]=1.0;

//System.out.println(gamma[0]);
//System.out.println(gamma[1]);
//System.out.println(gamma[2]);

for (int i=0;i<3;i++) {
m[i]=fv[i]/(gamma[i]*K[i]);
}

//System.out.println(m[0]);
//System.out.println(m[1]);
//System.out.println(m[2]);

double x[]= {0.0,0.0,0.0,0.0,0.0};
x[0]=m[0]/((1000.0/18.0)+m[0]+m[1]+m[2]+S);
x[1]=m[1]/((1000.0/18.0)+m[0]+m[1]+m[2]+S);
x[2]=m[2]/((1000.0/18.0)+m[0]+m[1]+m[2]+S);
x[4]=S/((1000.0/18.0)+m[0]+m[1]+m[2]+S);
x[3]=1.0-x[0]-x[1]-x[2]-x[4];

double xCO2=x[0];
double xN2=x[1];
double xO2=x[2];
double xH2O=x[3];
double xNaCl=x[4];

//System.out.println("xCO2 = " + xCO2);
//System.out.println("xN2 = " + xN2);
//System.out.println("xO2 = " + xO2);
//System.out.println("xH2O = " + xH2O);
//System.out.println("xNaCl = " + xNaCl);

System.out.println(m[0]);
return xCO2;
}
```

Appendix E

The fugacity coefficients for the vapor phase are easily calculated through the model of Li et al., since for the description of the vapor phase it uses Peng-Robinson model.

The fugacity coefficients for the liquid phase are calculated via the following equations.

Fugacity coefficient (ϕ) is defined as follows:

$$\varphi = \frac{f}{P}$$

where f=fugacity and P=pressure.

For an a-b dominant ideal solution (Henry solution), the proper choice of reference state is the so-called Henry's coefficient for the species $\widehat{f_i^o} = H_i$. Knowing that the activity coefficient, γ_i is defined as the ratio of the species fugacity in the liquid mixture to the ideal solution reference state fugacity, fugacity coefficient can be expressed by the following equation:

$$\varphi = \frac{\gamma_i H_i}{P}$$

This Henry coefficient is related to the Henry constant of Li et al. 2018 model as described below. The fugacity using the Herny constant of Li et al. 2018 is defined as follows:

$$f = K_H m_i \gamma_i$$

where m_i=molality of component i in aqueous phase.

Moreover, using the asymmetric convention, the fugacity is also defined as follows:

$$f = H_i x_i \gamma_i^* = H_i x_i$$

where x_i=mole fraction of component i in aqueous phase and γ_i^* is the correction factor of Henry's law.

As a result, the Henry coefficient is related to the Henry constant as follows:

$$H_i = \frac{K_H m_i \gamma_i}{x_i}$$

Therefore, the fugacities and the fugacity coefficients can now be calculated.

Appendix F

The comparison of the existing thermodynamic models in Unisim, like Peng-Robinson and Soave-Redlich-Kwong, with the model of Li et al. (2018), is presented in the following tables.

Table F.1 Errors % in CO_2 solubility - stream 1: Peng-Robinson

CO_2 solubility (mol/mol)					
Salinity (mol/kg solvent)	T(K)	P(bar)	Model of Li	Peng Robinson	% error
0	293.15	1	0.00021	0.00018	16.29
		2	0.00042	0.00035	16.34
		5	0.00105	0.00088	16.09
		10	0.00204	0.00172	15.66
		20	0.00387	0.00329	14.88
		30	0.00548	0.00470	14.24
		40	0.00692	0.00597	13.74
		50	0.00818	0.00709	13.35
		75	0.01072	0.00933	12.94
		100	0.01253	0.01088	13.18
		125	0.01381	0.01189	13.93
		150	0.01474	0.01254	14.94
		175	0.01543	0.01294	16.16
		200	0.01598	0.01319	17.47
Average (%) error					**14.94**
Salinity (mol/kg solvent)	T(K)	P(bar)	Model of Li	Peng Robinson	% error
0	298.15	1	0.00018	0.00015	14.99
		2	0.00037	0.00031	14.78
		5	0.00091	0.00078	14.46
		10	0.00177	0.00153	13.89
		20	0.00335	0.00292	12.84
		30	0.00475	0.00418	11.95
		40	0.00599	0.00532	11.20
		50	0.00708	0.00633	10.55
		75	0.00925	0.00838	9.42
		100	0.01079	0.00983	8.89
		125	0.01188	0.01083	8.83
		150	0.01265	0.01150	9.11
		175	0.01321	0.01194	9.62
		200	0.01364	0.01224	10.26
Average (%) error					**11.48**
Salinity (mol/kg solvent)	T(K)	P(bar)	Model of Li et al. (2018)	Peng Robinson	% error
0	303.15	1	0.00016	0.00014	13.55
		2	0.00032	0.00028	13.39
		5	0.00080	0.00069	13.00
		10	0.00156	0.00136	12.39
		20	0.00295	0.00261	11.39
		30	0.00419	0.00375	10.48
		40	0.00529	0.00478	9.68

		50	0.00626	0.00570	9.00
		75	0.00821	0.00758	7.70
		100	0.00963	0.00896	6.96
		125	0.01064	0.00993	6.63
		150	0.01137	0.01061	6.64
		175	0.01190	0.01109	6.87
		200	0.01231	0.01142	7.24
Average (%) error					**9.64**
Overall (%) error					**12.02**

Table F.2 Errors % in CO_2 solubility – stream 1: Soave-Redlich-Kwong

CO_2 solubility (mol/mol)					
Salinity (mol/kg solvent)	T(K)	P(bar)	Model of Li	Soave Redlich Kwong	% error
0	293.15	1	0.00021	0.00014	32.94
		2	0.00042	0.00028	33.12
		5	0.00105	0.00070	32.80
		10	0.00204	0.00138	32.46
		20	0.00387	0.00264	31.83
		30	0.00548	0.00377	31.32
		40	0.00692	0.00478	30.94
		50	0.00818	0.00568	30.64
		75	0.01072	0.00746	30.36
		100	0.01253	0.00869	30.67
		125	0.01381	0.00947	31.43
		150	0.01474	0.00995	32.49
		175	0.01543	0.01023	33.70
		200	0.01598	0.01039	34.96
Average (%) error					**32.12**
Salinity (mol/kg solvent)	T(K)	P(bar)	Model of Li	Soave Redlich Kwong	% error
0	298.15	1	0.00018	0.00012	31.55
		2	0.00037	0.00025	31.44
		5	0.00091	0.00063	31.08
		10	0.00177	0.00123	30.71
		20	0.00335	0.00235	29.85
		30	0.00475	0.00337	29.13
		40	0.00599	0.00428	28.52
		50	0.00708	0.00510	27.99
		75	0.00925	0.00674	27.11
		100	0.01079	0.00790	26.77
		125	0.01188	0.00869	26.86
		150	0.01265	0.00920	27.30
		175	0.01321	0.00952	27.93
		200	0.01364	0.00973	28.66
Average (%) error					**28.92**
Salinity (mol/kg solvent)	T(K)	P(bar)	Model of Li et al. (2018)	Soave Redlich Kwong	% error
0	303.15	1	0.00016	0.00011	30.08

		2	0.00032	0.00022	29.96
		5	0.00080	0.00056	29.69
		10	0.00156	0.00110	29.16
		20	0.00295	0.00211	28.35
		30	0.00419	0.00303	27.60
		40	0.00529	0.00386	26.93
		50	0.00626	0.00461	26.35
		75	0.00821	0.00614	25.29
		100	0.00963	0.00725	24.73
		125	0.01064	0.00802	24.59
		150	0.01137	0.00855	24.76
		175	0.01190	0.00891	25.14
		200	0.01231	0.00915	25.64
Average (%) error					**27.02**
Overall (%) error					**29.35**

Table F.3 Errors % in CO_2 solubility – stream 2: Peng-Robinson

CO_2 solubility (mol/mol)					
Salinity (mol/kg solvent)	T(K)	P(bar)	Model of Li et al. (2018)	Peng Robinson	% error
0	293.15	1	0.00063	0.00053	16.19
		2	0.00127	0.00107	15.87
		5	0.00313	0.00267	14.71
		10	0.00574	0.00527	8.18
Average (%) error					**13.73**

Table F.4 Errors % in CO_2 solubility – stream 2: Soave-Redlich-Kwong

CO_2 solubility (mol/mol)					
Salinity (mol/kg solvent)	T(K)	P(bar)	Model of Li et al. (2018)	Soave Redlich Kwong	% error
0	293.15	1	0.00063	0.00042	32.85
		2	0.00127	0.00085	32.68
		5	0.00313	0.00213	31.83
		10	0.00574	0.00422	26.53
Average (%) error					**30.97**

Appendix G (Smith, 2005, p.659)

Consider a two-stage compression in which the intermediate gas is cooled down to the initial temperature. The total work for a two-stage adiabatic gas compression of an ideal gas is given by:

$$W_s = \frac{\gamma}{\gamma-1} P_1 V_1 \left[1 - \left(\frac{P_2}{P_1}\right)^{\frac{\gamma-1}{\gamma}}\right] + \frac{\gamma}{\gamma-1} P_2 V_2 \left[1 - \left(\frac{P_3}{P_2}\right)^{\frac{\gamma-1}{\gamma}}\right] (1)$$

where P_1, P_2, P_3 = initial, intermediate and final pressures, V_1, V_2 = initial and intermediate gas volumes.

For an ideal gas with intermediate cooling to the initial temperature:

$$P_1V_1=P_2V_2 \ (2)$$

Combining Equations 1 and 2:

$$W_s = \frac{\gamma}{\gamma-1} P_1 V_1 \left[2 - \left(\frac{P_2}{P_1}\right)^{\frac{\gamma-1}{\gamma}} - \left(\frac{P_3}{P_2}\right)^{\frac{\gamma-1}{\gamma}}\right] (3)$$

The intermediate pressure P_2 can be chosen to minimize the overall work of compression. Thus:

$$\frac{dW_s}{dP_2} = 0 = \frac{\gamma}{\gamma-1} P_1 V_1 \left[\left(\frac{1}{P_1}\right)^{\frac{\gamma-1}{\gamma}} \left(\frac{\gamma-1}{\gamma}\right) {P_2}^{-1/\gamma} - {P_3}^{\frac{\gamma-1}{\gamma}} \left(\frac{\gamma-1}{\gamma}\right) {P_2}^{\frac{1-2\gamma}{\gamma}}\right] (4)$$

Simplifying and rearranging Equation 4 gives:

$$P_2^{\frac{2\gamma-2}{\gamma}} = (P_1 P_3)^{\frac{\gamma-1}{\gamma}}$$

or

$$P_2 = \sqrt{P_1 P_3} \ (5)$$

Rearranging Equation 4 gives:

$$\frac{P_2}{P_1} = \frac{P_3}{P_2} = \left(\frac{P_3}{P_1}\right)^{\frac{1}{2}} (6)$$

Thus, for minimum shaft work, each stage should have the same compression ratio, which is equal to the square root of the overall compression ratio. This result is readily extended to N stages. The minimum work is obtained when the compression ratio in each stage is equal:

$$\frac{P_2}{P_1} = \frac{P_3}{P_2} = \frac{P_4}{P_3} = \cdots = r \ (7)$$

where r=compression ratio.

Since

$$\left(\frac{P_2}{P_1}\right) = \left(\frac{P_3}{P_2}\right) = \left(\frac{P_4}{P_3}\right) \ldots = r^N = \frac{P_{N+1}}{P_1} (8)$$

The pressure ratio for minimum work for N stages is given by:

$$W_s = \frac{\gamma}{\gamma-1} P_{in} V_{in} N [1 - (r)^{\frac{\gamma-1}{\gamma}}] \quad (9)$$

Introducing the isentropic compression efficiency gives:

$$W = \frac{\gamma}{\gamma-1} \frac{P_{in} V_{in} N}{\eta_{IS}} \left[1 - (r)^{\frac{\gamma-1}{\gamma}}\right] \quad (10)$$

In principle, the isentropic efficiency might change from stage to stage. However, if the isentropic efficiency for a reciprocating compressor is assumed to be only a function of the pressure ratio and the pressure ratio is constant between stages, then it is legitimate to use a single value as in Equation 10. It should be noted that these results for staged compression are based on adiabatic ideal gas compression and are therefore not strictly valid for real gas compression. It is also assumed that intermediate cooling is back to inlet conditions, which might not be the case with real intercoolers. For fixed inlet conditions and outlet pressure, the overall power consumption is usually not sensitive to minor changes in the intercooler temperature.

The corresponding equation for a polytropic compression is given by:

$$W = \frac{n}{n-1} \frac{P_{in} V_{in} N}{\eta_P} [1 - (r)^{\frac{n-1}{n}}] \quad (11)$$

If the polytropic efficiency of a centrifugal or axial compressor is assumed to be a function of volumetric flowrate, then the efficiency, in principle, will change from stage to stage. This is because the density changes between stages, even if the gas is cooled back to the same temperature as a result of the pressure increase. However, such effects are not likely to have a significant influence on the predicted power.

Appendix H

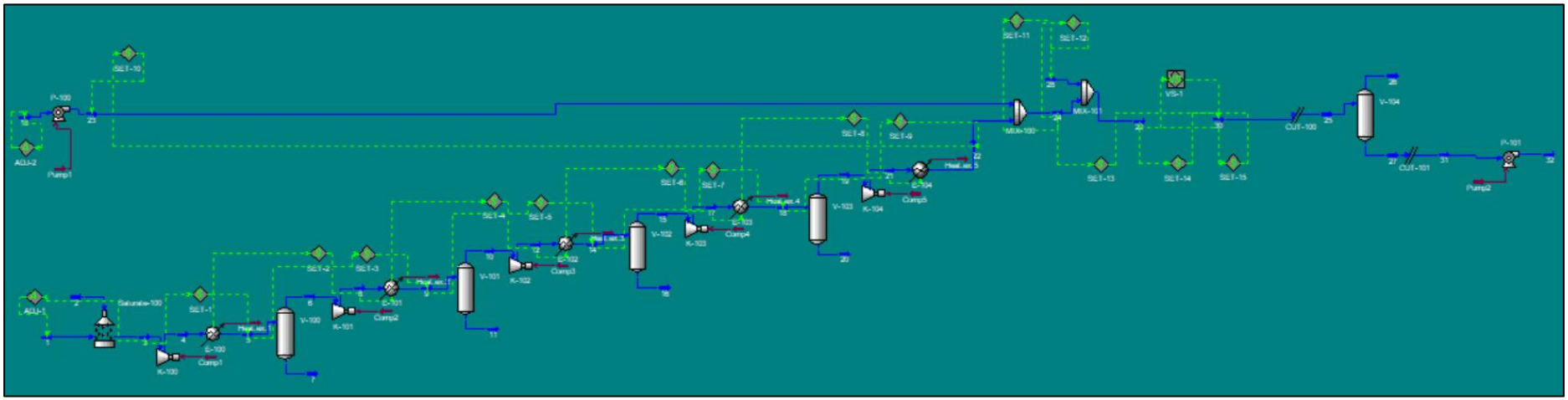

Figure H.1 Process Flow Diagram - Unisim

Appendix I

In this appendix, the mass balance between the streams 24 and 28 for fixing the salinity, at the right level, is described.

In order to fix the salinity's values, the mole flows of oxygen, nitrogen and carbon dioxide of stream 28 are set equal to these of stream 24. Moreover, the sum of the mole flows of pure water and sodium chloride in stream 28 is set the same as the one in stream 24. These are described by the following equations:

$$m_{O_2,24} = m_{O_2,28}$$

$$m_{N_2,24} = m_{N_2,28}$$

$$m_{CO_2,24} = m_{CO_2,28}$$

$$m_{H_2O,24} = m_{NaCl+H_2O,24} = m_{NaCl+H_2O,28}$$

Using the solver option in Excel, the mole flow of water in stream 28 is defined by setting the salinity in the stream 29 that occurs after the mixing.

Appendix J

The following tables represent the pressure ratios and the compression stages in the study of the effect of the thermodynamic approach to equilibrium.

Table J.1 Pressure Ratios – Thermodynamic Approach to Equilibrium

Thermodynamic Approach to Equilibrium	Pressure Ratios	
	IP-14	IP-28
95%	2.246	2.272
90%	2.289	2.314
85%	2.331	2.353

Table J.2 Compression Stages – Thermodynamic Approach to Equilibrium

Thermodynamic Approach to Equilibrium	Compression Stages	
	IP-14	IP-28
95%	3	4
90%	3	4
85%	3	4

Appendix K (Smith, 2005, p.661)

K.1 Pressure drop and heat transfer correlations for the tube-side

The total pressure drop for the tube-side includes the pressure drop in the tube, sudden contractions, sudden expansions and flow reversals. There are two major sources of pressure losses on the tube-side of a shell-and-tube exchanger:

a. friction loss in a tube, which can be calculated as:

$$\Delta P = 4c_f \frac{L}{d_I} \frac{\rho v_T^2}{2} \text{ (1)}$$

where ΔP=pressure drop, c_f= Fanning friction factor, L=length of tube, d_I=inside diameter of tube, ρ=fluid density and υ_T=fluid velocity inside the tubes.

b. losses due to the sudden contractions, expansions and flow reversals through the tube arrangement, which can be estimated per tube-pass as:

$$\Delta P = 2.5 \frac{\rho v_T^2}{2} \text{ (2)}$$

Thus, the total pressure drop for the tube-side is:

$$\Delta P_T = N_{TP}(4c_f \frac{L}{d_I} + 2.5) \frac{\rho v_T^2}{2} \text{ (3)}$$

where ΔP_T=tube-side pressure drop and N_{TP}=number of tube passes.

The friction factor for turbulent flow (Re>4000) can be approximated by:

$$c_f = 0.046 Re^{-0.2} \text{ (4)}$$

where Re=Reynolds number and μ=fluid viscosity.

Substituting this into equation 3:

$$\Delta P_T = N_{TP} 4\ x\ 0.046 (\frac{d_I \upsilon_T \rho}{\mu})^{-0.2} \frac{L}{d_I} \frac{\rho v_T^2}{2} + N_{TP} \frac{2.5}{2} \rho v_T^2 = K_{PT} N_{TP} L \upsilon_T^{1.8} + 1.25 N_{TP} \rho v_T^2 \text{ (5)}$$

where K_{PT}=$0.092\rho^{0.8}\mu^{0.2}d_I^{-1.2}$ (6).

Now, the relationship between velocity (υ_T) and the heat transfer coefficient (h_T) needs to be determined to relate pressure drop to h_T.

The tube-side heat transfer coefficient can be calculated from:

$$h_T = \mathrm{C} \frac{k}{d_I} Pr^{\frac{1}{3}} Re^{0.8} (\frac{\mu}{\mu_w})^{0.14} \text{ (7)}$$

where h_T=tube-side heat transfer coefficient, C=0.021 for gases, 0.023 for nonviscous liquids, 0.027 for viscous liquids, k=fluid thermal conductivity, Pr=Prandtl number=$\frac{C_p \mu}{k}$, C_p=fluid heat capacity, μ=fluid viscosity at the balk fluid temperature and μ_w=fluid viscosity at the wall.

Assuming μ/μ_w=1 and rearranging Equation 7 gives:

$$h_T = K_{hT} \upsilon_T^{0.8} \text{or} \upsilon_T = (\frac{h_T}{K_{hT}})^{\frac{1}{0.8}} \text{ (8)}$$

$$\text{where } K_{hT} = C\frac{k}{d_I}Pr^{\frac{1}{3}}(\frac{d_I\rho}{\mu})^{0.8} \text{ (9).}$$

Now, consider the relationship between the pressure drop and the surface area for the tube-side. The heat transfer surface area A, based on the outside tube surface area, is given by:

$$A=N_T\pi d_oL \text{ (10)}$$

where A=heat transfer surface area, N_T=number of tubes and d_o=outside diameter of tube.

Volumetric flowrate on the inside (tube-side) F_I is given by:

$$F_I = \frac{\pi d_I^2}{4}\frac{N_T}{N_{TP}}\upsilon_T \text{ (11)}$$

where F_I=volumetric flowrate on the inside (tube-side).

This equation can be rearranged to give an expression for the number of tubes N_T:

$$N_T = \frac{4F_IN_{TP}}{\pi d_I^2\upsilon_T} \text{ (12)}$$

Substituting N_T into the expression for surface area gives:

$$A = \frac{4F_IN_{TP}}{d_I^2\upsilon_T}d_oL \text{ (13)}$$

or

$$L = \frac{Ad_I^2\upsilon_T}{4F_IN_{TP}d_o} \text{ (14)}$$

Thus, Equation 5 can be rearranged to give:

$$\Delta P_T = K_{PT}\frac{Ad_I^2}{4F_Id_o}\upsilon_T^{2.8} + 1.25N_{TP}\rho\upsilon_T^2 \text{ (15)}$$

Substituting υ_T from Equation 8:

$$\Delta P_T = K_{PT}\frac{Ad_I^2}{4F_Id_o}(\frac{h_T}{K_{hT}})^{\frac{2.8}{0.8}} + 1.25N_{TP}\rho(\frac{h_T}{K_{hT}})^{\frac{2}{0.8}} = K_{PT1}Ah_T^{3.5} + K_{PT2}h_T^{2.5} \text{ (16)}$$

where

$$K_{PT1} = K_{PT}\frac{d_I^2}{4F_Id_o}(\frac{1}{K_{hT}})^{3.5} = \frac{0.023\rho^{0.8}\mu^{0.2}d_I^{0.8}}{F_Id_o}(\frac{1}{K_{hT}})^{3.5} \text{ (17)}$$

$$K_{PT2} = 1.25N_{TP}\rho(\frac{1}{K_{hT}})^{2.5} \text{ (18).}$$

K.2 Pressure drop and heat transfer correlations for the shell-side

The total pressure drop for the shell-side includes those in the two ends, cross sections and window sections (see Figure K.1). The resulting pressure drop is defined from the inlet to the outlet of an exchanger. Figure K.2 illustrates idealized axial and cross flow. Ideal cross flow gives the higher heat transfer coefficients than axial flow. Figure K.3 illustrates the actual flow pattern. Clearances between the tubes and baffles allow leakage (bypassing) of some of the fluid. This acts to reduce the outside heat transfer coefficient. The heat transfer coefficient and pressure drop is first estimated for ideal cross flow. Then the effects of leakage, bypassing and flow in the window zone are considered by applying correction factors.

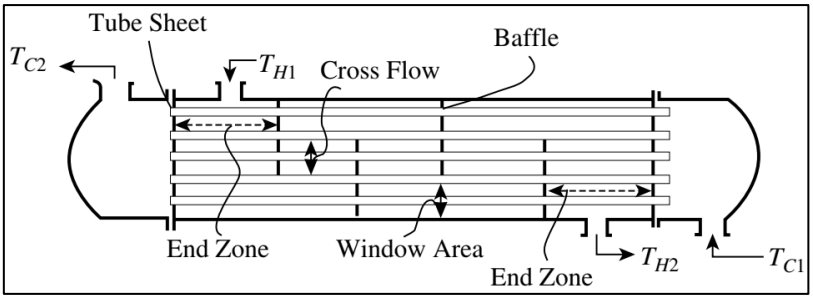

Figure K.1 Zone definition of the shell-side of the shell-and-tube heat exchangers

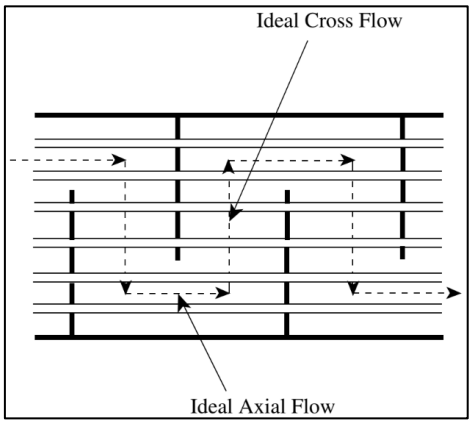

Figure K.2 Ideal shell-side flow

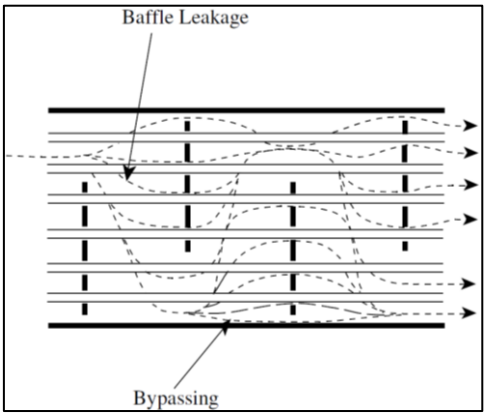

Figure K.3 Nonideal shell-side flow

The pressure drop for the shell-side has three components from inlet to outlet (see Figure K.1). These are the pressure drop for the ends (ΔP_e), the pressure drop for the cross-flow sections (ΔP_c), and the pressure drop for the window sections (ΔP_w).

The total pressure drop for the shell-side is given by summing the pressure drops over all the zones in series from inlet to outlet:

$$\Delta P_S = 2\Delta P_e + \Delta P_c(N_B - 1) + \Delta P_w N_B \quad (19)$$

where ΔP_S=shell-side pressure drop, ΔP_e=pressure drop for the end, ΔP_c=pressure drop for the cross-flow section, ΔP_w=pressure drop for the window section and N_B=number of baffles.

a. Pressure drop in the two ends. There will be only one baffle window in the end zones. The total number of restrictions in the end zone will be the sum of the number of tubes in the

cross-flow and window sections. The zone between tube sheet and the baffle (the end zone) pressure drop (ΔP_e) is given by:

$$\Delta P_e = F_{Pb}\Delta P_{IC}(1 + \frac{N_w}{N_c}) \text{ (20)}$$

where F_{Pb}=bypass correction factor for pressure drop to allow for flow between the tube bundle and the shell wall and is a function of the shell-to-bundle clearance. Typically, F_{Pb} lies between 0.5 and 0.8, depending on construction of the exchanger and the sealing arrangements. F_{Pb} = 0.8 can be used as a reasonable assumption for the clean condition. Fouling will tend to reduce bypassing and increase the pressure drop. Fouling will tend to increase the value to approach 1.0 in the worst case.

ΔP_{IC}=for ideal flow across the tubes based on the number of tubes in the cross-flow section

N_w=number of tube rows in the window section

N_c=number of tube rows in the cross-flow section

The ideal cross-flow pressure drop ΔP_{IC} can be expressed as:

$$\Delta P_{IC} = 8j_f N_C \frac{\rho v_S^2}{2}(\frac{\mu}{\mu_w})^{-0.14} \text{ (21)}$$

where j_F=cross-flow friction factor and υ_S=shell-side fluid velocity

The shell-side fluid velocity is normally based on the area of flow for a hypothetical row of tubes across the diameter of the shell between two baffles. Thus:

$$\upsilon_S = \frac{F_O}{A_S} \text{ (22)}$$

where F_O=volumetric flowrate on the outside (shell-side) ($m^3 \cdot s^{-1}$), A_S=mass cross-flow area (m^2)= number of tubes × space between the tubes × baffle spacing=$\frac{D_S}{p_T}$ ($p_T - d_o$)L_B, D_S=shell diameter (m), p_T=tube pitch, that is, center to center distance between adjacent tubes (m), L_B=distance between baffles (m)

Assuming μ/μ_W=1 in Equation 21 and substituting into Equation 20 gives:

$$\Delta P_e = F_{Pb}\left(1 + \frac{N_w}{N_c}\right)8j_f N_c \frac{\rho v_S^2}{2} = F_{Pb}(N_w + N_c)8j_f \frac{\rho v_S^2}{2} \text{ (23)}$$

The friction factor j_f for cross flow can be correlated for turbulent flow (Re > 4000) as:

$$j_f = 0.3245Re^{-0.17} \text{ (24)}$$

The number of restrictions for cross flow in the window zones NW can be calculated as:

$$N_w = \frac{B_C D_S}{p_T} \text{ (25)}$$

where N_w=number of tube rows in the window section (–) and B_C=baffle cut (–)

The number of tube rows in the cross-flow section Nc is:

$$N_C = \frac{D_S}{p_T} - 2\,x\,\frac{B_C D_S}{p_T} = \frac{D_S(1-2B_C)}{p_T} \text{ (26)}$$

Substituting N_w, N_c and j_f into Equation 23 gives:

$$\Delta P_e = F_{Pb}\frac{D_S(1-B_C)}{p_T}8j_f\frac{\rho v_s^2}{2} = F_{Pb}\frac{D_S(1-B_C)}{p_T}8\ x\ 0.3245Re^{-0.17}\frac{\rho v_s^2}{2} =$$
$$F_{Pb}\frac{D_S(1-B_C)}{p_T}8\ x\ 0.3245(\frac{\rho d_o}{\mu})^{-0.17}\frac{\rho}{2}v_s^{1.83} = K_{PS1}v_s^{1.83}\ (27)$$

where

$$K_{PS1} = 1.298\frac{F_{Pb}D_S(1-B_C)\rho^{0.83}\mu^{0.17}}{p_T d_o^{0.17}}\ (28)$$

b. Pressure drop for the cross sections. The pressure drop in the cross flow zones between the baffle tips is calculated from the correlation for ideal tube banks, and corrected for leakage and bypassing:

$$\Delta P_c=\Delta P_{IC}F_{Pb}F_{PL}\ (29)$$

where ΔP_c=pressure drop in cross-flow section, ΔP_{IC}=pressure drop for ideal cross flow and F_{PL}=leakage correction factor to allow for leakage through the tube-to-baffle clearance and the baffle-to-shell clearance. Typically, F_{PL} varies between 0.4 and 0.5. A value of F_{PL} = 0.5 can be used as a reasonable assumption for the clean condition. Fouling will tend to reduce leakage and increase the shell-side pressure drop. Fouling will tend to increase the value to approach 1.0 in the worst case.

The pressure drop for the cross-flow sections can be calculated as:

$$\Delta P_c(N_B-1) = (N_B-1)8j_f N_c\frac{\rho v_s^2}{2}F_{Pb}F_{PL}\ (30)$$

where NB = number of baffles..

The surface area A is given by:

$$A = N_T\pi d_o L\ (31)$$

For a square pitch, each one contains four quarter tubes. Thus, for a square pitch, each tube is contained in an area of p_2^T. The number of tubes can then be approximated as:

$$N_T = \frac{\frac{\pi}{4}D_S^2}{p_T^2}\ (32)$$

For a triangular pitch, each one with sides p_T, having an area of $0.5p_T^2$ sin60° contains half a tube. Thus, a single tube is contained in an area of p_T^2 sin60° = $0.866p_T^2$. The number of tubes can then be generalized as:

$$N_T = \frac{\frac{\pi}{4}D_S^2}{p_c p_T^2}\ (33)$$

where p_C=pitch configuration factor, 1 for square pitch, 0.866 for triangular pitch.

It should be noted that Equations 32 and 33 will tend to overestimate the number of tubes that can be contained in a given shell diameter. The larger the diameter shell, the smaller will be the error in the tube count. Substituting Equation 33 into Equation 31 gives:

$$A = \frac{\pi D_S^2}{4p_C p_T^2}\pi d_o L = \frac{\pi D_S^2}{4p_C p_T^2}\pi d_o L_B(N_B+1)\ (34)$$

The area for cross flow A_S is given by:

$$A_S = \frac{p_T - d_o}{p_T} D_S L_B \text{ (35)}$$

Rearranging Equation 35 gives:

$$L_B = \frac{A_S p_T}{(p_T - d_o) D_S} \text{ (36)}$$

Substituting L_B into equation 34 gives:

$$A = \frac{\pi D_S^2}{4 p_c p_T^2} \pi d_o \frac{A_S p_T}{(p_T - d_o) D_S} (N_B + 1) = \frac{\pi}{4 p_c p_T^2} \pi d_o \frac{A_S p_T}{(p_T - d_o)} D_S (N_B + 1) \text{ (37)}$$

Rearranging Equation 37 gives:

$$D_S (N_B + 1) = \frac{A}{\frac{\pi}{4 p_c p_T^2} \pi d_o \frac{A_S p_T}{(p_T - d_o)}} = \frac{A}{\frac{\pi}{4 p_c p_T^2} \pi d_o \frac{F_o p_T}{(p_T - d_o)}} \upsilon_s \text{ (38)}$$

Substituting the friction factor j_f and N_C into Equation 30 gives:

$$\Delta P_c (N_B - 1) = (N_B - 1) 8 \; x \; 0.3245 \left(\frac{\rho d_o \upsilon_s}{\mu} \right)^{-0.17} x \frac{D_S (1 - 2B_C)}{p_T} \frac{\rho \upsilon_s^2}{2} F_{Pb} F_{PL} \text{ (39)}$$

Combining Equations 38 and 39 gives:

$$\Delta P_c (N_B - 1) = \frac{8 \; x \; 0.3245 (\frac{\rho d_o}{\mu})^{-0.17}}{\frac{\pi}{4 p_c p_T^2} \pi d_o \frac{F_o p_T}{(p_T - d_o)}} \; x \; \frac{(1 - 2B_C)}{p_T} \frac{\rho}{2} A \upsilon_s^{2.83} F_{Pb} F_{PL} -$$
$$2 \; x \; 8 \; x \; 0.3245 \left(\frac{\rho d_o \upsilon_s}{\mu} \right)^{-0.17} x \; \frac{D_S (1 - 2B_C)}{p_T} \frac{\rho \upsilon_s^2}{2} F_{Pb} F_{PL} \text{ (40)}$$

where

$$K_{PS2} = \frac{0.5261 F_{Pb} F_{PL} p_C (1 - 2B_C) (p_T - d_o) \rho^{0.83} \mu^{0.17}}{d_o^{1.17} F_o} \text{ (41)}$$

$$K_{PS3} = \frac{2.596 F_{Pb} F_{PL} (1 - 2B_C) D_S \rho^{0.83} \mu^{0.17}}{d_o^{1.17} p_T} \text{ (42)}$$

c. Pressure drop for the window sections. The pressure drop calculation for the window zone is less accurate than that for the cross-flow sections. One correlation is:

$$\Delta P_w = F_{PL} (2 + 0.6 N_w) \frac{\rho \upsilon_s^2}{2} \text{ (43)}$$

The pressure drop for the window sections can be calculated as:

$$N_B \Delta P_w = N_B F_{PL} (2 + 0.6 N_w) \frac{\rho \upsilon_s^2}{2} = N_B F_{PL} \left(2 + 0.6 \frac{B_C D_S}{p_T} \right) \frac{\rho \upsilon_s^2}{2} \text{ (44)}$$

In order to remove N_B from the correlation, the following approximation can be made:

$$N_B + 1 \approx N_B \text{ (45)}$$

The bigger the exchanger, the better this assumption becomes. Using Equation 45 and 38 gives:

$$N_B \Delta P_w = F_{PL} \left(\frac{2}{D_S} + 0.6 \frac{B_C}{p_T} \right) D_S (N_B + 1) \frac{\rho \upsilon_s^2}{2} = F_{PL} \left(\frac{2}{D_S} + 0.6 \frac{B_C}{p_T} \right) \frac{A}{\frac{\pi}{4 p_c p_T^2} \pi d_o \frac{F_o p_T}{(p_T - d_o)}} \; x \; \upsilon_S \frac{\rho \upsilon_s^2}{2} =$$
$$K_{PS4} A v_s^3 \text{ (46)}$$

where

$$K_{PS4} = \frac{0.2026 F_{PL} p_C p_T (p_T - d_o)\rho}{d_o F_o} \left(\frac{2}{D_S} + \frac{0.6 B_C}{p_T}\right) \quad (47)$$

d. Shell-side heat transfer coefficient. The shell-side heat transfer coefficient is given by:

$$h_S = h_{IS} F_{hn} F_{hw} F_{hb} F_{hL} \quad (48)$$

where h_S=shell-side heat transfer coefficient, h_{IS}=shell-side heat transfer coefficient for ideal cross flow, F_{hn}=correction factor to allow for the effect of the number of tube rows crossed. The basic heat transfer coefficient is based on ten rows of tubes. For turbulent flow, F_{hn} is close to 1.0., F_{hw}=the window correction factor. This allows for flow through the baffle window and is a function of the heat transfer area in the window zones and the total heat transfer area. A typical value for a well-designed exchanger is near 1.0., F_{hb}=the bypass stream correction factor. This allows for flow between the tube bundle and the shell wall and is a function of the shell-to-bundle clearance. Typical values are in the range 0.7 to 0.9 for clean exchangers with effective sealing arrangements. Fouling will tend to reduce bypassing and increase the shell-side heat transfer coefficient by increasing the cross flow. A conservative assumption would be to assume a value of 0.8 both for the clean and fouled condition. However, fouling will tend to increase the value to approach 1.0. and F_{hL}=the leakage correction factor. This allows for leakage through the tube-to-baffle clearance and the baffle-to-shell clearance. Typical values are in the range 0.7 to 0.8 for clean exchangers. Fouling will tend to reduce leakage and also increase the shell-side heat transfer coefficient by increasing the cross flow. A conservative assumption would be to assume a value of 0.8 both for the clean and fouled condition. However, fouling will tend to increase the value to approach 1.0.

The heat transfer coefficient for ideal cross flow over a tube bank is given as:

$$h_{IS} = j_h C_p Pr^{-\frac{2}{3}} \rho v_s \quad (49)$$

The heat transfer factor j_h can be correlated for turbulent flow (Re > 4000) as:

$$j_h = 0.24 Re^{-0.36} \quad (50)$$

Substituting j_h into h_{IS} gives:

$$h_{IS} = 0.24 C_p Pr^{-\frac{2}{3}} \rho \left(\frac{\rho d_o}{\mu}\right)^{-0.36} v_s^{0.64} \quad (51)$$

From Equation 48:

$$h_S = F_{hn} F_{hw} F_{hb} F_{hL} 0.24 CpPr^{-\frac{2}{3}} \rho \left(\frac{\rho d_o}{\mu}\right)^{-0.36} v_s^{0.64} = K_{hS} v_s^{0.64} \quad (52)$$

where

$$K_{hS} = \frac{0.24 F_{hn} F_{hw} F_{hb} F_{hL} \rho^{0.64} Cp^{\frac{1}{3}} k^{\frac{2}{3}}}{\mu^{0.307} d_o^{0.36}} \quad (53)$$

Reasonable assumptions for the clean and fouled condition are F_{hn}=F_{hw}=1 and F_{hb}=F_{hL}=0.8. By rearranging Equation 52:

$$v_S = \left(\frac{h_S}{K_{hS}}\right)^{\frac{1}{0.64}} \quad (54)$$

e. Pressure drop correlation for the shell-side. Substituting Equations 27, 40, 46 and 54 into Equation 19 gives:

$$\Delta P_S = 2\Delta P_e + 2\Delta P_C(N_B - 1) + \Delta P_w N_B = 2K_{PS1}v_S^{1.83} + K_{PS2}Av_S^{2.83} - K_{PS3}v_S^{1.83} +$$
$$K_{PS4}Av_S^3 = 2K_{PS1}\left(\frac{h_S}{K_{hS}}\right)^{\frac{1.83}{0.64}} + K_{PS2}A\left(\frac{h_S}{K_{hS}}\right)^{\frac{2.83}{0.64}} - K_{PS3}\left(\frac{h_S}{K_{hS}}\right)^{\frac{1.83}{0.64}} + K_{PS4}\left(\frac{h_S}{K_{hS}}\right)^{\frac{3}{0.64}} =$$
$$K_{S1}h_S^{2.86} + K_{S2}Ah_S^{4.42} + K_{S3}Ah_S^{4.69} \quad (55)$$

where $K_{S1} = \frac{2K_{PS1} - K_{PS3}}{K_{hS}^{2.86}}$ (56), $K_{S2} = \frac{K_{PS2}}{K_{hS}^{4.42}}$ (57) and $K_{S3} = \frac{K_{PS4}}{K_{hS}^{4.69}}$ (58)

The constants in the heat transfer and pressure drop correlations are functions of the fluid physical properties, volumetric flowrate, tube size and pitch. In preliminary design, it is reasonable to assume either 20 mm outside diameter tubes with a 2 mm wall thickness or 25 mm outside diameter tubes with 2.6 mm wall thickness. The tube pitch is normally taken to be p_T=1.25d_o. A square tube pitch configuration can be assumed as a conservative assumption. Baffle cut can be assumed to be 0.25 in preliminary design.

It should be noted that the pressure drop calculation is much less accurate than the film transfer coefficient calculation. Moreover, calculations for the shell-side are less reliable than those for the tube-side. The pressure drop correlations for the shell-side should be treated with great caution. Even experimental data tends to show considerable scatter when correlated.

Appendix L

In the following tables the compression's pressures, the pressure ratios and the compression stages for each case, in the study of the effect of pressure drop, are studied.

Table L.1 Pressures for the dissolution of CO_2 for all cases, taking into consideration the pressure drops in the mixer

	Pressure Drop in the mixer-1 bar	**Pressure Drop in the mixer-3 bar**	**Pressure Drop in the mixer-5 bar**
	Dissolution Pressure (bar)		
HP-14	181	183	185
IP-14	17	19	21
HP-28	181	183	185
IP-28	38	40	42

Table L.2 Pressure ratios of the compression stages for each case

HP-14/HP-28					
Pressure Drop Mixer (bar)	**Pressure Drop Heat Exchanger (bar)**				
	0.1	**0.2**	**0.3**	**0.4**	**0.5**
1	2.630	2.652	2.675	2.698	2.722
3	2.635	2.658	2.680	2.704	2.727
5	2.641	2.663	2.686	2.709	2.733
IP-14					
Pressure Drop Mixer (bar)	**Pressure Drop Heat Exchanger (bar)**				
	0.1	**0.2**	**0.3**	**0.4**	**0.5**
1	2.283	2.320	2.358	2.397	2.436
3	2.367	2.404	2.441	2.479	2.517
5	2.446	2.482	2.518	2.556	2.593
IP-28					
Pressure Drop Mixer (bar)	**Pressure Drop Heat Exchanger (bar)**				
	0.1	**0.2**	**0.3**	**0.4**	**0.5**
1	2.273	2.303	2.333	2.364	2.396
3	2.302	2.331	2.361	2.392	2.424
5	2.329	2.359	2.389	2.419	2.451

Table L.3 Compression Stages for each case

	Compression stages
HP-14/HP-28	5
IP-14	3
IP-28	4

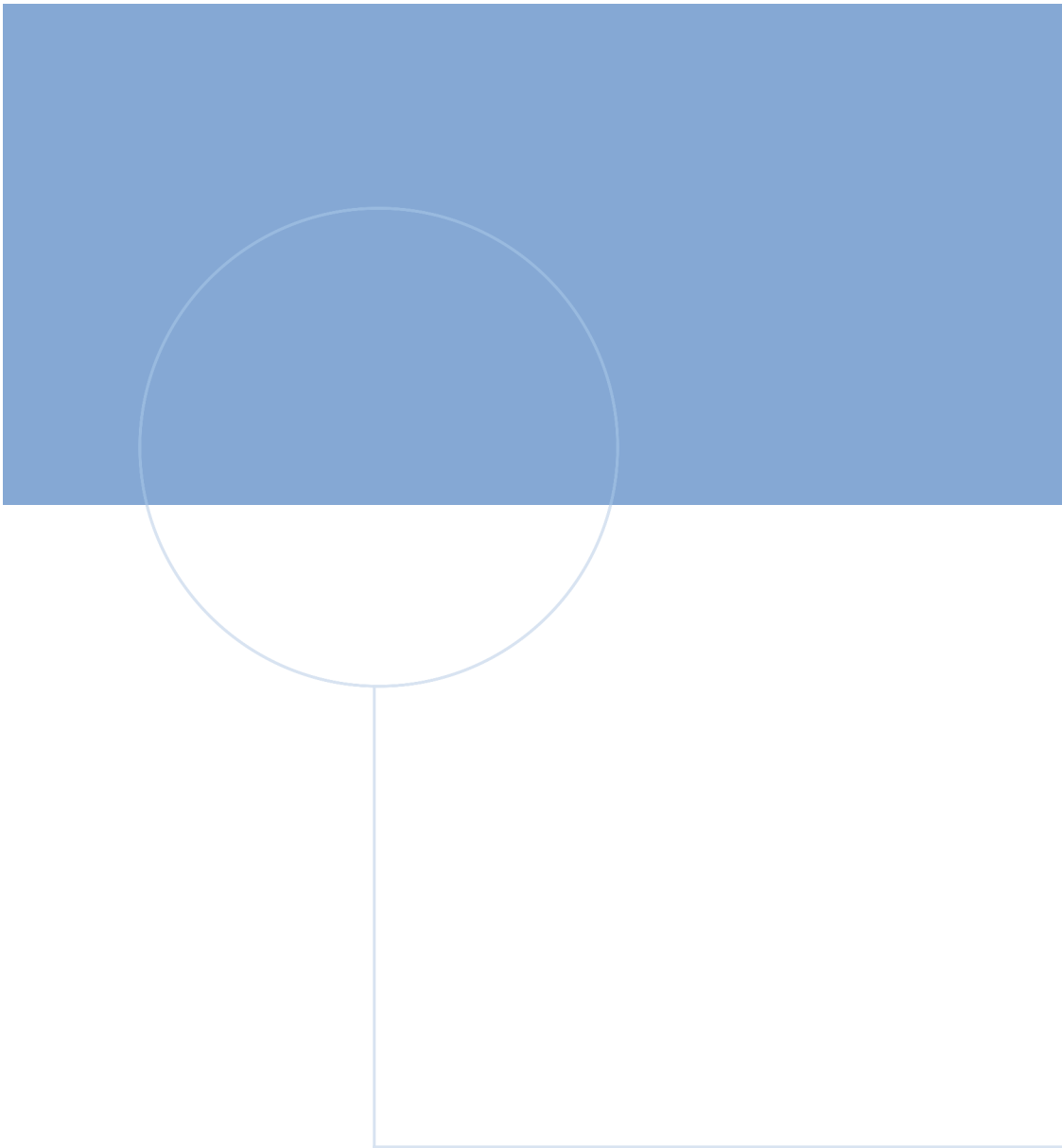

NTNU

Kunnskap for en bedre verden